Faculty of Aerospace Engineering

Incremental nonlinear control applied to tiltrotor aircraft

Master of Science Thesis

Ralph Krook

August 15, 2022

TU Delft Delft University of Technology

Challenge the future

Incremental nonlinear control applied to tiltrotor aircraft

Master of Science Thesis

by

Ralph Krook

in partial fulfillment of the requirements for the degree of

Master of Science
in Aerospace Engineering

at the Delft University of Technology,
to be defended publicly on Friday August 26, 2022 at 10:00.

Supervisor:	Dr. ir. M.D. Pavel	
Thesis committee:	Dr. ir. M.D. Pavel,	TU Delft
	Dr. ir. E. van Kampen,	TU Delft
	Dr. A. Bombelli	TU Delft

An electronic version of this thesis is available at `http://repository.tudelft.nl/`.

TU Delft Delft University of Technology

Preface

Completing this thesis marks the ultimate step in finalizing my studies at the TU Delft and obtaining the degree of Master of Science in Aerospace Engineering. I look back with great pleasure at the time I spent here in Delft, where I have learned more than I could have ever expected. I consider myself very fortunate for all the fantastic adventures I could take part in that took me around the world.

I would like to take this opportunity to thank all who have supported me during my thesis and the rest of my student career. First of all, Marilena, thank you for all the time and energy supervising me during my thesis. I am very grateful for having studied this exciting subject. Completing my thesis under your supervision was a pleasure and a great learning experience. Many thanks also to my friends for the best times I have had here in Delft, and thank you for your patience while I was so consumed by this work. Most importantly, I would like to thank my parents and brother. You have allowed me to take my time to learn and explore by virtue of your unwavering support. I am very grateful to you for always being there for me.

I am happy to finalize this chapter of my life, and I look forward to applying all that I have learned in the future.

Ralph Krook
Delft, August 2022

“Richtiges Auffassen einer Sache und Mißverstehn der gleichen Sache schließen einander nicht vollständig aus.”

—— *Franz Kafka - Der Prozess*

Contents

List of Figures

List of Tables

List of Abbreviations

ADOCS Advanced Ditigal/Optical control system

AFC Automatic Flight Control System

c.g. Center of gravity

CA Control allocation algorithm

CF Command Filter

FFS Force Feel System

INDI Incremental Nonlinear Dynamic Inversion

MF Control effectiveness mismatch factor

MPC Model Predictive Control

OP Operating point

PID Proportional-integrator-derivative controller

RPM Revolutions per minute

SCAS Stability and Control Augmentation System

VTOL Vertical Take-off and Landing

WLS Weighted least squares method

WPIM Weighted pseudo inverse method

List of Symbols

α Angle of attack $[rad]$

β Rotor flapping angle [rad]

χ Command filter compensation estimate

χ Aircraft position vector in inertial frame $[m]$

δ_e Elevator deflection angle $[rad]/[deg]$

η Nacelle angle $[deg]/[rad]$

γ Lock number

Ω Rotor speed [rad/s]

ω_n Natural frequency $[1/s]$

ψ Rotor azimuth angle [rad]

ρ Air density $[kg/m^3]$

θ_0 Collective swashplate angle $[rad]/[deg]$

θ_f Fuselage pitch angle $[deg]/[rad]$

θ_{1s} Longitudinal cylic swashplate angle $[rad]/[deg]$

g Gravitational accelerations $[m/s^2]$

G_c Rotational acceleration control effectiveness matrix

G_v Linear acceleration control effectiveness matrix

$G_{q,i}$ Control effectiveness of q with respect to actuator i

$G_{T,i}$ Control effectiveness of T with respect to actuator i

H_s Sensor filter

m Aircraft mass $[kg]$

M_i Pitch rate control derivative with respect to actuator i $[1/s^2]$

p_i Control allocation sensitivity on axis i

u rational velocity component about the body y-axis $[rad/s]/[deg/s]$

R Rotor radius $[m]$

T Proprotor thrust force $[N]$

T_i Thrust force control derivative with respect to actuator i $[N/deg]$

T_s Controller sample time $[s]$

u velocity component of the body x-axis $[m/s]$

V Control Lyapunov function

γ Flight path angle $[rad]$

V_∞ Flight speed $[m/s]$

w velocity component of the body z-axis $[m/s]$

W_u Control allocation weighting matrix considering deflections

W_v Control allocation weighting matrix considering axis

X_{COL} Collective stick deflection $[inch]$

X_{LON} Longitudinal stick deflection $[inch]$

1

Introduction

Tiltrotor aircraft combine the benefits from turboprop aircraft and helicopters by merging the ability to take off and land vertically (VTOL) with the performance that fixed wing turboprop aircraft have on endurance, range and speed. Although the tiltrotor concept was already introduced in the early stages of aviation history, the number of actual developed manned tiltrotor aircraft has been limited. Nowadays, the only manned tiltrotor in production is the Bell Boeing V-22 Osprey and is operated by the U.S and Japanese military. Current developments however, will soon enable civilian use of tiltrotor aircraft, that can leverage their operational flexibility to solve problems such as airport and airspace congestion.

The benefits of the tiltrotor configuration with its expanded operational envelope, also present many technical challenges of which one is the controllability of the aircraft. In an unaugmented state, tiltrotor aircraft exhibit poor and changeable handling qualities due to large nonlinearities in their dynamics. In hover mode for example, the aircraft appears sluggish and unstable while the behavior is mainly dominated by the complex rotor flapping-dynamics of the two rotors. To assist the pilot, currently deployed tiltrotor aircraft feature augmented controls via Fly-by-wire systems that maintains the necessary response characteristics throughout the entire mission. While the augmentation systems alleviate some of the pilot workload, pilots are still faced with demanding manoeuvres such as the conversion from forward flight to hover and sequential landing. In this critical phase of flight, the pilot is responsible for maintaining the desired flight path angle and speed trajectory by means of manually adjusting the throttle, mast angle and nose attitude. This can be a difficult task especially in instrument meteorological conditions.

The tiltrotor experiences a wide range of flight conditions at different airframe configurations and therefore the vehicle dynamics are highly nonlinear. This means that the conventional linear controllers that are in use now, require extensive gain scheduling with changes in mast angle, airspeed and altitude. Consequently, the development of such linear controllers can become costly and iterations are difficult. Additionally, these techniques can suffer from performance degradation due to nonlinearities, uncertainties and system failures.

To solve the shortcomings of linear flight control, many efforts have searched for alternatives. Feedback linearization methods such as nonlinear dynamic inversion have been studied extensively, and its derivative incremental nonlinear dynamic inversion has been applied to many aerospace applications. Incremental nonlinear dynamic inversion (INDI) has been introduced as aerospace control method twenty year ago and has an advantage over conventional nonlinear dynamic inversion because it is less model dependent. This could be beneficial for tiltrotor control as predicting accurate aircraft dynamics is difficult. Incremental control has been demonstrated in many aerospace applications such as fighter aircraft, passenger jets, drones and novel electric urban air mobility aircraft. Incremental control has also been applied to helicopters. Research into incremental control on tiltrotor aircraft however still remains while the benefits of INDI may fit this aircraft configuration very well. The aircraft dynamics are highly nonlinear due to its extended envelope and possible configuration changes. Control of a tiltrotor also poses a control allocation problem where in transition from a hover to a forward flight phase, the rotors can produce controlling moments as well as the aerodynamic surfaces such as the elevator and flaperons.

This research therefore addresses the question on how incremental nonlinear control can be applied to tiltrotor aircraft. Specific attention is given to the design of the attitude controller in combination with a control allocation solver and a global velocity controller which can steer the aircraft through a transition and conversion based on incremental logic.

The structure of the report is as follows. First, a paper is presented which addresses the controller design in short and discusses some of the particularities that have been identified during this project. Second, elements from the previously conducted literature study are presented as relevant background information. Third, the work done in this thesis is presented. This concerns controller design synthesis and evaluation. Lastly, this report is concluded with a summary of results and recommendations for future work.

Part I

Scientific Article

Incremental nonlinear control applied to a nonlinear tiltrotor model

Ralph R.J. Krook
Delft University of Technology, Faculty of Aerospace Engineering

Incremental nonlinear control is a promising control method that can be applied in controlling tasks that involve systems with highly nonlinear dynamics. Incremental nonlinear control is a feedback linearization method that requires less model knowledge than conventional Nonlinear Dynamic Inversion and is robust against model mismatches. This paper presents an incremental based control method to control a longitudinal model of the XV-15 tiltrotor aircraft. First, an attitude controller is designed that solves the over actuated system of longitudinal cyclic and elevator pitch control by using a weighted least squares control allocation method. Second, an incremental based velocity controller is designed which integrates the use of the nacelles. The controllers have been tested against attitude and speed tracking tasks to evaluate their performance. The attitude controller showed to be able to follow the reference signal while adjusting to changing aircraft dynamics. In combination with the velocity controller the aircraft was able to follow a complete speed profile from helicopter mode to fixed-wing and back in a fully coordinated way while remaining in the conversion corridor.

I. Introduction

Tiltrotor aircraft combine the benefits of turboprop aircraft and helicopters by merging the ability to take-off and land vertically (VTOL) with the performance of fixed wing turboprop aircraft on endurance, range, and speed. Although the tiltrotor concept was already introduced in the early stages of aviation history, the number of actual developed manned tiltrotor aircraft has been limited. Nowadays, the only manned tiltrotor in production is the Bell Boeing V-22 Osprey which the U.S and Japanese military operate. Current developments, however, will soon enable civilian use of tiltrotor aircraft, such as the Augusta Westland 609 that could leverage their operational flexibility to solve problems such as airport and airspace congestion [1, 2].

The benefits of the tiltrotor configuration with its expanded operational envelope also present many technical challenges, one of which is the aircraft's controllability [3]. In an unaugmented state, tiltrotor aircraft exhibit rather poor and changeable handling qualities due to large nonlinearities in their dynamics. In hover mode, for example, the aircraft appears sluggish and unstable while the behavior is mainly dominated by the complex rotor flapping-dynamics of the two rotors [4]. To improve handling qualities, currently deployed tiltrotor aircraft feature augmented controls via a Fly-by-wire system that maintains the necessary response characteristics throughout the entire mission [5]. While the augmentation systems alleviate some of the pilot workload, pilots are still faced with demanding maneuvers such as the conversion from forward flight to hover and sequential landing. In this critical phase of flight, the pilot is responsible for maintaining the desired flight path angle and speed trajectory by means of manually adjusting the throttle, mast angle, and nose attitude. This can be a difficult task, especially in instrument meteorological conditions.

The tiltrotor experiences a wide range of flight conditions at different airframe configurations and therefore, the vehicle dynamics are highly nonlinear. This means that the conventional linear controllers that are in use now require extensive gain scheduling with changes in mast angle, airspeed, and altitude. Consequently, developing such linear controllers can become costly, and iterations are complex. Additionally, these techniques can suffer from performance degradation due to nonlinearities, uncertainties and system failures [6].

To solve the shortcomings of linear flight control, many efforts have searched for alternatives. Feedback linearization methods such as nonlinear dynamic inversion have been studied extensively, and its derivative incremental nonlinear dynamic inversion has been applied to many aerospace applications. Incremental nonlinear dynamic inversion (INDI) has been introduced as aerospace control method twenty year ago [7–9] and has an advantage over conventional nonlinear dynamic inversion because it is less model dependent. This could be beneficial for tiltrotor control as predicting accurate aircraft dynamics is difficult. Incremental control has been demonstrated in many aerospace applications such as in [10–12]. Incremental control has also been applied to helicopters in the works of [13–15]. Research into incremental control on tiltrotor aircraft however still remains while the benefits of INDI may fit this aircraft configuration very well.

The aircraft dynamics are highly nonlinear due to its extended envelope and possible configuration changes. Control of a tiltrotor also poses a control allocation problem where in transition from a hover to a forward flight phase, the rotors can produce controlling moments as well as the aerodynamic surfaces such as the elevator and flaperons [16].

This research therefore addresses the question on how incremental nonlinear control can be applied to tiltrotor aircraft. Specific attention is given to the design of the attitude controller in combination with a control allocation solver and a global velocity controller which can steer the aircraft through a transition and conversion based on incremental logic.

The structure of this paper is as follows. First, the nonlinear tiltrotor model which will be used for the simulations is discussed. Second, the incremental control law for the attitude controller will be derived. Third, the velocity control laws will be derived. Next, the attitude controller design will be evaluated at multiple points in the flight envelope. The result section will be concluded with a demonstration of the global velocity controller.

II. Methods

A. Longitudinal nonlinear model

The tiltrotor configuration that will be considered in this study is that of the XV-15 tiltrotor [17]. The aircraft features two tiltable nacelles on which proprotors are installed. They are positioned at the left and right tip of the main wing. The nacelles can tilt from a vertical position when the aircraft is flying in helicopter mode all the way down to a horizontal position so they can provide thrust as propellers in fixed wing flight. An impression of this specific tiltrotor is shown in figure 1.

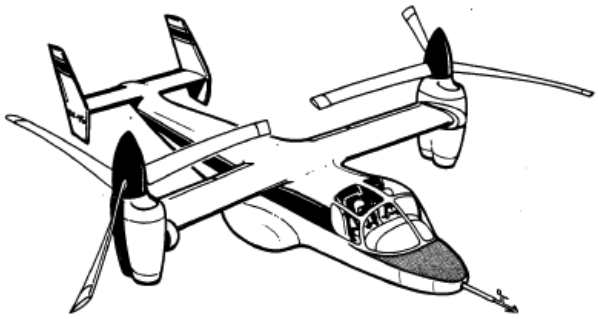

Fig. 1 Impression of the XV-15 tiltrotor. [17]

A three degree of freedom (3-DOF) tiltrotor nonlinear model of the XV-15 was used to evaluate the controller performances. The model was designed and validated previously in the works of [18, 19]. It is primarily based on the architecture and parameters of the XV-15 model as presented by Furgeson in [20]. The rotor dynamics and thrust calculations have been derived from [21]. For a detailed description of the model including parameters and values, the reader is referred to [18, 19].

The nonlinear model can be summarized via the system of differential equations:

$$\dot{\underline{x}} = f(\underline{x}, \underline{u}) \tag{1}$$

The four longitudinal states in $\underline{x}$ are:

$$\underline{x} = \begin{bmatrix} u & w & q & \theta_f \end{bmatrix}^T \tag{2}$$

with u is the linear velocity in the body axis x-axis, w is the linear velocity in the body z-axis, q the rotational rate about the body y-axis and θ_f is the fuselage pitch Euler angle. The model can be manipulated via 4 control inputs in $\underline{u}$:

$$\underline{u} = \begin{bmatrix} \theta_0 & \theta_{1s} & \delta_e & \eta \end{bmatrix}^T \tag{3}$$

Where θ_0 is the collective swashplate angle of the proprotors, θ_{1s} is the longitudinal cyclic swashplate angle and δ_e is the elevator deflection angle. Because this model only describes longitudinal motions, the collective and longitudinal

cyclic inputs to the 2 proprotors is symmetric. This means that both proprotors will receive the same input commands and these can therefore be described by two instead of four inputs. The nacelle angle η ranges from 0 degrees in hover mode to -90 in fixed-wing mode and only one command is used to control both nacelles symmetrically. All four actuators have maximum rate, time-constant and, position limits associated with them.

B. Attitude controller design

The attitude controller is the inner-loop of the control scheme and calculates required actuator positions from a pitch angle reference signal and a thrust reference signal. The attitude controller is designed based on the concept of incremental nonlinear control.

Consider the system in equation (1). Performing a Taylor series expansion around a trimmed operating point ($\underline{x}_0$,$\underline{u}_0$) and neglecting higher order terms, results in:

$$\begin{aligned}\dot{\underline{x}} &\simeq f\left(\underline{x}_0, \underline{u}_0\right) + \left.\frac{\partial f(\underline{x}, \underline{u})}{\partial \underline{x}}\right|_{\substack{x=\underline{x}_0 \\ u=\underline{u}_0}} \left(\underline{x} - \underline{x}_0\right) + \left.\frac{\partial f(\underline{x}, \underline{u})}{\partial \underline{u}}\right|_{\substack{x=\underline{x}_0 \\ u=\underline{u}_u}} \left(\underline{u} - \underline{u}_0\right) \\ &= \dot{\underline{x}}_0 + F\left(\underline{x}_0, \underline{u}_0\right)\left(\underline{x} - \underline{x}_0\right) + G\left(\underline{x}_0, \underline{u}_0\right)\left(\underline{u} - \underline{u}_0\right)\end{aligned} \tag{4}$$

In equation (4), the F refers to a matrix with stability derivatives and G refers to a matrix with the system's control effectiveness .

With small time increments, for example when implemented on a flight controller with a high sampling frequency, equation (4) can be simplified further when the considering the time-scale separation principle [22]. If the input $\underline{u}$ changes significantly faster than the state $\underline{x}$ can progress after one timestep, it can be assumed that $\underline{x} \approx \underline{x}_0$. This means that in equation (4), $\underline{x} - \underline{x}_0 \approx 0$ and thus that $F\left(\underline{x} - \underline{x}_0\right) << G\left(\underline{u} - \underline{u}_0\right)$. This notion gives:

$$\dot{\underline{x}} \simeq \dot{\underline{x}}_0 + G\left(\underline{x}_0, \underline{u}_0\right)\Delta\underline{u} \tag{5}$$

Where $\Delta\underline{u} = \left(\underline{u} - \underline{u}_0\right)$ and indeed only the direct control actions of u affect the state derivative. Assuming that the previous state of $\dot{\underline{x}}_0$ is available through measurements, the incremental control law can now be formulated as:

$$\underline{u} = \underline{u}_0 + \Delta\underline{u} = \underline{u}_0 + \Delta\underline{u} = G^{-1}\left(\underline{x}_0, \underline{u}_0\right)\left(\underline{v} - \dot{\underline{x}}_0\right) \tag{6}$$

The predicted acceleration $\dot{\underline{x}}$ is now denoted by v and considered a virtual control input. Equation (6) is an incremental control law and computes the required increment Δu to achieve the desired acceleration v. An incremental control law like this has the advantage that only the aircraft parameters in G need to be known. The rest of the vehicle dynamics need not to be predicted. On the other hand, because the control inputs are based on increment calculations, the position of the actuators in $\underline{u}$ needs to be known each timestep. Either from modeling or measurements.

In the case of an attitude controller for this tiltrotor application, equation 6 can be implemented to control the pitch axis and thrust of the aircraft.

$$\begin{bmatrix} \theta_0 \\ \theta_{1s} \\ \delta_e \end{bmatrix} = \begin{bmatrix} \theta_0 \\ \theta_{1s} \\ \delta_e \end{bmatrix}_0 + \Delta \begin{bmatrix} \theta_0 \\ \theta_{1s} \\ \delta_e \end{bmatrix} = G_c^{-1} \begin{bmatrix} \Delta T \\ v - \dot{q}_0 \end{bmatrix} = \begin{bmatrix} G_{T,\theta_0} & G_{T,\theta_{1s}} & G_{T,\delta_e} \\ G_{q,\theta_0} & G_{q,\theta_{1s}} & G_{q,\delta_e} \end{bmatrix}^{-1} \begin{bmatrix} \Delta T \\ v - \dot{q}_0 \end{bmatrix} \tag{7}$$

To control the attitude and thrust of the aircraft it was chosen to only employ the swashsplate and elevator controls and disregard the nacelle angle control. The increment in thrust ΔT refers to the required change in proprotor thrust. This value will be calculated by the velocity controller as will demonstrated in the next section. The control effectiveness matrix G_c is populated with the control derivatives from the linearization of the model f. The model has been linearized at trimpoints where the aircraft was in steady horizontal flight at all different flight speeds and nacelle angles throughout the flight envelope.

Figures (2) and (3) show the control derivatives of the pitch rate with respect to longitudinal cyclic, elevator deflection and of the thrust with respect to longitudinal cyclic and collective angle. The results are shown against the conversion corridor in which the aircraft is required stay during a transition to fixed wing flight or conversion back to helicopter mode. In fixed wing flight, the longitudinal cyclic control is phased out and is not available for flight control anymore. Looking at these figures, one can see that in all cases the control derivatives keep the same order of magnitude in the entire flight envelope. In the longitudinal cyclic case, in figure (2), the effectiveness on pitch rate becomes weaker and

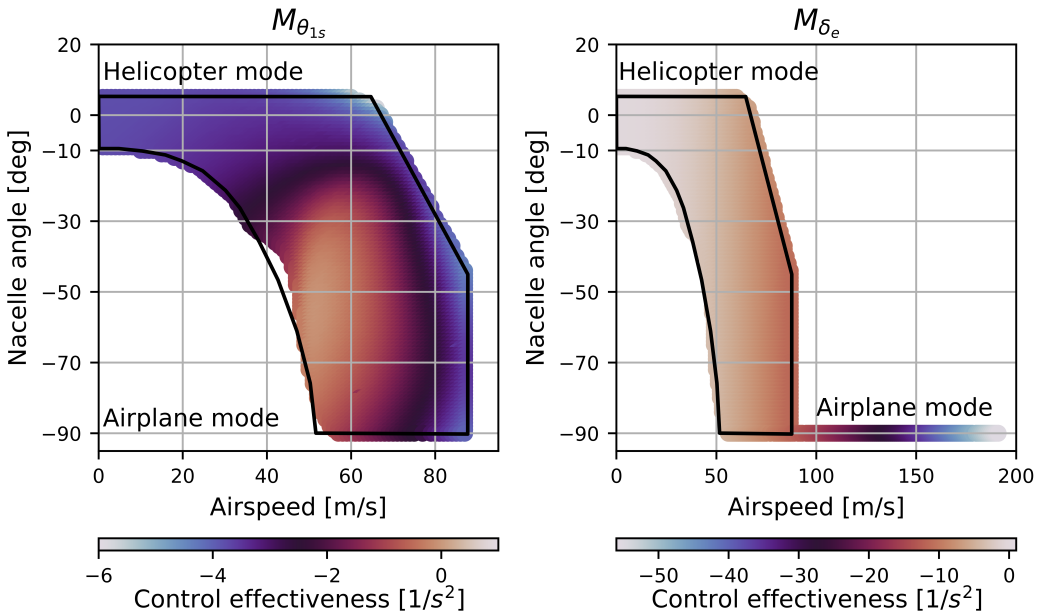

Fig. 2 Control derivatives of pitch rate q with respect to θ_{1s} and δ_e.

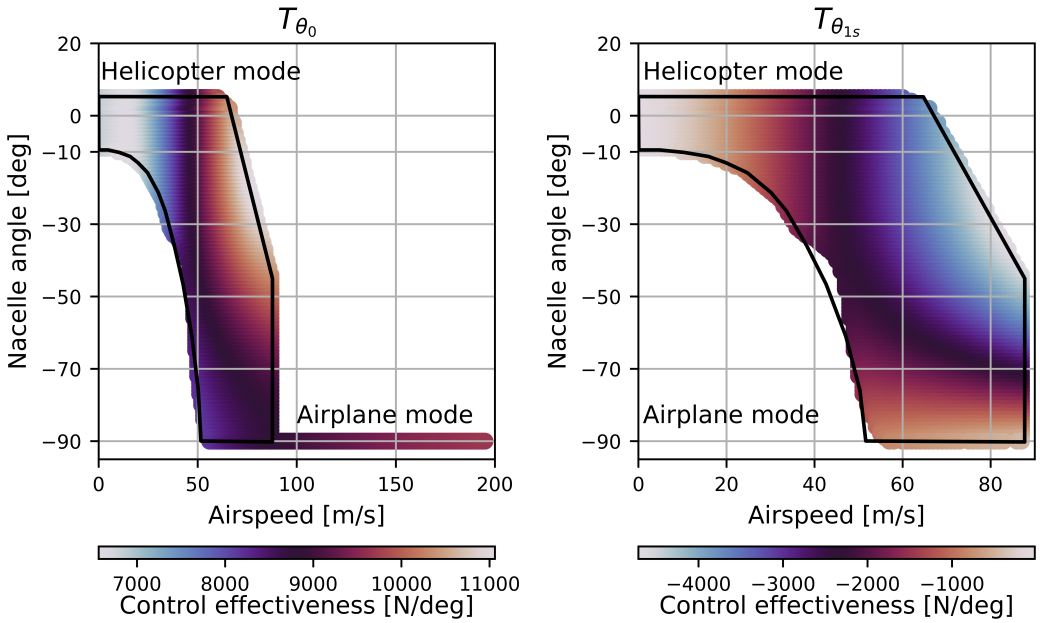

Fig. 3 Control derivatives of thrust T with respect to θ_0 and θ_{1s}.

even close to zero between the nacelle angles -30 and -70 degrees. If the control derivative in reality would cross over and become positive the system could become unstable.

As a base scenario it was chosen to disregard the cross-coupling effects of the collective input to the pitch axis and to disregard the effect of longitudinal cyclic on thrust. This finally leaves G_c as:

$$G_c = \begin{bmatrix} T_{\theta_0} & 0 & 0 \\ 0 & M_{\theta_{1s}} & M_{\delta_e} \end{bmatrix} \tag{8}$$

The entries in G_c are updated every timestep with look-up tables depending on the current flight speed and nacelle angle.

The control effectiveness matrix from equation (8) is a non-square matrix and cannot be inverted as is required in the calculation of equation (7). The over-actuated system is a result of the elevator and cyclic who both have an effect on the pitch dynamics. To solve the control allocation problem, a weighted least squares problem is formulated and solved with an active set method. This method has been introduced to solve aerospace control allocation problems in [23] and was applied to an incremental controller for a quadcopter and tailsitter drone in [24]. The objective function is formulated as:

$$\Delta \underline{u} = \arg \min_{\Delta \underline{u}_{min} \leq \Delta \underline{u} \leq \Delta \underline{u}_{max}} \gamma \left\| W_v (G_c \Delta \underline{u} - \begin{bmatrix} \Delta T \\ \nu - \dot{q}_0 \end{bmatrix}) \right\|^2 + \left\| W_u \left(\Delta \underline{u} - \Delta \underline{u}_p \right) \right\|^2 \tag{9}$$

The goal is to minimize the objective function and its effect is twofold. The first term refers to the error between the requested pitch and thrust effort and provided pitch and thrust effort by the input Δu. The second term concerns the deviation of the control inputs from their preferred values in Δu_p. The factor γ is set to 1000 and ensures that priority is given to solving the control effort in stead of solving for the preferred actuator increment. Furthermore, each term has a weighting matrix associated with it. The weighting matrix W_v can be used to prioritize one axis over another. In this case, since the inputs are decoupled in G_c the matrix W_v is set to I. When the inputs are coupled in G_c, the weighting matrix W_v can be tuned by considering the relative sensitivity of the actuators to one axis versus another axis. In principle, because the controls in G_c are decoupled, the prioritization of control axis is not required and the thrust axis can even be left out of the optimization problem altogether. However, to employ this method in the future with coordinated controls this base case is evaluated first. The second weighting matrix looks like this:

$$W_u = \begin{bmatrix} w_{\theta_0} & 0 & 0 \\ 0 & w_{\theta_{1s}} & 0 \\ 0 & 0 & w_{\delta_e} \end{bmatrix} \tag{10}$$

A higher weight in W_u means that the solver will find a solution for $\Delta \underline{u}$ with the specific actuator input closer to u_p. In this set up, the entries in W_u are : $w_{\theta_0} = 1$,$w_{\theta_{1s}} = 1$, $w_{\delta_e} = 1/5$. The elevator is allowed to deviate more from its preferred state than the cyclic control. The incremental changes Δu_p have been defined as:

$$\Delta \begin{bmatrix} \theta_0 \\ \theta_{1s} \\ \delta_e \end{bmatrix}_p = \begin{bmatrix} \theta_{0,min} - \theta_{0,0} \\ -1 \cdot \theta_{1s,0} \\ -1 \cdot \delta_{e,0} \end{bmatrix} \tag{11}$$

This means that for the elevator and cyclic control the preferred increment is in the direction to a neutral deflection and for the collective input the preferred increment is in the direction to minimize its deflection. The objective function is finally solved under the constraints of the increment space that is available ($\Delta \underline{u}_{min}$ and $\Delta \underline{u}_{max}$).

Incremental control is based on acceleration information. In this case, the pitch acceleration is required to solve equation (7). Ordinarily, pitch acceleration is not measurable and must be derived from gyroscope rate measurements. These are generally noisy. A second order low-pass filter is employed to suppress measurement noise so that an accurate acceleration estimation can be made. The dynamics of the filter are shown in equation (12) and the filter parameters are set to a cut-off of $5Hz$ with $\omega_n = 25$ and $\zeta = 0.55$.

$$H_s(s) = \frac{\omega_n^2}{s^2 + 2\zeta\omega_n s + \omega_n^2} \tag{12}$$

The lag on the estimated signal can influence the performance of the controller severely [25]. The phase lag imposed on the estimated signal for $\dot{q}$ and $\dot{q}$ must therefore be synchronized by a synchronization filter on the actuator position signals.

$$u_f = H_s \cdot u_0 \tag{13}$$

$$q_f = H_s \cdot q_s \tag{14}$$

The control law of equation (7) can now be rewritten to:

$$\underline{u} = \underline{u}_f + \Delta\underline{u} = G_c^{-1} \begin{bmatrix} \Delta T \\ v - \dot{q}_f \end{bmatrix} \tag{15}$$

The control signals v and subsequently q_{ref} are calculated via :

$$v = K_1(q_{ref} - q_f) \tag{16}$$

$$q_{ref} = K_2(\theta_{ref} - \theta) \tag{17}$$

C. Velocity controller design

The velocity controller is the outer loop and will calculate the required pitch angle, thrust and nacelle angle based on velocity or positional input in the inertial North-East-Down (NED) frame. The controller is also based on incremental logic. Instead of considering the state $\underline{x}$, the control laws will be derived based on Newton's second law of motion. The changes in pitch angle, thrust and nacelle angle will be calculated to achieve a desired linear acceleration. The vector $\underline{\chi} = [\chi_x, \chi_y, \chi_z]$ describes the position of the aircraft in the NED frame and the inputs are $u = [\theta_f, T, \eta]$. The motion of the aircraft can be described by:

$$\ddot{\underline{\chi}} = \underline{f}(\underline{\chi}, \underline{u}) = \underline{g} + \frac{1}{m}\underline{L}(\dot{\underline{\chi}}, \underline{u}) + \frac{1}{m}\underline{T}(\dot{\underline{\chi}}, \underline{u}) + \frac{1}{m}\underline{D}(\dot{\underline{\chi}}, \underline{u}) + \frac{1}{m}\underline{H}(\dot{\underline{\chi}}, \underline{u}) \tag{18}$$

To derive the control law, the Taylor series expansion is performed on equation (18) and similar to the attitude controller, the assumption of time scale separation has been applied. This results in

$$\ddot{\underline{\chi}} = \ddot{\underline{\chi}}_0 + \frac{1}{m}G_v(\underline{x}, \underline{u})(\underline{u} - \underline{u}_0) \tag{19}$$

The G_v matrix is an effectiveness matrix that relates increments in $\underline{u}$ with the inertial linear accelerations $\ddot{\underline{\chi}}$. In the case of equation (18), there are four forces to be considered. Thrust, lift, drag and H-force. In this derivation of the velocity control law, only the thrust and lift force will be considered further to derive the INDI control law. This decision is made on the basis that the H-force is relatively small and difficult to model and the drag force is also relatively small compared to the lift force.

Note that the forces that are not included in the control law derivation are not disregarded. The effects of these forces are still measured by the acceleration feedback signals and will be dealt with accordingly as long as the effectiveness of G_v permits (in magnitude and direction). The only decision that has been made at this point is that only the lift and thrust force will be used to actively steer the aircraft.

The entries in G_v concern the lift force and the thrust force. For the derivation of the lift force derivatives, it is assumed that the flight path angle is small and that the angle of attack is equal to the pitch angle. The lift force is modelled as:

$$L = \frac{1}{2}\rho V_\infty^2 S C_{l_\alpha}(\alpha - \alpha_0) \tag{20}$$

In this equation, the lift force is expressed in the aerodynamic frame. The thrust force is modelled as:

$$T = gm\left(1.2 + \frac{1}{10}\left(\frac{8}{90}\eta - 2\right)\right) \tag{21}$$

This is a simple linear approximation of the thrust force as a function of nacelle angle. It has been derived by evaluating the following two cases. In helicopter mode, the nacelles are upright at 0 degrees. This means that the proprotors must provide approximately 100% of the aircraft's weight in thrust. In fixed-wing mode, the nacelles have rotated to -90 degrees so that the thrust is approximately equal to the drag of the aircraft. Estimating that in this configuration the drag of the aircraft will be approximately 20% of the weight, the thrust will be that as well.

is equal to the weight when the aircraft is in helicopter mode and about 20% of the weight when the aircraft is in fixed wing mode. The direction of the thrust force is assumed to be in line with the nacelle angle.

Both forces are transformed to the inertial NED frame and their derivatives with respect to $\underline{u}$ are calculated. This results in:

$$G_v = \begin{bmatrix} -Tc(\theta_f+\eta) + K_l(-\theta_f+\alpha_0) & -Tc(\theta_f+\eta) & -s(\theta_f+\eta) \\ Ts(\theta_f+\eta) - K_l & Ts(\theta_f+\eta) & -c(\theta_f+\eta) \end{bmatrix} \tag{22}$$

Where $K_l = \frac{1}{2}\rho V_\infty^2 S C_{l_\alpha}$.

By rearranging the terms in equation (19) the incremental control law can be formulated.

$$\begin{bmatrix} \theta_f \\ \eta \\ \Delta T \end{bmatrix}_{ref} = mG_v^{-1}\left(\begin{bmatrix} \ddot{\chi}_x \\ \ddot{\chi}_z \end{bmatrix}_{ref} - \begin{bmatrix} \ddot{\chi}_x \\ \ddot{\chi}_z \end{bmatrix}_f\right) + \begin{bmatrix} \theta_f \\ \eta \\ 0 \end{bmatrix}_f \tag{23}$$

Where sine and cosine function have been abbreviated by $s()$ and $c()$.

Similarly to the attitude controller, the linear acceleration measurements are noisy and are therefor filtered. The controller is synchronized by also filtering the previous actuator states $\underline{u}$. The matrix G_v is non-square and can again not be inverted. For this control allocation problem again the WLS solver is used. The objective function of equation (9) remains the same in its form. The weighting matrix $W_v = I$ and the matrix W_u is set to $I \cdot [10, 1, 1]$ such that the pitch attitude is minimized. The problem is constraint by the minimum and maximum increment limits of $\underline{u}$ and the preferred increments $\underline{u}_p$ are:

$$\Delta \begin{bmatrix} \theta_f \\ T \\ \eta \end{bmatrix}_p = \begin{bmatrix} -1 \cdot \theta_f \\ T_{min} \\ \eta_{min}/\eta_{max} \end{bmatrix} \tag{24}$$

The preferred thrust increment is the minimum allowable thrust decrease, as an attempt to fly the aircraft more efficiently. The preferred increment in fuselage pitch angle directs the attitude to a nose level attitude. The preferred nacelle angle increment is set to the maximum or minimum allowable nacelle angle set point depending on if the goal is to transition to fixed wing flight or the convert back to helicopter mode.

Finally, the acceleration reference signal $\ddot{\chi}$ is calculated via a cascaded p-loop structure.

$$\ddot{\chi}_{ref} = K_3(\dot{\chi}_{ref} - \dot{\chi}_f) \tag{25}$$

$$\dot{\chi}_{ref} = K_4(\chi_{ref} - \chi) \tag{26}$$

The reference signals are also constraint by minimum and maximum limits because the large differences in distances and velocities encountered would otherwise require gain scheduling.

The model and controllers have been implemented in the `Simulink/Matlab` simulation environment.

III. Results

First, the attitude controller will be evaluated. It has been tuned in helicopter mode and tested on multiple points in the flight envelope. The points are summarized in table 1. These points were chosen to give an impression on the performance in helicopter mode, during the transition at intermediate nacelle angles and during cruise in fixed wing mode. Note that the nacelles are in helicopter mode pointing upwards when $\eta = 0$ degrees and are pointing forwards in fixed wing mode when $\eta = -90$ degrees.

Figure 4 shows the response to a pitch doublet command at the evaluation points from table 1. The responses have been corrected with the the fuselage pitch angle at the trimpoint so they all start off from zero degrees. The responses for P1, P2, and P4 are similar and are all able to track the command. The response in fixed wing mode, P4 shows some overshoot. This may be explained by the fact that at that in fixed wing flight, the pitch is only controlled by the elevator. The performance of INDI is in general very sensitive to actuator dynamics so if these change, the original gains of K_1 and K_2 are perhaps not be optimal anymore. And this is the case here, the elevator moves faster than the cyclic. If the actuator can move faster, the attitude controller could be tuned more stiff. The overshoot can also be explained by a model mismatch where the control effectiveness in G_c has been overestimated compared to the actual "real world" control effectiveness. In figure 5, the actuator commands are presented and it shows that for P4 the commands are not clipped when the response overshoots. Note that the cyclic limits for all cases changes because the cyclic control is phased out with decreasing nacelle angle. The longitudinal cyclic is not available in fixed wing flight.

Table 1 Attitude controller evaluation points

ID	Flight speed m/s	Nacelle angle deg
P1	0	0
P2	40	-10
P3	60	-60
P4	150	-90

P3 is the only response that cannot track the commanded signal, as it does not reach the upper step input. Looking at the actuator commands in figure 5 reveals that for P3 both the elevator and cyclic controls are clipped during the tracking deviation. This indicates that the controller does try to resolve the error but the deviation originates from inherent aircraft limitations. This result is also in line with the results from the linearization process in figure 2 where the cyclic effectiveness in this region of the flight envelope is relatively weak and the elevator control is also still marginally effective.

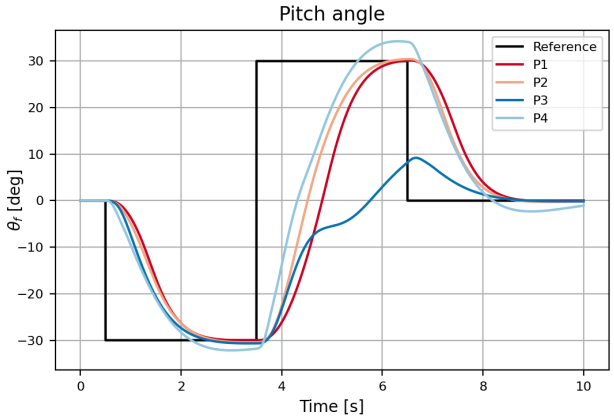

Fig. 4 Pitch attitude response to doublet maneuver at evaluation points P1,P2,P3, and P4.

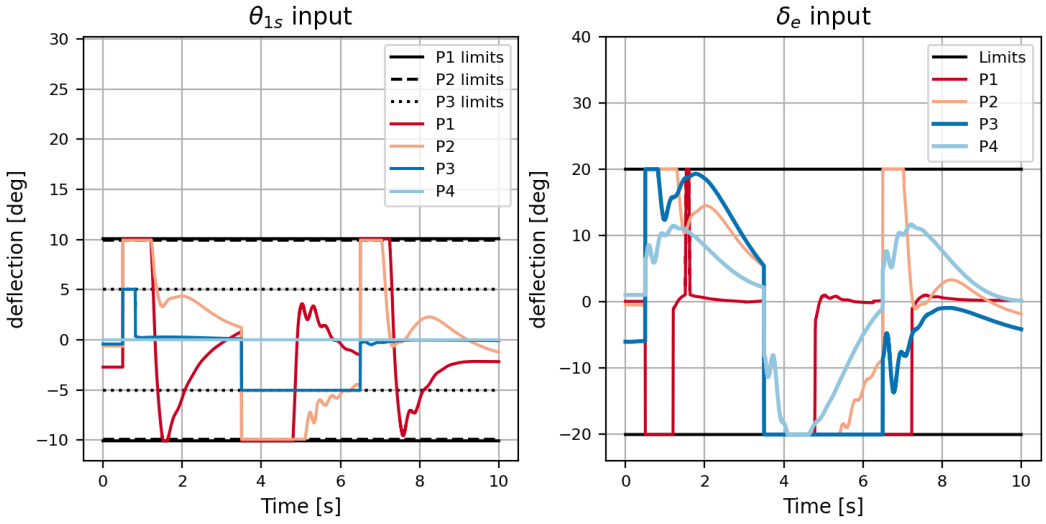

Fig. 5 Actuator control commands after pitch doublet maneuver at evaluation points P1,P2,P3, and P4.

Next the velocity controller is evaluated. To demonstrate the performance of the velocity controller, a speed profile

is tracked in which the aircraft transitions from helicopter mode to fixed wing mode and converts back to a helicopter.

The speed profile is shown in figure 6 together with the vehicle response in horizontal and vertical direction. The aircraft is able to track the horizontal speed profile. In the tuning process the maximum and minimum horizontal acceleration limits on the reference signal ($\ddot{\chi}$) were set to -3 and 3 m/s^2. These limits are clearly visible in the response of the aircraft. In the tuning process these limits were found to be important to keep the system stable. If the limits are increased, the system becomes unstable.

The vertical velocity tracking appears noisy but the order of magnitude and overall direction is the same. This can also be concluded from the altitude data. During the maneuver, the maximum deviation from the starting altitude is 6 meters and the maximum altitude loss is 2 meters.

In figure 7, the outputs of the velocity controller are shown. The aircraft can track the commanded pitch angle closely. Also when flying through the region of weaker control effectiveness as shown in figure 2 and where the attitude tracking task showed poor results, the aircraft can still follow the commanded signal.

In figure 8 the flight is graphed versus the conversion corridor. The velocity controller is able to remain within the limits of the corridor during the transition to fixed wing mode and also reversing back to helicopter mode.

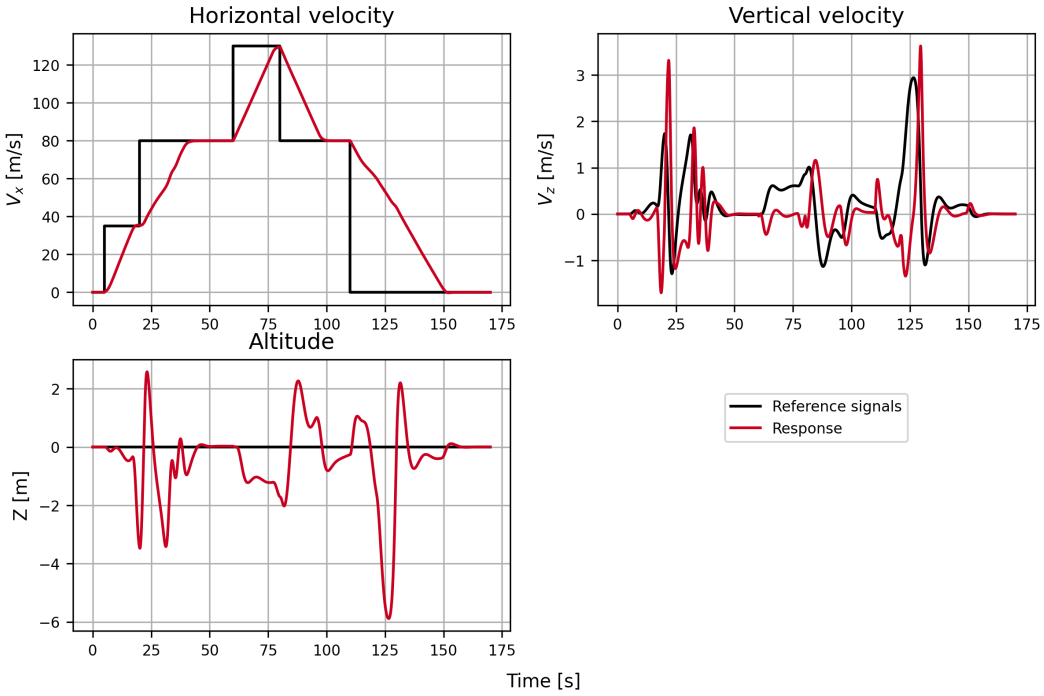

Fig. 6 Speed profile and the response of the aircraft.

IV. Conclusions & Recommendations for future work

The goal of this paper was to present how incremental nonlinear control can be applied to the tiltrotor aircraft. An attitude controller was developed including a control allocation solver as well as a cascaded incremental velocity controller.

The attitude controller was evaluated at four points in the flight envelope with a doublet maneuver. In the middle of the conversion corridor, the doublet maneuver revealed that the longitudinal cyclic and elevator controls were not effective enough to follow the tracking task. In this light it would be interesting to investigate how the control effectiveness of the collective control behaves and if using the WLS algorithm, the collective actuator could be used to coordinate joint control effort in regions where the cyclic and elevator are relatively weak.

The global incremental velocity controller that was presented integrates the use of the nacelle attitude to coordinate control effort to track of linear accelerations. The controller showed to be able to follow a horizontal speed profile from hover to cruising speed in fixed wing mode. During the maneuver the control actuators were saturated only rarely. The

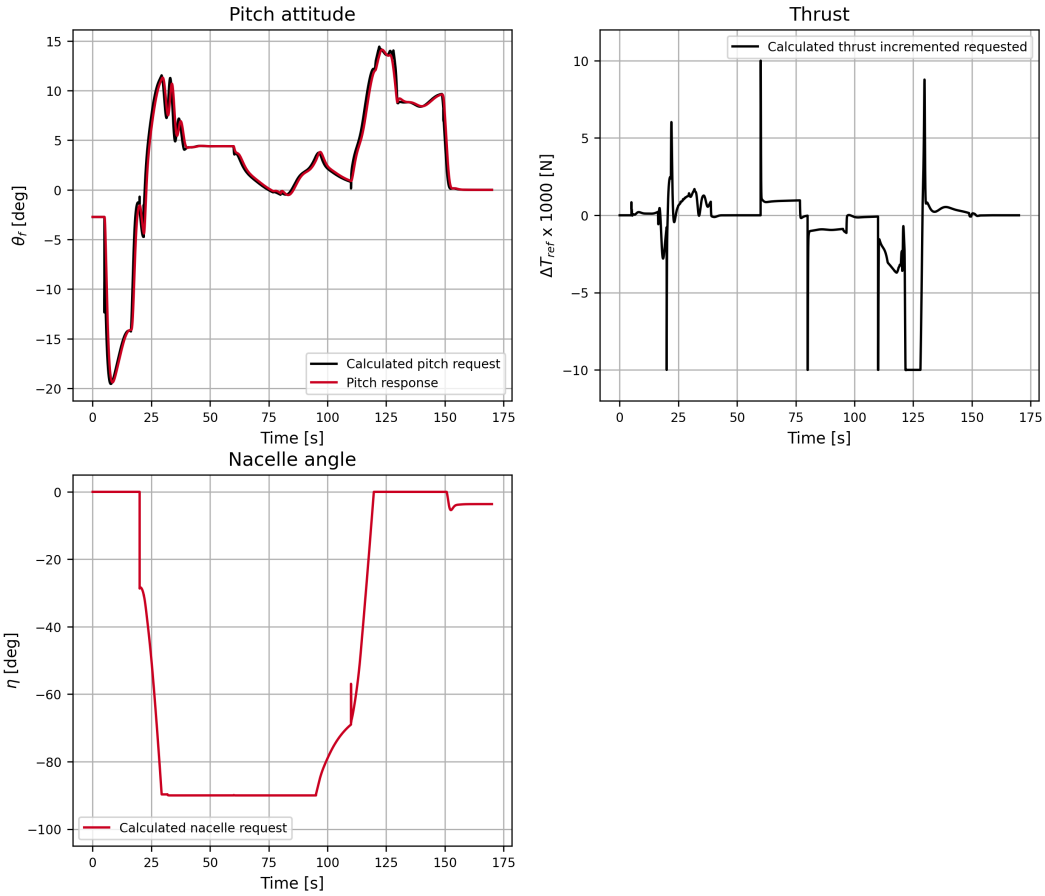

Fig. 7 Calculated command inputs of the velocity controller.

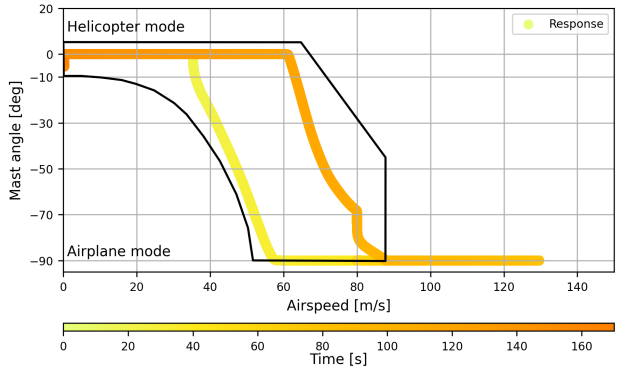

Fig. 8 Flight profile of the tracking maneuver against the conversion corridor.

maximum altitude deviation was 6 meters. During the tuning process it was noticed that the accelerations reference signal $\ddot{\chi}_{ref}$ must be limited in order for the system to remain stable. This limits the agility of the aircraft and may be undesirable. For future work it is recommended to investigate how the G_v matrix could be populated with more accurate information on the lift and thrust force derivatives by modeling these forces more accurately, especially the thrust force for which a relatively simple approximation has been used. Additionally, it would be interesting to investigate which other forces contribute significantly to the aircraft's linear dynamics and to investigate how to include these in G_v in a simple way. The method that has been developed and implemented in this work should be easily extendable to also

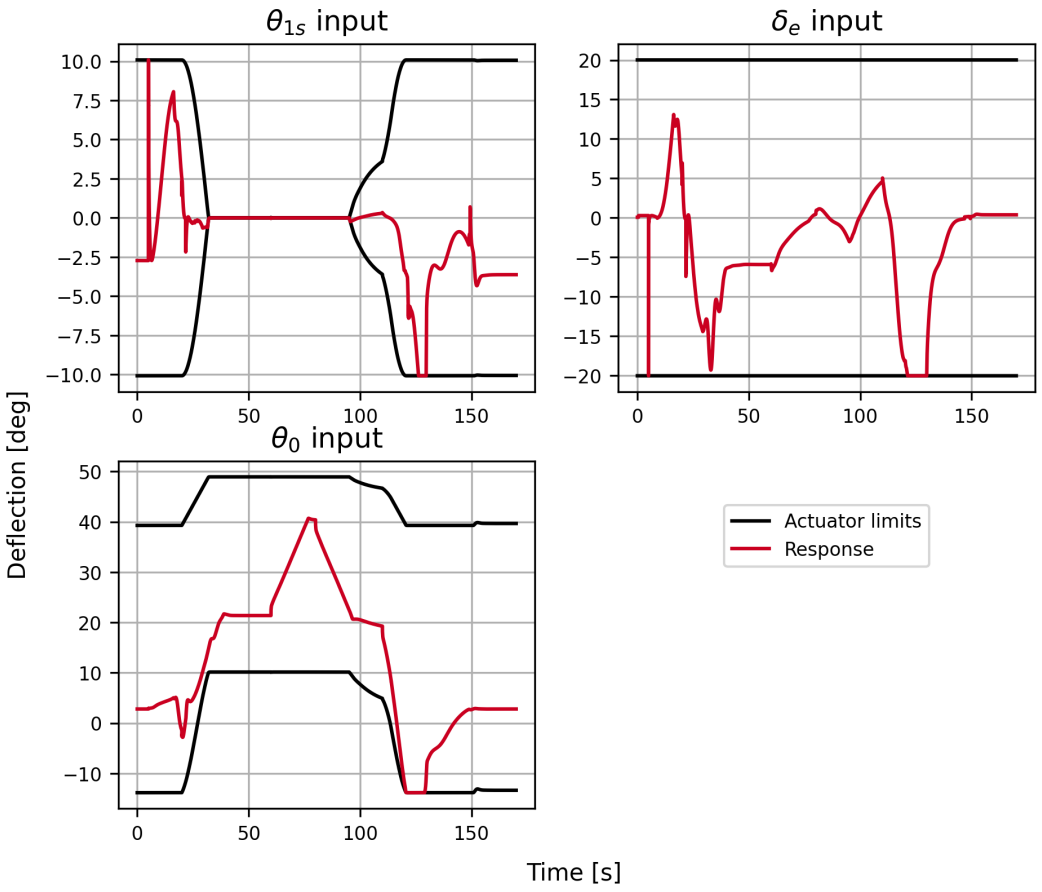

Fig. 9 Actuator inputs calculated by the attitude controller

include the lateral dynamics of the tiltrotor aircraft. It is recommended that in future work these motions will also be considered.

References

[1] Chung, W. W., Linse, D., Paris, A., Salvano, D., Trept, T., Wood, T., Gao, H., Miller, D., Wright, K., Young, R., and Cheng, V., "Modeling High-Speed Civil Tiltrotor Transports in the Next Generation Airspace," Tech. Rep. October, NASA Ames Research Center, Moutain View, 2011.

[2] US, "Addressing the future challenges of the operation of power lift category/tiltrotor class aircraft in international air navigation, ICAO AE35-WP," , 2004.

[3] Maisel, M., Giulianetti, D. J., and Dugan, D. C., *The History of the XV-15 Tilt Rotor Research Aircraft from Concept to Flight*, NASA, Washington D.C., 2000. URL https://www.researchgate.net/publication/24295050.

[4] Perfect, P., "Optimising Handling Qualities For Tilt Rotor Aircraft," Ph.D. thesis, University of Liverpool, Liverpool, 7 2009.

[5] Goldstein, K. W., and Dooley, L. W., "V-22 Control Law Development," *42nd Annual Forum of the American Helicopter Society*, Washington D.C., 1986, pp. 673–684.

[6] Slotine, J.-J. E., and Li, W., *Applied nonlinear control*, Prentice Hall, 1991.

[7] Smith, P. R., and Patel, Y., "Translational motion control of VSTOL aircraft using nonlinear dynamic inversion," *20th Atmospheric Flight Mechanics Conference*, American Institute of Aeronautics and Astronautics Inc, AIAA, 1995, pp. 238–252. https://doi.org/10.2514/6.1995-3452.

[8] Bacon, B. J., and Ostroff, A. J., "Reconfigurable flight control using nonlinear dynamic inversion with a special accelerometer implementation," *AIAA Guidance, Navigation, and Control Conference and Exhibit*, , No. August, 2000. https://doi.org/10.2514/6.2000-4565.

[9] Bacon, B. J., Ostroff, A. J., and Joshi, S. M., "Reconfigurable NDI controller using inertial sensor failure detection & isolation," *IEEE Transactions on Aerospace and Electronic Systems*, Vol. 37, No. 4, 2001, pp. 1373–1383. https://doi.org/10.1109/7.976972.

[10] Sieberling, S., Chu, Q. P., and Mulder, J. A., "Robust flight control using incremental nonlinear dynamic inversion and angular acceleration prediction," *Journal of Guidance, Control, and Dynamics*, Vol. 33, No. 6, 2010, pp. 1732–1742. https://doi.org/10.2514/1.49978.

[11] Acquatella, B. P., Falkena, W., van Kampen, E. J., and Chu, Q. P., "Robust nonlinear spacecraft attitude control using incremental nonlinear dynamic inversion," *AIAA Guidance, Navigation, and Control Conference 2012*, , No. August, 2012. https://doi.org/10.2514/6.2012-4623.

[12] Smeur, E. J., De Croon, G. C., and Chu, Q. P., "Cascaded incremental nonlinear dynamic inversion for MAV disturbance rejection," *Control Engineering Practice*, Vol. 73, No. July 2017, 2018, pp. 79–90. https://doi.org/10.1016/j.conengprac.2018.01.003, URL https://doi.org/10.1016/j.conengprac.2018.01.003.

[13] Howitt, J., "Application of Non-linear Dynamic Inversion to Rotorcraft Flight Control," *American Helicopter Society 61st Annual Forum*, AHS, Grapevine, 2005.

[14] Simplício, P., Pavel, M. D., van Kampen, E. J., and Chu, Q. P., "An acceleration measurements-based approach for helicopter nonlinear flight control using incremental nonlinear dynamic inversion," *Control Engineering Practice*, Vol. 21, No. 8, 2013, pp. 1065–1077. https://doi.org/10.1016/j.conengprac.2013.03.009.

[15] Pavel, M. D., Shanthakumaran, P., Chu, Q. P., Stroosma, O., Wolfe, M., and Cazemier, H., "Incremental nonlinear dynamic inversion for the apache AH-64 helicopter control," *Journal of the American Helicopter Society*, Vol. 65, No. 2, 2020, pp. 1–16. https://doi.org/10.4050/JAHS.65.022006.

[16] Berger, T., "Handling Qualities Requirements and Control Design for High-Speed Rotorcraft," Ph.D. thesis, Pennsylvania State University, 2019. URL https://etda.libraries.psu.edu/catalog/17211tub246.

[17] Maisel, M., "Tilt rotor research aircraft familiarization document," Tech. rep., NASA Aimes Research Center, Moutain View, 1975.

[18] Sokolowski, P., "Liturature study: Flight Dynamics Modelling of a Tiltrotor Aircraft," , 2020.

[19] Steinbusch, G., "A Theoretical Approach for Analysing the Stability Characteristics of Tiltrotor Aircraft," Tech. rep., TU Delft, Delft, 2022.

[20] Ferguson, S. W., "A Mathermatical Model for Real Time Flight Simulation of a Generic Tilt-Rotor Aircraft," Tech. rep., NASA Ames Research Center, Moutain View, 1988.

[21] van Holten, T., Melkert, J., Marrant, B., and Pavel, M. D., *Helicopter Performance, Stability, and Control (AE4314 Diktaat)*, November, TU Delft, Delft, 2002.

[22] Saksena, V., O'Reilly, J., and Kokotovic, P., "Singular Perturbations and Time-scale Methods in Control Theory : Survey 1976-1983 "," *Automatica*, Vol. 20, No. 3, 1984, pp. 273–293.

[23] Härkegård, O., "Efficient active set algorithms for solving constrained least squares problems in aircraft control allocation," *Proceedings of the IEEE Conference on Decision and Control*, Vol. 2, No. December, 2002, pp. 1295–1300. https://doi.org/10.1109/cdc.2002.1184694.

[24] Smeur, E. J., "Incremental Control of Hybrid Micro Air Vehicles," Ph.D. thesis, TU Delft, 2018. https://doi.org/10.4233/uuid:23c338a1-8b34-40a6-89e9-997adbdafd75.

[25] Smeur, E. J., Chu, Q. P., and De Croon, G. C., "Adaptive incremental nonlinear dynamic inversion for attitude control of micro air vehicles," *Journal of Guidance, Control, and Dynamics*, Vol. 39, No. 3, 2016, pp. 450–461. https://doi.org/10.2514/1.G001490.

Part II

Literature Study

2

Tiltrotor fundamentals

In this chapter the defining properties of the tiltrotor aircraft configuration are discussed. First, the purpose and mission characteristics of the tiltrotor configuration is discussed. Second, the flight mechanical capabilities with special attention to the transition maneuver. Third, the control mechanism are discussed and pilot control strategies. Lastly the general dynamics of the aircraft are briefly mentioned.

2.1. Purpose and mission characteristics

Tiltrotor aircraft combine the benefits from turboprop aircraft and helicopters by merging the ability to take-off and land vertically (VTOL) with the performance that fixed wing turboprop aircraft have on endurance, range and speed. Although the tiltrotor concept was already introduced in the early stages of aviation history (see for example the tiltrotor patent filed by Blount [10] in 1933), the number of actual developed manned tiltrotor aircraft has been limited. The first full scale tiltrotor aircraft was built by the Transcendental Aircraft Company and achieved a forward speed of 100 kts in helicopter mode and a rotor tilt angle of 35 degrees [11]. Later, the XV-3 tiltrotor was developed as part of a research program contracted by the US Air Force. The XV-3 was the first tiltrotor that was able to demonstrate a full conversion maneuver. During flight testing the specific aircraft configuration revealed critical aeroelastic and aircraft stability problems that had to be solved before the tiltrotor could be designed to reach its full potential.

Another major stepping stone in the development of tilrotor aircraft was the XV-15 research aircraft, and was a joint collaboration between NASA, the US Army and the Bell Helicopter Company [1]. Following its predecessor the XV-3, the XV-15 was conceived as a proof-of-concept vehicle and a V/STOL research tool for integrated windtunnel, flight-simulation, and flight-test investigations[7].

Nowadays the only manned tiltrotor in production is the Bell Boeing V-22 Osprey [2] which is only operated by the U.S and Japanese military. The full scale development of the V-22 started in the 1980's and found most of its technical basis in the research program of the XV-15. Next to that the V-22 Osprey was also the first ever all-composite rotorcraft and was fitted with sophisticated fly-by-wire controls as opposed to the mechanical control system of the XV-15 [12]. Current developments however, will soon enable civilian use of tiltrotor aircraft, with the Augusta Westland 609 [13], that could leverage its operational flexibility to solve problems such as airport and airspace congestion [14][15].

Tiltrotor aircraft share several distinctive features that enable them to operate in the hover, horizontal cruise and conversion flight regime. In figure 2.2 a schematic overview of the Bell Boeing V-22 Osprey is shown in which the important physical attributes of the configuration are visible. As can be seen from the figure, tiltrotor aircraft do share features similar to ordinary fixed wing aircraft such as the main wing and the empennage. With the difference that at each wingtip an engine nacelle is mounted that also facilitates as the suspension point for the gimballed rotors. Each nacelle can swivel around the wingspan axis approximately 90 degrees from a vertical to a horizontal attitude and back. This tilting ability enables the tiltrotor to use its rotors to serve a dual purpose in different phases of flight. In the cruise phase, the nacelles and rotors are oriented horizontally in the direction of flight serving as a source of thrust. While in the hover phase, the nacelles and rotors are pointed upwards to generate lift. When transitioning from hover to fixed wing flight, the aircraft converts its configuration and changes the nacelle angle from a vertical to a horizontal

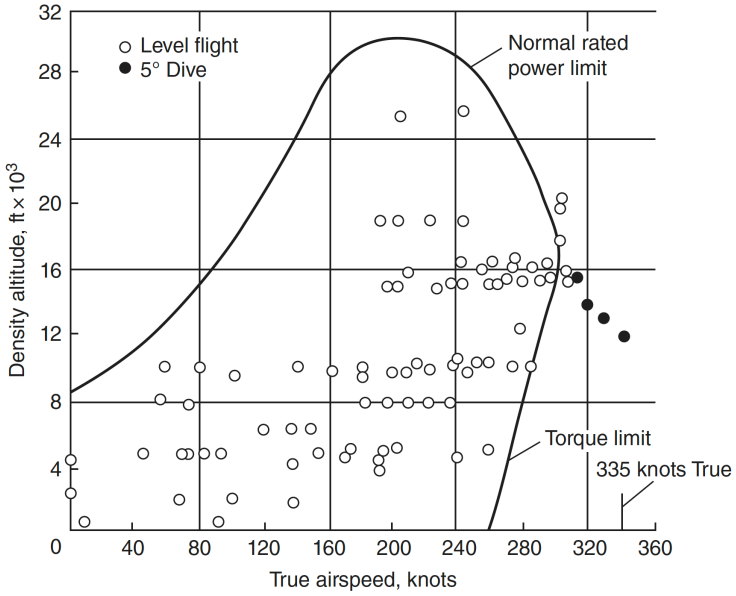

Figure 2.1: XV-15 height-velocity flight envelope [1]

orientation. This maneuver also involves accelerating forward and gaining airspeed such that at the end the wings generate enough lift to remain airborne.

The wide flight envelope of the tiltrotor can be illustrated in a height-velocity diagram as shown in figure 2.1. The figure shows the height-velocity combinations at which the XV-15 tiltrotor aircraft can sustain trimmed level flight and illustrates the true potential for tiltrotor aircraft.

2.2. Conversion corridor

The transition from hover to forward flight is performed by flying through the conversion corridor. This effectively means tilting the nacelles forward and accelerating. The standard conversion maneuver is completed successfully when the aircraft has reached its fixed wing trimmed state without altitude loss [16]. The corridor is set of airspeed and nacelle angle combinations that allow for a transition. The lower limit on the nacelle angle is defined by wing-loading limits whereas the upper limit is determined by the torque limit and structural limits (namely rotor/hub endurance limits). For the XV-15, the maximum conversion velocity V_t has been defined by aeroelastic effects when the nacelles are not in their locked in 0 degree fixed wing position[4]. Exceeding the upper bound of the conversion corridor can cause structural damage caused by unsteady rotor loads [17]. Figure 2.4 shows the conversion corridor of the XV-15. The figure also shows a maximum nacelle angle of 95 degrees which is 5 degrees back from the hover attitude of 0 degrees. This extra degree of freedom allows for faster backwards flight.

The normal nacelle tilt rate for the XV-15 is 7.5 degrees/second, which allows for a full conversion from 90 to 0 degrees in 12 seconds. A second slower tilt rate can be selected by the pilot of 1.5 degrees/second. It is also possible to stop the tilting motion at an arbitrary nacelle angle within the conversion envelope and remain in steady flight [1].

2.3. Control mechanisms

To fly throughout the various flight regimes provided by the tiltrotor configuration, the flight control system combines both rotor and fixed surface controls. The rotor system is a three-bladed prop-rotor with a stiff in-plane gimbal mounting to the hub and the tip-path-plane orientation is controlled through standard cyclic and collective feathering of the individual blades to create controlling forces and moments. In contrast to conventional articulated rotors, the resulting hub moments in the gimbal rotor cause the entire rotor system to rotate or flap as a unit rather than each blade independently [4].

Additionally, aerodynamic surfaces such as the elevator, rudder and ailerons/flaperons may be found to

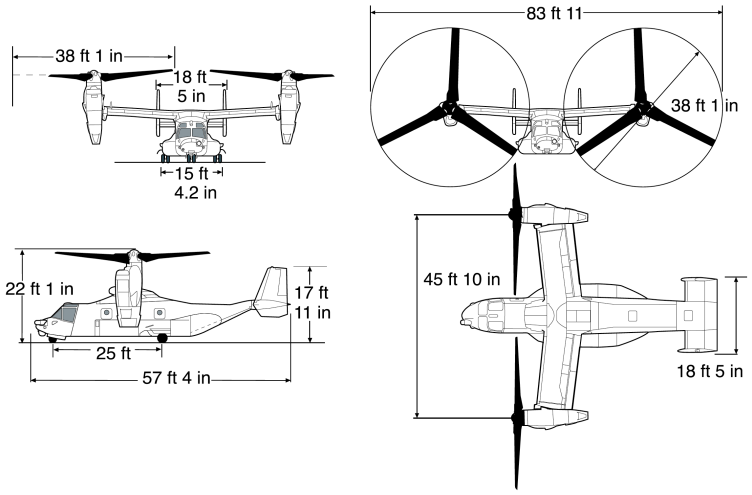

Figure 2.2: Schematic overview of the Bell-Boeing V-22 Osprey [2]

control the aircraft in fixed wing flight. During hover, when the nacelles are oriented vertically, pitch control is provided by applying longitudinal cyclic symmetrically to both rotors. Roll control is generated by applying differential thrust (i.e. change in collective pitch) between the two rotors. The horizontal orientation of the aircraft is controlled by applying asymmetrical (differential) cyclic to the two rotors [18]. The V-22 and later tiltrotor aircraft also feature a complementary hover control mode which allows for generating side force and move laterally across the ground without rolling the aircraft excessively [3]. This lateral side-force is generated by applying lateral cyclic symmetrically to both rotors. The heaving motion in hover is generated by applying collective pitch to both rotors symmetrically.

During flight in fixed wing configuration, with the nacelles horizontal, the pitch attitude of the aircraft is controlled by applying elevator deflections quite similar to conventional aircraft. Likewise the ailerons/flaperons and rudder control the lateral orientation of the aircraft. Figure 2.3 gives an overview of the different control mechanisms.

For the XV-15, throughout the entire transition process within the corridor, the control power was designed to be equal, or to be greater than recommended in [19] about all axes [7]. Nevertheless, the rotor controls are phased out during the conversion as a function of nacelle angle.

2.4. Pilot controls

Before the Bell-Boeing V-22 Osprey, the earlier XV-15 was equipped with a mechanical flight control system. The cockpit layout is similar to that of a helicopter featuring a center control stick for pitch and roll, rudder paddles for yaw. Power changes are made with the power lever which is located in the same location as the helicopter collective stick. Tilt-control itself is facilitated in the cockpit to the pilot via a three-position switch on each power lever control [7].

Following the pilot interface the control inputs are then send to the actuators via a system of mechanical linkages and mixing boxes which takes care of control phasing and mixing throughout the flight envelope. The controls are supplemented by a force feel system FFS and a stability and control augmentation system (SCAS) to provide for better handling qualities [18]. The basic design philosophy was to provide level 1 handling qualities in airplane mode with SCAS off and FFS on. In hover, level 1 handling qualities should be achieved with both SCAS and FFS active. The SCAS is implemented in series with the pilot's control motion and is scheduled by nacelle angle to provide the desired response characteristics throughout the flight envelope. The SCAS also provide attitude retention in the pitch and roll axis to reduce pilot workload in stead flight. The pilot is furthermore assisted by a RPM governor to manage the RPM of the rotors.

In contrast, the V-22 was one of the earliest aircraft equipped with a fully (triple) redundant Fly-by-wire system and featured the Advanced Digital/Optical control system ADOCS control law architecture [3]. The Fly-by-wire system featured stability augmentation to assist the pilot by maintaining at least level 2 handling qualities. Next to that the Automatic Flight Control system featured four extra modes to alleviate pilot workload. These modes include Altitude Hold, Airspeed Hold, Hover Trim and Hover Hold.

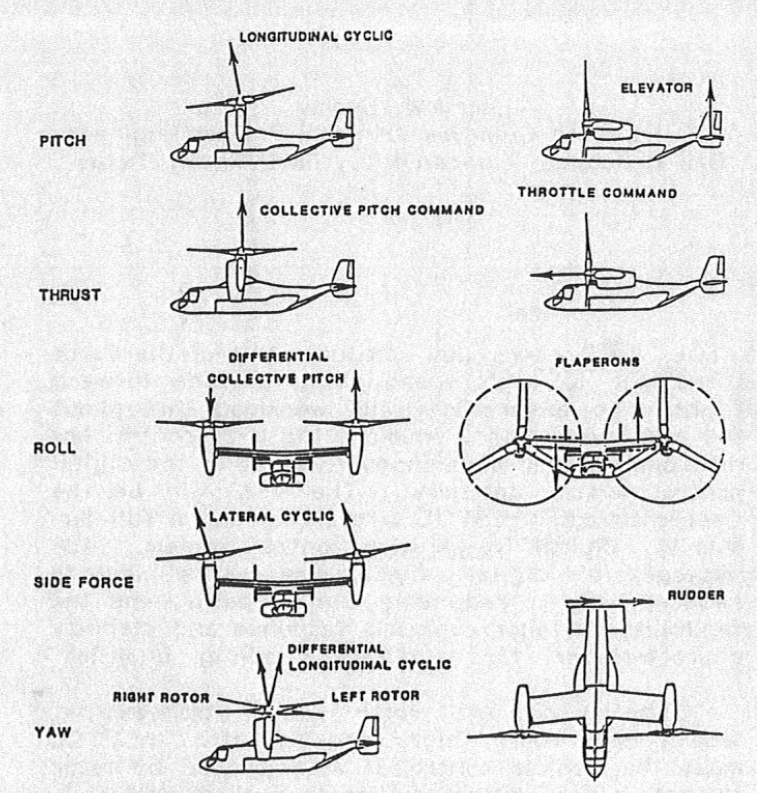

Figure 2.3: Control mechanisms of the Bell-Boeing V-22 Osprey [3]

The control law architecture from the ADOCS system is based on the linear control concept of explicit model following [20]. The benefit of this control method is that the dynamics apparent to the pilot can be very precisely chosen such that they in fact completely resemble the handling qualities specifications. The downside of this method is that it is a linear control method and that it requires extensive gain scheduling. Moreover, with this method the plant dynamics also need to be known to a very precise extent [21].

For the earlier XV-15, the amount of control input to the rotors and aerodynamic surfaces was managed by the flight control system to give minimum pilot efforts in all modes of flight and to provide conventional control characteristics[18].

2.5. Aircraft dynamics

From the XV-3 research program, it was clear that next to aeroelastic effects, the tiltrotor configuration is subject to severe handling-qualities deficiencies. These had a major influence on the control system design of the XV-15. The major deficiencies of the XV-3 included[18]:

- Large variations in power requirements during approach to hover
- Nose down pitching during transition
- Lateral instability during hover in ground effect
- Lightly damped dynamic stability
- Low control response
- Unsatisfactory control harmony

The first three characteristics are said to be intrinsic to the tiltrotor configuration with its laterally displaced rotors combined with a wing and horizontal stabilizer. These would have to be resolved by augmentation via the flight control system. The latter three items have been solved by designing the XV-15

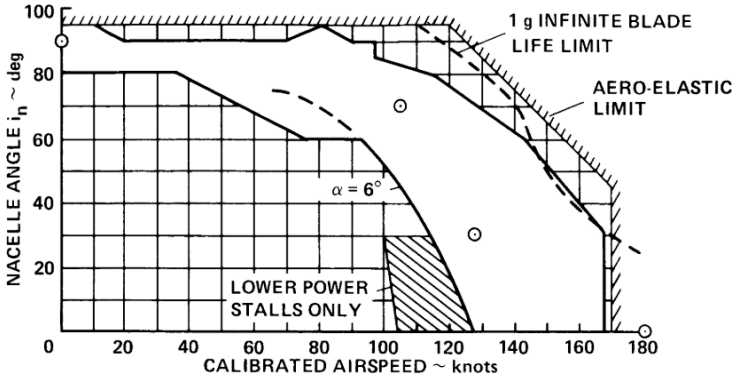

Figure 2.4: Conversion corridor of the XV-15 [4]

with an increased tail volume to improve damping by offsetting the rotor destabilizing effects, adding a rotor hub spring for increased control power and the addition of a force feel system [18].

The dynamic characteristics of the XV-15 were later also identified by Tischler in [4]. In helicopter mode for instance, the open-loop dynamics of the XV-15 were found to be typical of hovering aircraft, while there were a lot less cross-coupling effects noticeable. The planar symmetric rotor configuration yields vehicle dynamics which are decoupled between longitudinal and lateral/directional motions. There is one-way coupling from roll input to yaw response which is noticeable to a significant degree. This is caused by the differential rotor torque which is a result of the differential thrust (differential collective) to activate a roll maneuver. Open-loop pitch and roll dynamics have been found to show highly unstable low-frequency phugoid motions. The heave and yaw dynamics are as opposed to conventional rotorcraft decoupled and show essentially first-order dynamics. Because the tiltrotor configuration has large disk-loading(heave) and no tail-rotor (yaw) these dynamics show to be fairly slow with large time-constants of approximately 10 seconds. [4].

2.6. Rotor dynamics

Understanding of rotor dynamics is key to understand how a rotorcraft is controlled. These dynamics are complicated and complex and are not justified with a short discussion in this literature review. But to understand one of the reasons for this research the key concept of rotor dynamics is highlighted.

To vector the thrust of a rotor around its hub, the individual rotor blades (or as a system in gimballed rotors) flap up and down such that the plane that is spanned by the tips of the blades tilts forward, backwards or sideways. The reason for this flapping behaviour is twofold [22]. It can be caused by the oncoming flow, generating more lift on the advancing side of the rotor and less lift on the retreating side of the rotor. Secondly the lift can be cyclically controlled by applying cyclic pitch to the rotor blades. This effectively increases or decreases the angle of attack of the rotor blade and creates thus more or less lift and thus accelerating the blade up or down. Because the pitch is controlled cyclically, the lift load on the rotor disk plane can be asymmetrical therefore tilting the disk in a certain direction. The dynamics of the disk eventually create moments and forces on the hub to which the helicopter itself will respond again.

An approximation of the flapping dynamics of a helicopter in hover with a constant inflow velocity as a function of the azimuth angle was given in [17]:

$$\beta'' + \frac{\gamma}{8}\Omega\beta' + \lambda_\beta^2\beta = \frac{2}{\Omega}(p\cos\psi - q\sin\psi) + \frac{\gamma}{8}\left(\theta - \frac{4}{3}\lambda_i + \frac{p}{\Omega}\sin\psi + \frac{q}{\Omega}\cos\psi\right) \tag{2.1}$$

In this equation the control input θ is given by:

$$\theta = \theta_0 + \theta_{1c}\cos\psi + \theta_{1s}\sin\psi \tag{2.2}$$

Where θ_0 is the collective pitch angle and θ_{1s} and $\theta_1 c$ are the longitudinal and lateral cyclic pitch respectively. Furthermore in equation 2.1, β is the flapping angle defined with respect to the plane perpendicular to the rotor shaft, Ω is the rotor speed and λ_β is the flapping frequency ratio given by the expression:

$$\lambda_\beta^2 = 1 + \frac{K_\beta}{I_\beta \Omega^2} \tag{2.3}$$

, with K_β the equivalent flapping hinge spring stiffness. Furthermore are p and q rotational rates of the rotor shaft (or fuselage) and ψ is the azimuth angle of the rotor. Lastly, γ, the Lock number is given by:

$$\gamma = \frac{\rho c a_0 R^4}{I_\beta} \tag{2.4}$$

, with ρ the air density, c the rotor blade chord, a_0 the zero lift angle, R the blade length and I_β the blade mass moment of inertia around the flapping hinge.

Although the equation of motion from 2.1 is a simplification of the real world, some important dynamic characteristics can be observed from this expression. Firstly as can be seen, the dynamics can be described as a second order differential equation. A typical response from such a flapping system is shown in figure 2.1.

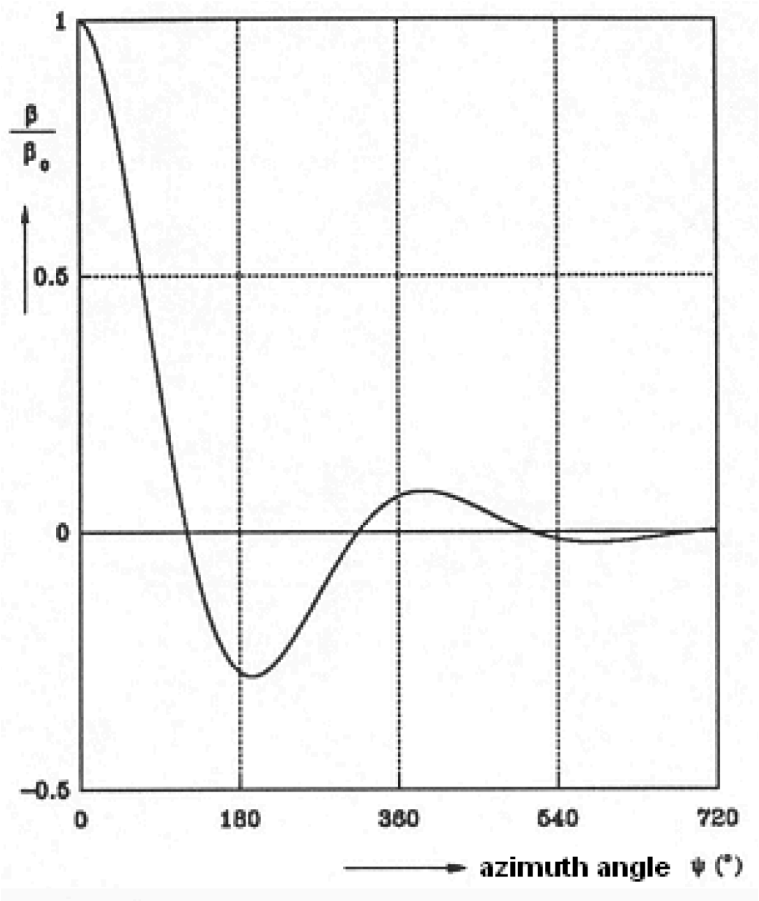

Figure 2.5: Non-dimensional flapping angle after an initial disturbance as a function of the azimuth angle for a blade with a Lock number γ equal to 6 and spring constant K_β equal to zero, only the homogeneous solution of equation 2.1 is shown [5]

After applying a cyclic pitch input to the rotor system or after a disturbance, the system will react accordingly by balancing changing aerodynamic, rotational and spring forces by eventually settling to a steady state flapping angle [23]. The steady state flapping angle will thus not be reached instantaneously. This reaction time between the control inputs and the forces and moments that are being generated by the rotor disk will show to be an important factor when designing incremental control laws for rotorcraft as was shown in [24]. Despite the different rotor configurations, some generality can be drawn with respect to the lag between input and response which can be quantified time constant τ_β and calculated via:

$$\tau_\beta = \frac{16}{\gamma \Omega} \tag{2.5}$$

The tiltrotor aircraft uses a gimballed proprotor systems, in stead of an articulated rotorsystem. This results in slighty different equations of motion [17] however the overall structure can be regarded the same and similar dynamic lag effects are to be expected.

3

Advanced nonlinear control methods

This chapter presents the advanced control methods that are of interest for solving the tiltrotor control challenges. First, some background information is given on the concept of nonlinear dynamic inversion on which most subsequent methods are based. Second, the derivatives of standard nonlinear dynamic inversion are presented as they may be a possible solution. Lastly the state of the art control research in the field of nonlinear tiltrotor control is presented.

3.1. Tiltrotor control, linear approach

Up to the 1980's flight control theory and practice had progressed from very simple fixed-form feedback structures (e.g. pitch rate to elevator) with gains tuned by control engineers in flight, to complex multivariable feedback laws, designed with modern multivariable tools that optimally trade off command responses, disturbance responses, and robustness characteristics of the final closed-loop airframe/controller combination. Rotorcraft specifically with their highly nonlinear cross-coupled dynamics and non-minimum phase zeros had already seen a wide range of control methods. These included time-domain techniques such as linear quadratic regulators/Gaussian methods, eigenstructure assigment methods, and singular perturbation methods. Frequency-domain approaches included the H_∞ method, quantitative feedback theory, the Nyquist array and characteristic locus methods [25].

3.2. Nonlinear Dynamic Inversion

During the 1980's these previous methods were complemented by a new concept of nonlinear flight control called dynamic inversion or feedback linearization as presented in [20]. In [26] the concept of dynamic inversion is derived and implemented on a UH-1H simulation model. Dynamic inversion was found to be especially useful in flight control design for aircraft that can encounter extreme nonlinear dynamics, as are encountered for example in the flight regime with very high angles of attack where wing stall occurs. This new method could be the solution to the divide and concur strategy of previous flight control design where the flight envelope was divided into smaller segments. For each segment a linear dynamics model is used to design the specific controller and satisfy desirable closed-loop characteristics. Next the individual controllers are stitched together with gain schedules to cover the complete flight envelope [27]. The chief advantage of this new method is that it avoids the time consuming development step of designing and testing the gain scheduler. Next to this, it would also have the potential to improve safety and performance.

Nonlinear dynamic inversion (NDI) is a concept where the nonlinear plant dynamics are cancelled out by effectively multiplying state feedback signals with the inverse of the dynamic equations. The full derivation has been presented in many studies such as [20], [26], [27], [28] or in the books of [29] and [30]. A brief overview of the important equations is given here.

Considering a nonlinear system MIMO system of the form:

$$\dot{x} = f(x) + G(x)u \tag{3.1}$$

$$y = h(x) \tag{3.2}$$

Where $x \in R^n$ is the system's state vector, $u \in R^m$ is the control input vector, $y \in R^m$ is the system output vector, f and h are smooth vector fields on R^n, and $G \in R^{n \times m}$ is a matrix whose columns are smooth vector fields. Considering a system which is controlled directly via its state vector and equals the output vector, i.e.

$$y = x \tag{3.3}$$

Furthermore, when assuming that $G(x)$ is inverteble in the domain of interest for all x, the control law to find the desired solution for u can be calculated takes the form of:

$$u = G^{-1}(x) = [v - f(x)] \tag{3.4}$$

The solution of 3.4 cancels all nonlinearities and relates the desired output y to the new input v via a simple linear function.

$$\dot{y} = v \tag{3.5}$$

This relation between the desired output $(\dot{y})$ and the virtual input (v) is not only linear but decoupled. All elements in v each only corresponds to their counterpart in y and no cross-coupled dynamics are present. The equation 3.5 is called the single-integrator form and this system can be forced exponentially stable via linear feedback control. The linear feedback control can be designed to guarantee time- or frequency-domain requirements. A tracking problem can be solved to follow the desired output y_{ref} based on the error $e = y_{ref} - y$:

$$v = \dot{y}_{ref} + K(e, \dot{e}, ...) \tag{3.6}$$

The linear controller can again be forced to be exponentially stable by proper gain tuning. This controller scheme is depicted in 3.1 where the two parts of the controller are distinguished. The desired-dynamics part that can be tuned via a linear controller and the plant dependent part that linearizes the plant dynamics.

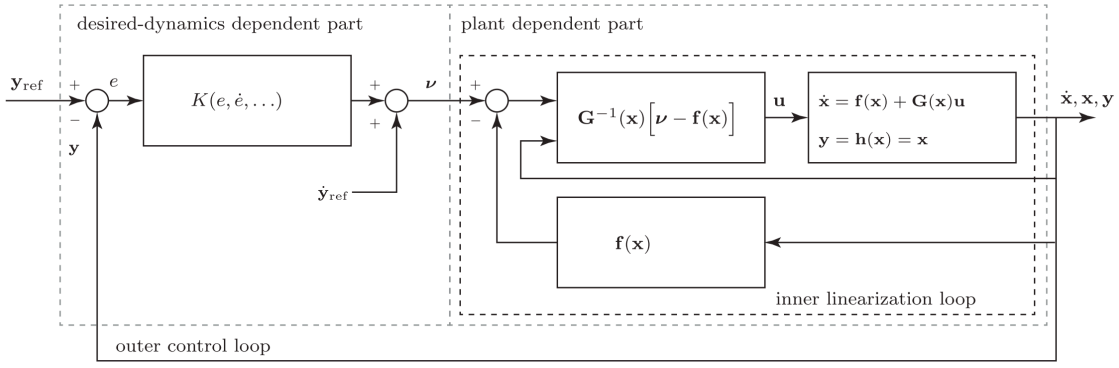

Figure 3.1: Tracking controller of a MIMO system with Nonlinear Dynamic Inversion [6]

The resulting controller works perfectly while making two assumptions that can show to be disadvantages when comparing NDI to other nonlinear control methods:

1. Complete knowledge of system dynamics is available and the describing model simulates the plant dynamic exactly. This is never the case and robustness to modeling errors is an important issues in the use of dynamic inversion. Model residuals can be compensated for by imposing loop shaping requirements on the linear controller (desired-dynamics part)[27]. A powerful method of μ-synthesis is presented in [31] and [32] but the robustness guarantees only hold for the case where the model residuals behave linearly.

   Alternatively, in stead of compensating for large model discrepancies, the flight controller can be complemented with an online parameter estimator. The estimator updates the model during the flight in an attempt to match it with real world dynamics. These adaptive methods include for example Neural Networks as presented in [33].

2. Knowledge of the state of the system i.e. x, is always available [27]. For fixed-wing aircraft control this is generally not an issue since most modern aircraft carry an arsenal of sensors ranging from rate gyros to complete navigators providing inertial orientation, velocity and position. For rotorcraft however, this could pose an issue when considering rotor flapping angles as states. Measurements of flapping angles are generally not available in flight.

   This issue may be solved via state reconstruction on states that are visible from the system. However state reconstruction does involve a certain amount of knowledge of the system.

3.3. Incremental nonlinear control

One of the methods that has been developed to robustify NDI is incremental nonlinear dynamic inversion and was demonstrated in the 1990's by [34] and [35]. The method is sometimes also referred to as acceleration measurement based. Especially in aerospace application where INDI is used to stabilize/control the attitude of the aircraft via acceleration feedback. The method is based on the principle of time scale separation [36] which makes a distinction between slow and fast dynamics.

In aircraft control for example, the vehicle is steered by applying changes to aerodynamic surfaces. These surfaces induce a moment and "instantaneously" accelerate the aircraft around a certain axis. The stabilizing drag forces to counteract the movement only increase with the increase of rate instead of acceleration. Therefore these two effects are considered to act on a different timescale.

Having made this distinction between fast and slow dynamics enables control laws to be designed that only calculate control efforts based on measured accelerations. These control efforts are calculated in increments instead of fixed actuator set points. Consider a system that is described via the nonlinear dynamics of:

$$\dot{x} = f(x,u) \tag{3.7}$$

Performing a Taylor series expansion around the operating point (x_0,u_0) results in:

$$\begin{aligned}\underline{\dot{x}} &\simeq \underline{f}\left(\underline{x}_0,\underline{u}_0\right) + \left.\frac{\partial \underline{f}(\underline{x},\underline{u})}{\partial \underline{x}}\right|_{\substack{x=\underline{x}_0\\u=\underline{u}_0}} \left(\underline{x}-\underline{x}_0\right) + \left.\frac{\partial \underline{f}(\underline{x},\underline{u})}{\partial \underline{u}}\right|_{\substack{x=x_0\\u=u_u}} (\underline{u}-\underline{u}_0) \\ &= \underline{\dot{x}}_0 + F\left(\underline{x}_0,\underline{u}_0\right)\left(\underline{x}-\underline{x}_0\right) + G\left(\underline{x}_0,\underline{u}_0\right)\left(\underline{u}-\underline{u}_0\right)\end{aligned} \tag{3.8}$$

Assuming time scale separation as described above the system of equation 3.8 can be simplified to:

$$\underline{\dot{x}} \simeq \underline{\dot{x}}_0 + G\left(\underline{x}_0,\underline{u}_0\right)\Delta\underline{u} \tag{3.9}$$

Where $\Delta\underline{u} = \left(\underline{u}-\underline{u}_0\right)$ and indeed only the direct control actions of u affect the state derivative. The incremental control law can now be formulated as:

$$\underline{u}_{des} = \underline{u}_0 + \Delta\underline{u} = \underline{u}_0 + \Delta\underline{u} = G^{-1}\left(\underline{x}_0,\underline{u}_0\right)\left(\underline{v}-\underline{\dot{x}}_0\right) \tag{3.10}$$

The control law can thus be synthesized without any knowledge required from $F\left(\underline{x}_0,\underline{u}_0\right)$ other than knowing if the timescale separation assumption is justified. The matrix $G\left(\underline{x}_0,\underline{u}_0\right)$ is called the control effectiveness matrix and relates the change in controlling forces and moments to the change in control input.

3.3.1. Model uncertainties and model adaptation

Because of its incremental nature, the system is quite robust to uncertainty in the control effectiveness matrix. If the virtual control demands a specific magnitude, the controller will increment the control effort in a time step. If in the next time step the demanded setpoint has not been reached because of the controller effectiveness was overestimated, the controller will again demand an increment. The controller will do this up until the required virtual control has been reached. In combination with a high controller sampling rate which can compensate for the increments that are too small, this method will always reach the desired virtual control setpoint. Previous studies in rotorcraft have shown that a controller sampling rate of 100Hz would be fast enough [37] [38].

If the control effectiveness is underestimated the system is can show undesired behavior. In the extreme case the effectiveness can be underestimated by such a degree that a single increment can saturate the

controller in one timestep causing a sort of bang-bang control which not only can cause a strain on the actuators but can ultimately also inflict instability.

The most detrimental case, caused by modelling errors, is when the control effectiveness sign is actually opposite in the model to the real world. In this case the virtual control input will never be reached and the system is not controllable. Each timestep an actuator increment will be calculated that will force the system in the opposite direction then was intended.

Many different strategies have been studied for model adaptation. Examples of those online parameter identification techniques are the use of neural networks [33], multivariate splines [39]. In this scenario, may be most applicable is the use of a Least Mean Squares adaptive filter [40]. A method that was also used to complement the INDI controller in the research of [41] and [42]. The adaptation law is shown in equation 3.11. Where μ_1 and μ_2 are diagonal matrices whose entries can adjust the learning rate per axis. This tuning freedom is necessary to account for different signal to noise ratios for the different axis. The signals in $\underline{\dot{x}}$ is filtered to account for sensor noise similar to the INDI controller itself. To synchronize the system finally also the input increment $\Delta\underline{u}$ needs to be filtered.

$$G(k) = G(k-1) - \mu_2 \left(G(k-1)\Delta\underline{u}_f - \Delta\underline{\dot{x}}_f \right) \underline{u}_f^T \mu_1 \tag{3.11}$$

As can be seen this is a very simple and modular estimator and fits in nicely with the compactness of the INDI control law.

3.3.2. External systems

For aircraft control the performance of INDI has shown to depend on more than only the control effectiveness matrix. Other system attributes can influence the controller until instability is inflicted. Most notably these are:

- **Actuator dynamics** The demanded actuator position that was calculated in equation 3.10 will generally not be achieved instantaneously. The actuators have their own dynamics that have an impact on the system. For conventional aircraft control surface actuators these include a first order lag system with a rate and position limit. For INDI it is important that in equation 3.10 $\underline{u}_0$ is the actual current actuator position and not the instantaneous position that was calculated in the previous timestep [42].
- **Sensor dynamics** The control axis chosen to steer the aircraft are almost always the rotational states p, q, r. The virtual control in that case would be the derivative of these rates. Rotational accelerations however, are often not measured directly but constructed from rate signals of the gyros. These signals are differentiated to estimate the acceleration and differentiation of sensor signals can amplify noise to a large degree. Therefor these signals must be filtered first. Normally via a second order low-pass filter [43]. The lag that is introduced caused by the filter needs to be compensated for in the controller design to synchronize the controller demands with the measured signals. In [41] the synchronization is done at the point where

A schematic of INDI is shown in figure 3.2 were next to the increment computation also the sensor dynamics $H(s)$ and the actuator dynamics $A(s)$ are included.

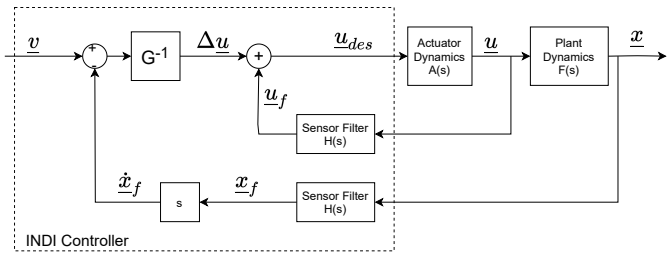

Figure 3.2: INDI schematic

In some instances of the application of INDI, the actuator state $\underline{u}$ cannot be measured by a sensor and actuator state feedback is not available. In these cases it is still important to account for actuator dynamics in the controller. This can be done by simulating the actuator dynamics and compute the actual actuator state as part of INDI controller as was presented in [41]. This is shown in figure 3.3. The degree by which

the actuator dynamics are simulated wrongly will impact the stability and performance of the system. Not having actuator states available as measurements will thus increase the requirement on system knowledge.

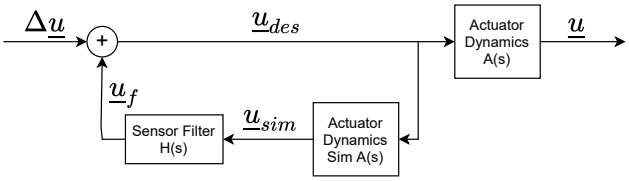

Figure 3.3: Simulating actuator dynamics, when actuator sensor feedback is not available

3.4. Backstepping

Besides nonlinear dynamic inversion, backstepping is another nonlinear control method that has been developed since the 1990s. Backstepping is a recursive control law design method which steps back from the plant's EOM towards the control inputs. The design is similar to feedback linearization, but in stead of transforming the system into its companion form and solving for the virtual input v straight away, first a stabilizing feedback is constructed for each set of states appearing in one integrator step. The stabilizing feedback is constructed via a Lyapunov function [30]. Major advantages of Backstepping versus NDI are that the use of the Lyapunov function alleviates the need for very precise model information and shows more robustness in this sense. Another advantage over NDI is that the system dynamics can be used to stabilize and control [44]. As apposed to NDI where all dynamics are cancelled out and linearized. Applying the Lyapunov stability criteria forces the system to remain stable, as can be mathematically proven, with gains free to choose. In real world applications however, it was shown that this is not necessarily the case because of actuator dynamics and sensor signal delays which the mathematical proofs never take into account [45].

3.4.1. Integrator backstepping

The full derivation and proof of stability of the backstepping methodology has been presented in many earlier works such as, [46] and [47], and in the books of [30], [29], [48]. Backstepping has many derivatives and variations amongst which is also an incremental version that similar to INDI assumes time scale separation and computes incremental control inputs as was demonstrated in [6]. This control law only needs model information on the control effectiveness, actuator states and state derivatives.

In the next part, the design methodology of a general incremental backstepping control-law is shown. Following the work of Acquatellla et al in [6]. Starting with a derivation of a non-incremental backstepping control-law.

Consider a physical system which can be represented via the following strict-feedback second order cascaded form:

$$\dot{x_1} = h(x_1) + k(x_1)\underline{x} \tag{3.12}$$

$$\dot{\underline{x}} = f(x_1, \underline{x}) + G(x_1, \underline{x})\underline{u} \tag{3.13}$$

In this system, equation 3.12 would represent a kinematic equation, for example the relation between body angular rates and inertial Euler angles [49]. Equation 3.13 would then represent a dynamic relation between forces and moments and accelerations for example a set of equations of motions in the form of Newton's second law.

Now the control law design can be started by introducing an error state between the reference signal of x_{des} and x

$$\underline{z} = \underline{x} - \underline{x}_{\text{des}} = \underline{x} - \alpha(x_1) \tag{3.14}$$

In this equation $\alpha(x_1)$ is s stabilizing feedback that will be designed later on. The function $\alpha(x_1)$ is called a stabilizing function. With the definition in equation 3.14, equation 3.12 can be rewritten as:

$$\dot{x_1} = h(x_1) + k(x_1)(\underline{z} + \alpha) \tag{3.15}$$

From here a Control Lyapunov Function (CLF) is designed. This function needs to be positive definite and radially unbounded, $V_1(x_1) : R^3 \mapsto R^+$. The property "radially unbounded" means that for a function, if the input goes to infinity the function becomes infinite as well. Like this: $\|x\| \to \infty \Rightarrow f(x) \to \infty$. A function that meets this property and often used in the derivation of backstepping control laws is:

$$V_1(x_1) = \frac{1}{2} x_1^\top x_1 \tag{3.16}$$

After this CLF has been defined the stabilizing function of $\alpha(x_1)$ can be chosen. The derivative of $V_1(x_1)$ needs to be non-positive when $x = \alpha$. This means that the designer is free to choose the function $\alpha(\chi)$ as long as $\dot{V}_1$ is negative. Efficient control via a control law $\alpha(\chi)$ can therefore be very dependent on plant dynamics.

$$\dot{V}_1 = \frac{\partial V_1(x_1)}{\partial x_1}[h(x_1) + k(x_1)\alpha(x_1)] \leq -W(x_1) \leq 0, \quad \forall x_1 \in R^n \tag{3.17}$$

Where $W : R^n \mapsto R$ is positive semi-definite. The derivative of $\alpha(x_1)$ is:

$$\dot{\alpha}(x_1, \underline{x}) = \frac{\partial \alpha(x_1)}{\partial x_1}\dot{x_1} = \frac{\partial \alpha(x_1)}{\partial x_1}[h(x_1) + k(x_1)(\underline{z} + \alpha(x_1))] \tag{3.18}$$

The control law of $\alpha(x_1)$ is the control law to steer x_1 to $x_{1_{des}}$ with x. But x itself is also dependent on dynamics from equation 3.13. Thus the error state z from equation 3.14 needs to be considered, because the desired state of x calculated in $\alpha(x_1)$ is certainly not instantaneously achieved by u. Therefore the derivative of $dotz$ is written as:

$$\dot{\underline{z}} = \dot{\underline{x}} - \dot{\alpha}(x_1, \underline{x}) = f(x_1, \underline{x}) + G(x_1, \underline{x})\underline{u} - \dot{\alpha}(x_1, \underline{x}) \tag{3.19}$$

With this in mind, the CLF can be augmented to also take into account this error state:

$$V_2(x_1, \underline{x}) = V_1 + \frac{1}{2}\underline{z}^\top \underline{z} \tag{3.20}$$

Then, the control law for u can be found by observing that to reach a asymptotically stable system, the derivative of the CLF V_2, needs to be nonpositive.

$$\begin{aligned} \dot{V}_2 &= \dot{V}_1 + \underline{z}^\top \dot{\underline{z}} \\ &\leq -W(x_1) + \underline{z}^\top \left[f(x_1, \underline{x}) + G(x_1, \underline{x})\underline{u} - \dot{\alpha}(x_1, \underline{x}) + \frac{\partial V_1(x_1)}{\partial x_1} k(x_1) \right] \end{aligned} \tag{3.21}$$

If $G(x_1, x)^{-1} \neq 0$ and invertable for all x and x_1, a possible solution for u could be:

$$\underline{u} = G^{-1}(x_1, \underline{x}) \left[-c_1 \underline{z} - f(\underline{x}) + \dot{\alpha}(x_1, \underline{x}) - \frac{\partial V_1(x_1)}{\partial x_1} k(x_1) \right] \tag{3.22}$$

For $c_1 > 0$, equation 3.21 will yield $\dot{V}_2 \leq -W(x_1) - c_1 \underline{z}^\top \underline{z} \leq 0$, which will guarantee an asymptotically stable system. The control law for u is only one possible control law and can be substituted by every solution which satisfies the inequality of equation 3.21.

3.4.2. Incremental backstepping

This backstepping methodology can be changed to an incremental form. The incremental form is especially of interest in when designing the controller which has to deal with unknown or difficult to predict nonlinearities. In the system of equations 3.12 and 3.13, the latter set contains relations of dynamical nature. Forces and moments are generated by control inputs to cause accelerations. These forces can be complex and therefor relying on precise modeling to create a control input like in equation 3.22 is a risk. Modelling inaccuracies can render the CLF of equation 3.20 unstable and therefore upset the whole control scheme. The incremental form is conceptually similar to the INDI approach that was presented before and relies on assumption that the slow dynamics of a system can be disregarded while the fast dynamics can be used to steer the plant. Consider again the dynamical system of:

$$\dot{\underline{x}} = f(\underline{x}) + G(\underline{x})\underline{u} \tag{3.23}$$

Applying a Taylor series expansion, similar to what was done for the derivation of the INDI control law in equation 3.8, the plant dynamics can be described like:

$$\underline{\dot{x}} \cong f\left(\underline{x}_0\right) + G\left(\underline{x}_0\right)\underline{u}_0 + \frac{\partial}{\partial \underline{x}}[f(\underline{x}) + G(\underline{x})\underline{u}]\Big|_{\substack{\underline{x}=\underline{x}_0 \\ \underline{u}=\underline{u}_0}} \left(\underline{x} - \underline{x}_0\right) + G\left(\underline{x}_0\right)\left(\underline{u} - \underline{u}_0\right) + \text{ H.O.T.} \tag{3.24}$$

Where here as well, the higher order terms will be neglected. And thus, the derivative of $\underline{x}_0$ is defined as:

$$\underline{\dot{x}}_0 \equiv f\left(\underline{x}_0\right) + G\left(\underline{x}_0\right)\underline{u}_0 \tag{3.25}$$

Or using standard notation for LTI-systems with:

$$A_0 = \frac{\partial}{\partial \underline{x}}[f(\underline{x}) + G(\underline{x})\underline{u}]\Big|_{\substack{\underline{x}=\underline{x}_0 \\ \underline{u}=\underline{u}_0}} \tag{3.26}$$

and,

$$B_0 = \frac{\partial}{\partial \underline{u}}[G(\underline{x})\underline{u}]\Big|_{\substack{\underline{x}=\underline{x}_0 \\ \underline{u}=\underline{u}_0}} = G\left(\underline{x}_0\right) \tag{3.27}$$

the taylor series expansion of equation 3.24 can be written as:

$$\underline{\dot{x}} \cong \underline{\dot{x}}_0 + A_0\left(\underline{x} - \underline{x}_0\right) + B_0\Delta\underline{u} \tag{3.28}$$

Now that there is a linear approximation of the dynamic relation between forces and moments and accelerations in equation 3.13. The CLF of equation 3.20 and its derivative in equation 3.21 can be reformulated to calculate a new incremental control law. The derivation of this step can be found in [50]. The control law calculates the desired input increment ($\Delta\underline{u} = \left(\underline{u} - \underline{u}_0\right)$) as:

$$\Delta\underline{u} = G^{-1}\left(\underline{x}_0\right)\left[-c_1\underline{z} - \underline{\dot{x}}_0 - A_0\left(\underline{x} - \underline{x}_0\right) + \dot{\alpha} - \frac{\partial V_1(x_1)}{\partial x_1}k(x_1)\right] \tag{3.29}$$

And again, similar to the INDI control law derivation, a high sampling rate is assumed such that $x - x_0 \approx 0$ while $u \neq u_0$. This leaves:

$$\Delta\underline{u} = G^{-1}\left(\underline{x}_0\right)\left[-c_1\underline{z} - \underline{\dot{x}}_0 + \dot{\alpha} - \frac{\partial V_1(x_1)}{\partial x_1}k(x_1)\right] \tag{3.30}$$

With the actual command signal calculated as:

$$\underline{u} = \underline{u}_0 + \Delta\underline{u} \tag{3.31}$$

3.4.3. Command filtering

The backstepping controller still depends on model information. The information in G but also the virtual control law α. and even its time derivative $\dot{\alpha}$. With absolute model knowledge the analytic derivation of α would be possible. However even if absolute model knowledge is available, if the degree of the cascaded system grows to past 3, the algebraic solutions of the control laws become very complex. A solution to solve this issue is called command filtering and is discussed in [51]. The concept here is that instead of finding the analytic solutions to the command laws, the command law is estimated with a filter. The filtering approach relieves some of the derivation complexities but does introduce lag which has to be compensated.

3.4.4. Parameter estimation

What could be of interest when looking at Backstepping control, is that it allows for the integrated parameter estimation in the controller itself. This has been studied in [47] where also a comparison study was done on integrated parameter estimation via backstepping and modular or separated least-squares estimators similar to the one presented in equation 3.11. It was found that the least squares method was superior to the integrated parameter update laws of the backstepping controller. The Lyapunov-based update laws of the integrated adaptive backstepping designs, in general, do not estimate the true value of the unknown parameters. It was shown that especially the estimate of the control effectiveness of damaged surfaces is much more accurate using modular adaptive design. Also the tuning of the update laws for the integrated design turned out to be quite time consuming.

3.5. Control allocation

In section 2.3 the control actuators of the tiltrotor configuration were discussed. From that discussion can be concluded that from the moment the aerodynamic surfaces become active, the aircraft is overactuated. This means that there are more control inputs available then there are control variables. During the conversion the elevator becomes active caused by the oncoming flow while the longitudinal collective is also still operative giving 2 actuators control over the pitch axis. A similar situation exists in the lateral axis where roll can be induced via differential longitudinal cyclic commands as well as the flaperons. Lastly the yaw axis can be controlled via both the rudder surface as well as differential thrust from the proprotors. In the XV-15, the cyclic commands are progressively phased out as a function of the nacelle angle where at a 0 degree nacelle angle in fixed wing flight, the cyclic commands are not available for flight control anymore. Nevertheless this control allocation problem needs to be solved especially when the aircraft is in the critical conversion maneuver. An overactuated system is characteristed by a control effectiveness matrix which is not square. This is the result of more actuators being availabe than control axes. The problem here is evident, the control law in equation 3.10 demands the inverse of the effectiveness matrix G but linear algebra on its own has not defined the solution to the inverse of a nonsquare matrix.

The easiest way to solve this problem would be to use the straight forward Moore-Penrose pseudoinverse operation [52] to find an approximation of the inverse dynamics. Although this method would lead to a solution to the allocation problem, by itself, it does not allow to leverage the extra control options for control optimization.

In the study of [53] a tiltrotor sort of NDI controller is designed for a configuration with redundant controls. The controller also uses a Moore-Penrose pseudoinverse operation, however it is complimented by weighting factors to increase the importance of some actuators over others. This is shown in equation 3.32

$$\underline{u}_{des} = W^{-1}G^T(GW^{-1}G^T)^{+}\underline{v} \tag{3.32}$$

Where W is a diagonal matrix with the individual weightings w_i for the different actuators. For this design it was chosen to prioritize actuators that were the quickest for a specific axis. Since the lag induced by the actuators affects the aircraft response and can result in pilot induced oscillations. Therefore, the weights w_i in W were calculated via

$$w_i = \frac{1}{\dot{u}_{i_{max}}} \tag{3.33}$$

Where $\dot{u}_{i_{max}}$ is the max response rate of the actuator u_i.

Another approach to solve the control allocation problem was presented in [54]. This approach solves a weighted least squares (WLS) problem of the form:

$$u_W = \arg\min_{\underline{u}\leq u\leq \bar{u}} \gamma \left\|W_v(Gu - v)\right\|^2 + \left\|W_u\left(u - u_p\right)\right\|^2 \tag{3.34}$$

Equation 3.34 defines the objective function of an optimization problem. The objective function penalizes two effects.

1. **Control performance** The first term looks at the computed actuator input u and checks if the input matches the demanded virtual control v. This is of course the most important part of the controller where the control input is calculated that actually realizes the demanded virtual input. The weighting

matrix W_u allows to prioritize control axes over each other. This would be beneficial for example in the case where there are unwanted cross-coupling effects or when one actuator controls multiple axis. The weighting matrix would for example allow the optimisation solver to find a control solution u which benefits one axis at the expense of another. For tiltrotor control this extra degree of freedom in the controller design could be of interest when looking at a hover maneuver where yaw control is demanded simultaneously to pitch control. These to axis share the same actuators, namely the longitudinal cyclic pitch. In the case where the actuators are near their saturation limit, it could be preferred to maintain control over the pitch axis at the expense of the yaw axis, since pitch induces a linear motion and yaw does not. These considerations can be implemented via the W_u matrix.

2. **Actuator usage** The second term in the objective function penalizes the demanded actuator position away from the preferred actuator position u_p. This can be useful to distribute the control work across different actuators to for example minimize drag. The weighting matrix W_u can be used to prioritize this as well. For tiltrotor control for example this can be used to minimize the usage of cyclic control at higher speeds during the conversion to minimize aeroelastic effects. The weighting factor γ in front of the first term is usually 1000 and ensures that whatever the preferred positions u_p of the actuators are, the optimization scheme will always first compute a control input that satisfies the demanded virtual input. Only after the control demand has been satisfied the second term is minimized.

This objective function is then solved via an active set method as described in [54] and is summarized in this report in appendix C. Using an active set method as a solver is efficient when a good estimate of the optimal active set is available. This means that the number of solver iterations will be small. In control allocation, a good estimate of the active set is given by the solution of the previous timestep. Especially with high sampling rates, the state between two solutions will not change much. Another appealing property of this method is that after every iteration, the solution will yield a lower cost value then the previous. This way a maximum number of iterations can be set to limit computational time. The WLS problem formulation for the redundant or over-actuated aircraft has been used with incremental control in [42] and [41] with good results. The method has been tested on a quadcopter configuration and a hybrid tailsitter. For these airframes it as especially important to be able to prioritize control axes over eachother. For the quadcopter for example, pitch and roll control are more important then the yawing motion. While yawing itself requires a lot of control effort from the propellers.

3.6. Previous ffforts on tiltrotor nonlinear control

This section presents some of the work that has already been performed on tiltrotor nonlinear control

An adaptive model inversion flight control method for tiltrotor aircraft has been proposed by [55] and further developed in [56] [57]. This method uses the concept of NDI as was discussed in the previous section. The model uncertainty issue is addressed by using neural networks to cancel the residuals that remain between the inaccurate model and real world system. This method was evaluated via computer simulation and proved to be working well. In a later publication [58], one of the authors made the remark however that the problem for neural networks is that:

1. It is not possible to prove that the controller will never adapt incorrectly causing the controller performance to deteriorate, and

2. it is not possible to prove that the controller has the ability to recover from faulty adaptation.

A MPC flight control system was proposed in [59] which uses model predictive control to steer the vehicle. The results of the work were promising however, the research had only been performed on linearized dynamics of the XV-15 and the controller was not tested on a nonlinear system.

In the work [60] a nonlinear dynamic inversion control law is designed. The model input for the control law was deduced from a 13th order linear model of the FXV-15 and was reduced to a third order model to only include angular rates. To cope with the discrepancies of the control law with the actual system dynamics, the controller included dynamic compensators. A PD compensator was used for the attitude command and attitude hold response type and a PI compensator was used for a rate command and attitude hold response type.

In [61], an adaptive θ-D backstepping based controller is proposed. The method had been tested on a simulator and was specifically designed to provide robustness to time-varying system parameters and

disturbances. The controller was performing very well in the simulator, however the simlulation model did not take flapping dynamics into account so this real world effect was not tested against the controller. Similarly, in [62] a dynamic surface adaptive backstepping approach was proposed which also did not include rotor flapping dynamics.

The paper of [63] proposes a time-varying linear controller for tiltrotor aircraft. This method also uses feedback linearization to cancel the nonlinear dynamics. The problem with this method however is, as was discussed earlier, that a complete nonlinear model of the aircraft is required. Which in real world is may not be very accurate or even available.

3.7. Previous efforts on Helicopter Incremental control

As can be seen the public available research on tiltrotor flight control is limited. Which may indicate that there are knowledge gaps to fill. Because a tiltrotor shares many dynamic characteristics with rotorcraft, efforts on rotorcraft incremental nonlinear control methods were also taken into consideration during the literature review.

In the paper of [64] an INDI method was proposed for rotorcraft control. In this work the author differentiated between helicopter dynamics and rotor-flapping dynamics and included state feedback of the rotor flapping states. The method was tested on a fixed rotor jig bolted on the floor but the results were encouraging and showed that feedback of rotor-flapping states can of significant value to the performance of the controller.

In [38] a INDI controller was proposed on a simulation model of the Bo-105. The results on performance and robustness against handling qualities of ADS-33-PHF were promising however the model did not include dynamic of rotor-flapping states and only steady state flapping angles were modelled.

In [24] a simulation model of the Apache AH-64 is used to test different variations of stability augmentation system based on INDI. The simulation model this time did include rotor-flapping states and the results showed that the INDI controller was sensitive to delays in the feedback of the acceleration signals. Further analysis showed that the cause might be the delayed response of the rotordisk to cyclic inputs. Earlier [42] showed that delayed signals can cause severe performance degradation with INDI. The INDI controller for the Apache AH-64 was modified include a delay and synchronize the control inputs with the rotordisk. This proved to work well. Later efforts of [65] and [66] investigated more parameters of the rotor dynamics to see what the influence was on INDI and proposed backstepping methods synchronized to rotordynamics.

3.8. Scientific gap

Based on the literature review presented, a knowledge gap can be identified. Present literature does not cover the use of incremental nonlinear control on tiltrotor aircraft that include rotor dynamics and does not discuss the control allocation problem based on incremental nonlinear control.

Part III

Thesis Work

4

Aircraft model

This chapter discusses the aircraft models that will be used for the design and evaluation of the incremental tiltrotor control laws. First the full predeveloped three degrees of freedom model will be discussed. Later derivatives from and additions to this model will be discussed .

4.1. Description of the longitudinal tiltrotor model

In the following discussion the model architecture is presented together with the main modelling assumptions. This model has been developed previously in the work of Sokolowski [8]. The model is primarily based on the model architecture of the XV-15 modelling structure presented by Furgeson in [67] and on rotor dynamics and thrust are approximated with an inflow model as shown in [5]. The aircraft parameters have been chosen such to resemble the dynamics of the XV-15, either by what was found in literature or estimated.

For the development of the model the assumptions were made that:

- There are no cross-coupling effects between symmetric and asymmetric motions and these can therefore be decoupled.
- The structure of the aircraft behaves like a rigid body. This does not include the movement of the rotordisc with respect to the fuselage.
- The mass of the aircraft remains constant and the c.g. does not move.
- the vertical stabilizers do not produce symmetric forces and moments
- Gravity remains constant
- Atmospheric conditions such as temperature and density remain constant.
- the dynamics can be derived referenced to a flat non-rotating earth.

In general four different systems are modelled that contribute to the forces and moments that govern the longitudinal motions of the aircraft. There are the wing, the fuselage, the horizontal tail and the rotor system. Regarding the rotor system these specific assumptions were made to simplify the development.

- The rotor is modelled with only a flapping hing without hing-offset. Lead-lag hinges and lead-motions are disregarded.
- The angular velocity (rotor RPM) of the rotors is constant.
- The rotor-induced velocity is assumed to be uniform across the rotor-disk.
- The blades have constant twist and are assumed to have a constant cross-sectional shape.
- The blades are assumed to be rigid.
- Regarding inertia calculations, the blade is modelled as a slender rod.
- Only linear aerodynamics are considered. The blade experiences a constant lift slope with respect to angle of attack. Stall characteristics are not modelled.

- The aerodynamic center of the blade profile lies at the quarter-chord point.
- The blade feathering axis is assumed to coincide with the blade quarter-chord point.
- Rotor flapping angles are achieved instantaneously and there is no lag to reach the rotor-body equilibrium.

Regarding the fuselage system the following assumptions were made:

- The fuselage only generates aerodynamic drag and lift and pitching moments are disregarded.
- The lift force acts in the c.g. of the aircraft.
- The fuselage drag is independent of angle of attack.

The model has been designed with the original control inputs variables. Namely, the X_{COL}, X_{LON} and η. The first two are pilot control stick inputs as they were designed for the XV-15. These inputs first go through a mixer of the flight control system before they are send through to the actual flight controls. A schematic of the original mixer of the XV-15 is shown in figure 4.5. the original control inputs have been substituted by the actual inputs that influence the flight dynamics of the aircraft namely the longitudinal cyclic, collective control, elevator control and nacelle angle control.

The full system of equations of motion can be found in appendix A. The list of aircraft and environmental parameters can be found in appendix B. The derivation of the equations of motion including a description of sign conventions and reference frames can be found in the work of Sokolowski [8].

The nonlinear model can be summarized via the system of differential equations:

$$\dot{\underline{x}} = f(\underline{x}, \underline{u}) \tag{4.1}$$

As was discussed previously, the model for this analysis describes the three longitudinal degrees of freedom with the four states in $\underline{x}$.

$$\underline{x} = \begin{bmatrix} u & w & q & \theta_f \end{bmatrix}^T \tag{4.2}$$

with u, the linear velocity in the body axis x-axis, w is the linear velocity in the body z-axis, q the rotational rate about the body y-axis, and θ_f the fuselage pitch angle. The model can be manipulated via 4 control inputs in $\underline{u}$:

$$\underline{u} = \begin{bmatrix} \theta_0 & \theta_{1s} & \delta_e & \eta \end{bmatrix}^T \tag{4.3}$$

Where θ_0 is the collective swashplate input, θ_{1s} is the cyclic swashplate input and δ_e is the elevator input. Because the model only describes longitudinal motions, the collective and cyclic input to the 2 proprotors is symmetric. This means that both proprotors will receive the same input commands and these can therefore be described by two in stead of four inputs.

4.2. Trim procedure

All simulations in this analysis start from a trimmed operating point of the model. Trimming was performed by formulating an objective function that would be minimized as a function of the initial operating point (OP), the system inputs $\underline{u}$ and the system states $\underline{x}$. The operating point is defined with:

$$OP = \begin{bmatrix} V_\infty & \gamma & q & \eta \end{bmatrix}^T \tag{4.4}$$

Via these initial conditions an operating point can be chosen at a desired flight speed V_∞, a flight path angle γ, a pitch rate q and a nacelle angle η. The available inputs to trimming function to minimize the cost function are:

$$\underline{u}_{trim} == \begin{bmatrix} \theta_0 & \theta_{1s} & \delta_e & \theta_f \end{bmatrix}^T \tag{4.5}$$

The fuselage pitch angle θ_f was added as a trimming variable in stead of operating point to allow the system to be trimmed with V_{inf} and γ in stead of the actual system states u, w. The body velocities will then follow from the basic flight mechanics equations:

$$\alpha = \gamma + \theta_f \tag{4.6}$$

$$u = \sqrt{\frac{V_\infty^2}{(1 + \tan^2 \alpha)}} \tag{4.7}$$

and,

$$w = u * \tan \alpha \tag{4.8}$$

The cost function for the trimming procedure is then formulated as

$$cost = \underline{\dot{x}}_0^2 = f(OP, \underline{u}_{trim}) \tag{4.9}$$

Where again, the initial conditions in OP are fixed and the variables in $\underline{u}_{trim}$ are allowed to vary. The optimization problem of equation 4.9 was solved in `MATLAB` via the fmincon() solver to find the initial states $(\underline{x}_0, \underline{u}_0)$.

4.3. Model linearization

After trimming the equations of motion may be linearized in order to find the stability and control derivatives in the form as shown in equation 4.10. With A carrying the stability derivatives and B the control derivatives. Linearization is performed by perturbing each one of the states in x and u around a trimmed operating point and evaluating its influence on $\dot{x}$. In this case the function `linmod` from `Matlab/Simulink` was used.

$$\underline{\dot{x}} = A\underline{x} + B\underline{u} \tag{4.10}$$

To get an insight in the dynamics of the system linearization of the equations of motion has been performed throughout the entire flight envelope. The results that are generated are only valid within a certain region close to the trimmed state as they can change fast when moving away from it. Especially along the conversion corridor where the changes in dynamic pressure and aircraft configuration are very large.

4.4. Control derivatives and effectiveness

Implementation of incremental control requires knowledge of the effective force of the aircraft its control mechanics. In the case of the attitude controller of the tiltrotor, this means the effective rotational acceleration that is achieved after an incremental change in actuator state $\Delta\underline{u}$.

The control effectiveness of the actuators can be estimated offline using model data or online via different online parameter estimation techniques as presented in section 3.3.1. In this work, the control effectiveness of the control actuators is estimated offline. If the control effectiveness changes significantly throughout the flight envelope, a look-up table can be used to update these parameters. For the estimation, equation 4.10 can be used since the results from the linearization in this form provide the relation between change in $\dot{x}$ induced by a change in u (i.e. Δu as shown in 4.11 and rewritten in 4.12 in its standard matrix form G.

$$\Delta\underline{\dot{x}} = B\Delta\underline{u} \tag{4.11}$$

$$G = \frac{\Delta\underline{\dot{x}}}{\Delta\underline{u}} \tag{4.12}$$

The entries of G, the control derivatives from B look like:

$$\begin{bmatrix} X_{\theta_0} & X_{\theta_{1s}} & X_{\delta_e} & X_\eta \\ Z_{\theta_0} & Z_{\theta_{1s}} & Z_{\delta_e} & Z_\eta \\ M_{\theta_0} & M_{\theta_{1s}} & M_{\delta_e} & M_\eta \end{bmatrix} \tag{4.13}$$

The plots in figure 4.1 show the effectiveness of the longitudinal cyclic control actuator θ_{1s} and the elevator actuator δ_e on the pitch acceleration $\dot{q}$, i.e. $M_{\theta_{1s}}$ and M_{d_e}. As mentioned in section 2.3, these two actuators are primarily used to control the pitch axis of the aircraft. The effectiveness has been estimated

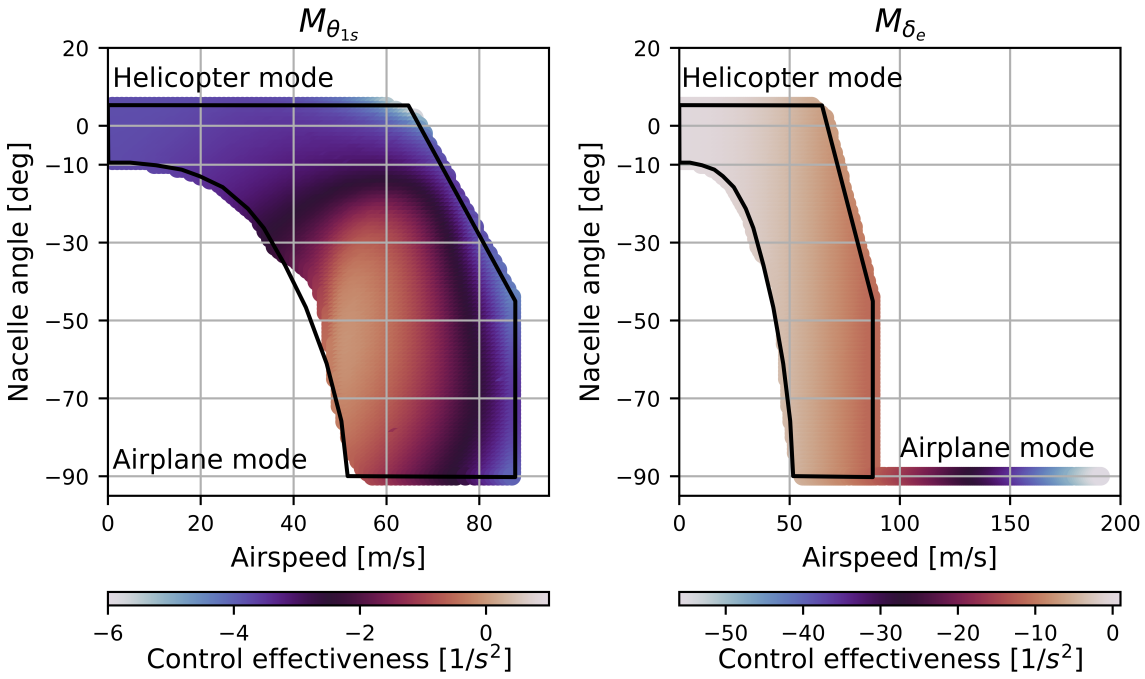

Figure 4.1: Control effectiveness of longitudinal cyclic ($M_{\theta_{1s}}$)and elevator (M_{δ_e}) control shown against the conversion corridor (V, η).

for different nacelle angles and airspeeds in and around the conversion corridor. The corridor is shown in black and may be found in [17]. The data shown in the graphs are the control derivatives that have been estimated from trim conditions in steady and horizontal flight within the corridor. Because the elevator is also active outside the corridor at higher airspeeds, the control derivative M_{δ_e} has been plotted up to the maximum achievable trimmed forward airspeed for this model.

Looking at figure 4.1 one can identify that the data do not exactly overlap with the conversion corridor. A small gap exists at the lower boundary in the middle of the conversion. Especially noticeable when looking at the $M_{\theta_{1s}}$. This gap indicates that the model was not trim-able at for steady horizontal flight in those flight conditions. The contours of the XV-15 conversion corridor have been based on multiple factors such as flight mechanical and structural limitations of the aircraft. Flight mechanical limits include for example wing stall phenomena in the lower speed regime or thrust limitations. Structurally, the corridor is designed to prevent the aircraft from exceeding airframe structural limits.

Looking at the effect of θ_{1s} on $\dot{q}$, the sign of the relation remains negative throughout the corridor. In this case this means that a positive cyclic input results in a negative pitch down acceleration. At lower airspeeds and intermediate nacelle angles ($V = [50, 65]$ and $\eta = [-80, -30]$), the effectiveness is close to zero and relatively weak compared to outside of this region. Weak effectiveness in G can pose a problem later one when designing the controller, since the control law is based on taking the inverse of G (G^{-1}). If the control effectiveness becomes to weak ($M_{\theta_{1s}} <<$) the inverse will grow very large and implicitly result in a higher control gain.

Regarding the control derivative M_{δ_e}, the sign remains negative independent of nacelle angle or airspeed. Positive elevator deflection results in a negative pitch down moment. As expected the effectiveness increases with increasing flight speed or dynamic pressure.

Alternatively, one can also look at the other control actuators that may have a secondary or "cross-coupling" effect on the pitching dynamics of the aircraft. Figure 4.2 shows the control derivatives of the nacelle and collective pitch control, M_η and M_{θ_0}. Regarding M_η it may be observed that the derivative changes sign from negative in helicopter mode to positive in a more forward flight position. The collective control is available in the entire flight envelope, from helicopter mode through higher speeds in fixed-wing mode. This is why its effectiveness has been plotted outside of the conversion corridor as well. Looking at the sign of M_{θ_0}, one can see that it changes from positive to negative multiple times. The collective function primarily controls the rotor thrust which in turn may generate a moment around the aircraft c.g..

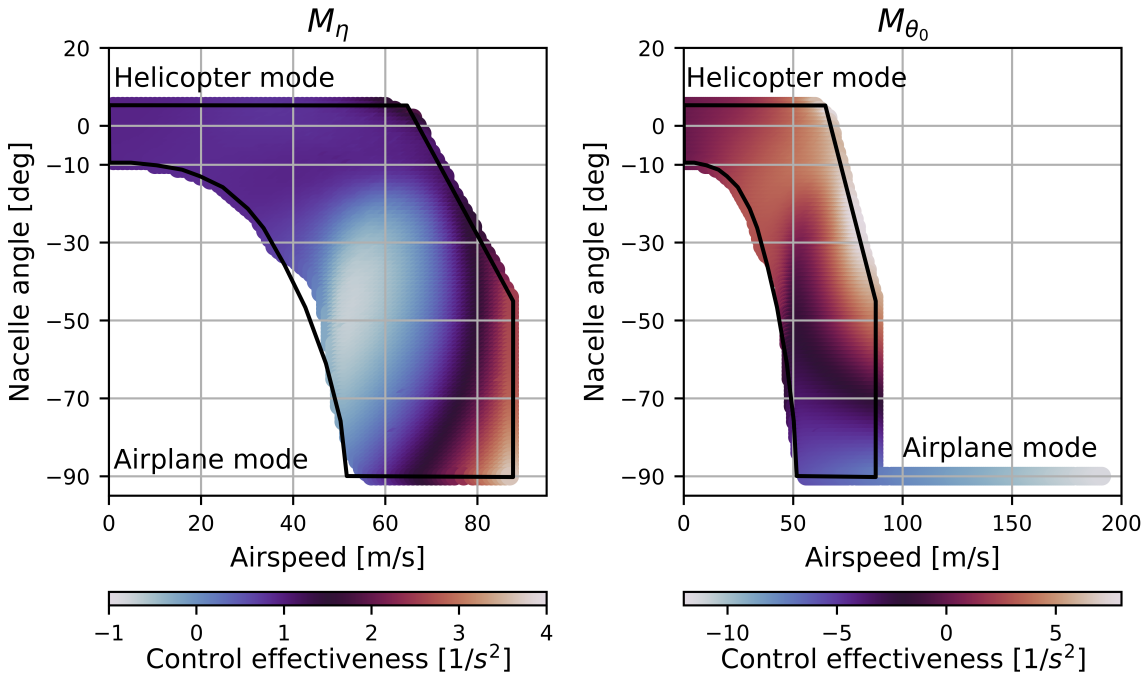

Figure 4.2: Control effectiveness of nacelle angle (η) and collective pitch (θ_0) control shown against the conversion corridor (V, η).

Because the nacelle angle changes also the hub direction and location with respect to the c.g. changes and consequently may impact the sign and magnitude of the thrust generated moment of θ_0. The actual incremental thrust force that is generated with an increment of collective pitch angle can also be obtained. This will be important later when considering the heave and surge motion of the aircraft. The derivative of thrust force to collective angle $T_{\theta_0} = \frac{\partial T}{\partial \theta_0}$ is shown in left plot of figure 4.3 against the conversion corridor. The figure shows the result for the thrust derivative of the effect of the two proprotors together. The results are calculated by first trimming the aircraft and then measuring the effect on the combined thrust force after a small perturbation in collective angle. The thrust derivative remains relatively constant throughout the flight envelope. The maximum deviation from the mean value of $8.8 \cdot 10^3 N/deg$ is 25%. A change in cyclic angle can also affect the proprotor thrust as can be seen in the right plot of figure 4.3. The thrust derivative to cyclic input is defined as $T_{\theta_{1s}} = \frac{\partial T}{\partial \theta_{1s}}$. In the plot it becomes apparent that a change in cyclic angle has a significant effect on the generated thrust. A positive change in cyclic angle has a negative contribution on the generated thrust. The order of the magnitude of the is about 50% to 25% of the contribution of collective on the thrust force. This is a severe cross-coupling effect that needs to be taken into account when designing control laws. Regarding the effect of the elevator on the generated thrust of the proprotors, $T_{\delta_e} = \frac{\partial T}{\partial \delta_e}$, this is assumed to be zero. This means that the elevator has no effect on the thrust.

4.5. Single degree of freedom model reduction

The complete 3-DOF model presented in the section above has been reduced to a SISO model to isolate and make more clear the influence of controller parameters on the overall system performance. The 3-DOF model is trimmed and linearized first after which linear body velocities u, w and their derivatives are forced zero. This leaves a SISO transfer function as shown in 4.14 in the continuous laplace domain s. The function $H(s)$ relates the cyclic input θ_{1s} to the pitch rate q of the tiltrotor.

$$H(s) = \frac{G}{s + F} \tag{4.14}$$

Looking at earlier examples from literature, this structure resembles simple pitching dynamics for a helicopter while it's movement is constrained to stay fixed in position. As shown in 4.15 by [68]. Where k

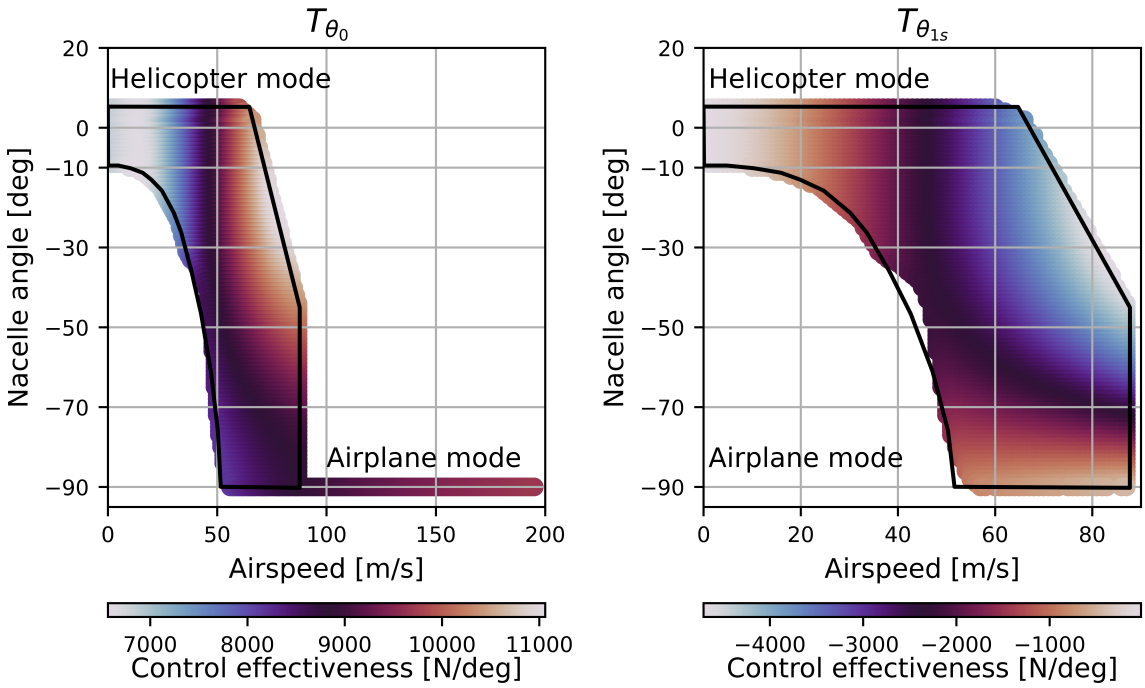

Figure 4.3: Control effectiveness of collective pitch angle (θ_0) and longitudinal cyclic angle (θ_{1s})on the rotor thrust force shown against the conversion corridor (V, η).

refers to the rotor stiffness, γ the rotor lock number.

$$\mathcal{L}(\dot{q} = -K\frac{16}{\gamma}\frac{1}{\Omega}q - K\theta_{1s}) = \frac{-k}{s + \frac{16k}{\gamma\Omega}} \tag{4.15}$$

A simplification that removes multiple controller inputs and linear velocities impacts the system response to a large degree. Especially when moving far away from the trim point. The figure 4.4 displays the SISO response conformance to a simple doublet input with the actual nonlinear 3-DOF model and a linearized 3-DOF model. By remaining relatively close to the trim point and limiting the input magnitude the system behaves very similar to the original model. In this case a trim point in hover mode was chosen where the aircraft its position is stationary (i.e. u and w are zero) and the nacelles are in the upright position. The direction and order of magnitude of the response are almost equal for the first 1.5 seconds and only diverge later on. The similarity in the very earliest stage of the response is most important when considering the behaviour of an incremental controller.

4.6. Control actuation system

To evaluate the performance of a flight control method, the constraints of the actuation system also need to be considered. These were not included in the original model. The constraints include mostly physical limits of input actuators such as mechanical position limits, rate limits and other dynamics. The flight control mechanical system of the XV-15 is complex. The control inputs of the pilot are mixed and combined with a force-feel system, SCAS, governor and engine control system. Next to that, control inputs are with the mast angle. A schematic overview is presented in figure 4.5 in which the longitudinal cockpit controls and how those commands progress through the system are highlighted.

The control input space of $\underline{u}$ that is considered in this work is the actual free available physical space of the actuators of the aircraft. Compared to the normal configuration, this means that the flight control system under consideration has control over the space that is available to the pilot via the cockpit control sticks and the space that is available to the control augmentation systems such as the SCAS and governor and engine control system.

The discussion below will substantiate the behaviour of all four the actuators. Two rotor control inputs,

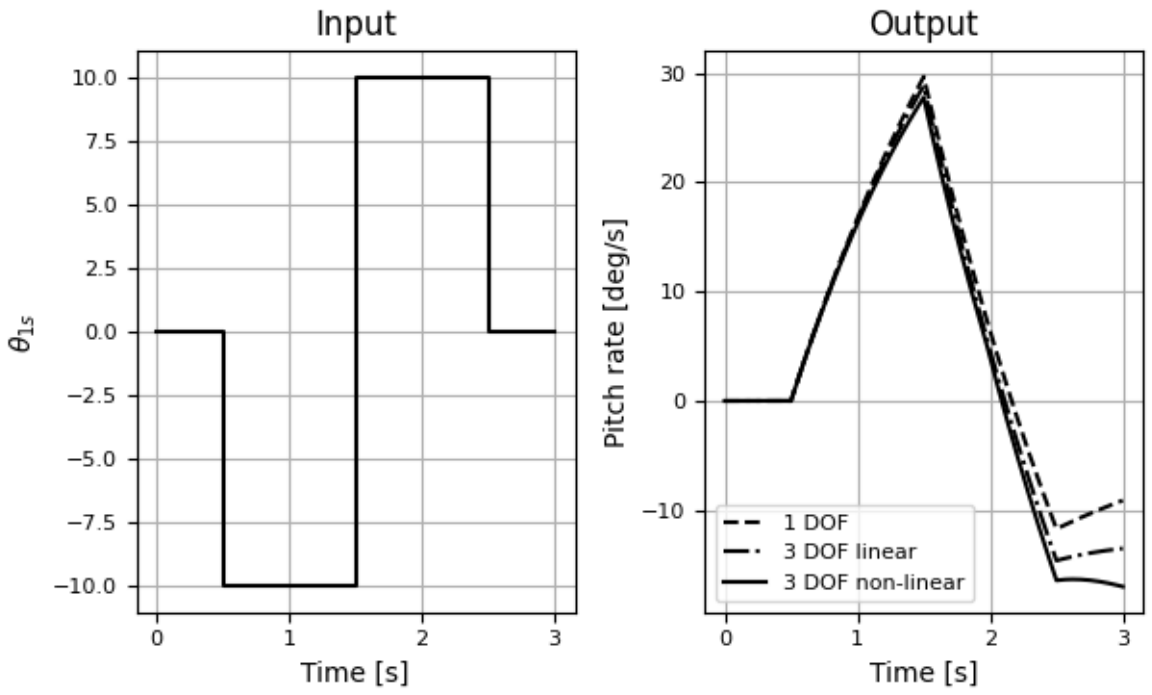

Figure 4.4: Comparison of pitch rate response to longitudinal cyclic input between different model complexities.

the elevator control input and the nacelle control input. In principle, the free allowable movement of the actuator that is considered is the same as the original XV-15 and available space is reversed engineered wherever necessary from the available data from Ferguson [9].

4.6.1. Collective swashplate control

The physical limits of the pitch control system have been derived following the reference data of the actual XV-15 from [67]. In the XV-15, the pitch angle command is a combination of different flight control systems that are integrated with each-other. The actual command can be calculated via:

$$\theta_0 = (\partial\theta_0/\partial X_{COL})X_{COL} + \theta_{0G} + \theta_{0LL} \tag{4.16}$$

Equation 4.16 only takes into account the command inputs for longitudinal motions. The factor $(\partial\theta_0/\partial X_{COL})$ is the gearing ratio that maps the collective control stick input from the pilot to collective pitch angle input. The collective control stick inputs limits are given by:

$$0 \leq X_{COL} \leq 10\ inch \tag{4.17}$$

In helicopter mode, the pilot has direct access to the collective input via the collective stick to control the heave motion of the aircraft. In airplane mode, the $(\partial\theta_0/\partial X_{COL})$ gearing ratio is completely phased out and the collective pitch angle is only controlled via the governor. The RPM governor sends commands through the input θ_{OG}. During normal operations, the governor automatically changes the collective pitch to control the rotor and maintain the RPM which has been pre-selected by the pilot. In this case, the governor control is disregarded and the available governor control space is also added to the available collective actuator space. The governor has a fixed operational space:

$$-5 \leq \theta_{OG} \leq 33.5\ deg \tag{4.18}$$

Finally, the system has a global lower limit θ_{0LL}, which has been measured at 75% away from the root of the blade. This value is first correct for the local blade twist. This lower limit is also phased with nacelle angle as shown in table 4.1.

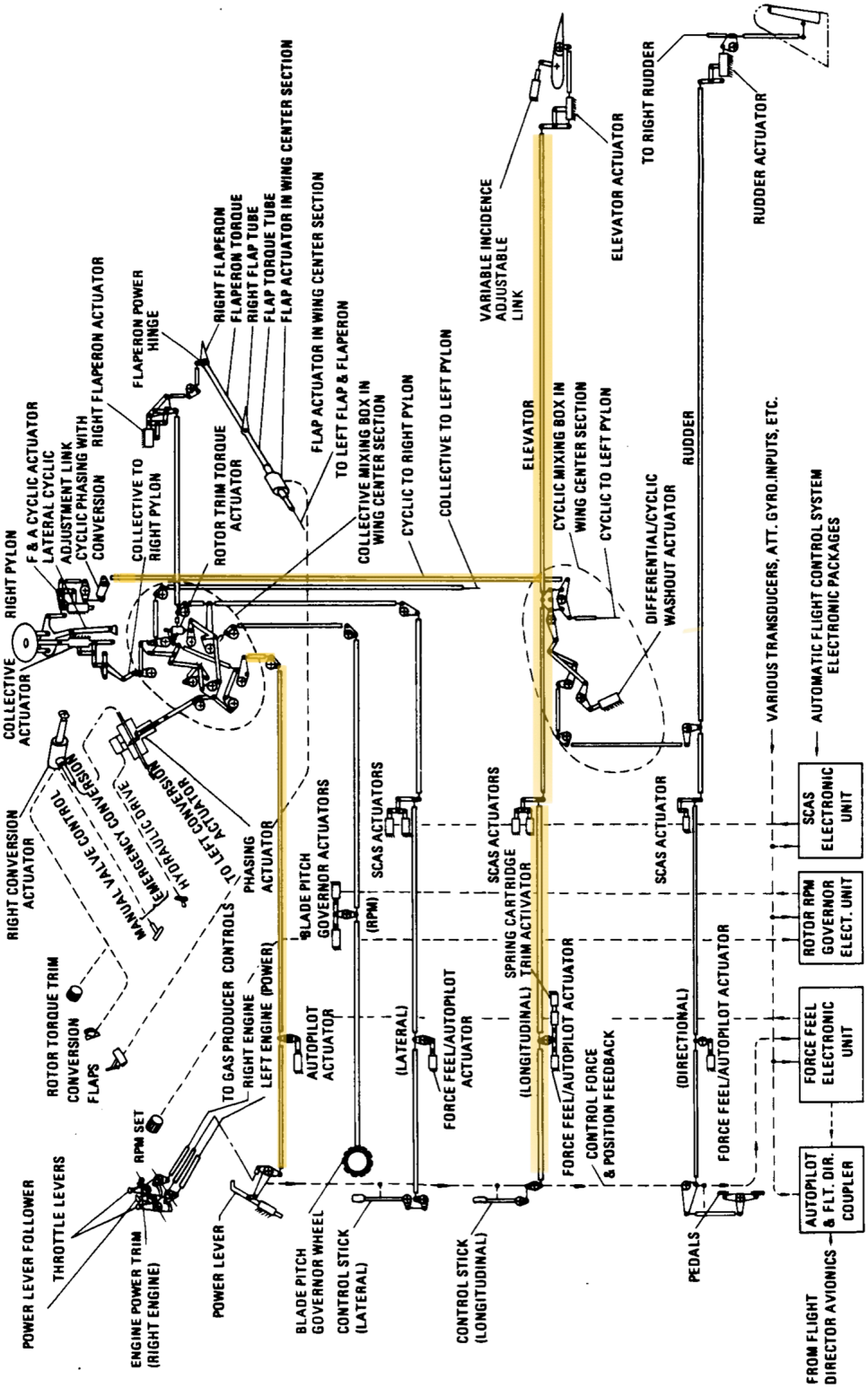

Figure 4.5: Original flight control mechanical schematic XV-15. [7]

Nacelle angle, η, [deg]	$\frac{\partial\theta_0}{\partial X_{COL}}$, [deg/in]	θ_{0LL} @75%R, [deg]	$\theta_{0LL,0tw}$ [8] (zero twist) [deg]	$\theta_{0_{min}}$ [deg]	$\theta_{0_{max}}$ [deg]
0 (helicopter mode)	1.6	-2.3	-8.7	-14	41
-10	1.5	-1	-7.4	-12	41
-20	1.4	1	-5.4	-10	42
-30	1.1	4	-2.4	-7.4	42
-40	0.92	7	0.6	-4.4	43
-50	0.71	10.2	3.8	-1.2	44
-60	0.52	13.5	7.1	2.1	46
-70	0.34	16.7	10	5.3	47
-80	0.15	19.5	13	8.1	48
-90 (airplane mode)	0	21.3	15	10	49

Table 4.1: Collective control gearing and lower pitch bounds.

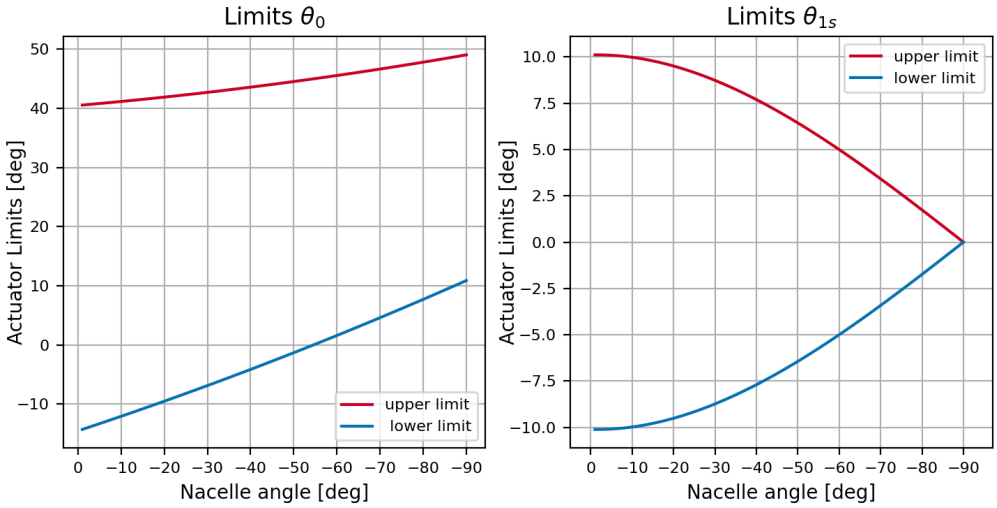

Figure 4.6: Command limits of the collective and longitudinal cyclic pitch angle against nacelle mast angle.

To find the lower and upper limits of the collective actuator the data from table 4.1 is used. The data entries are from discrete measurement points of smooth phasing function. The upper and lower limit can be found via equations 4.19 and 4.20. The results are also shown in table 4.1.

$$\theta_{0_{max}}(\eta) = \frac{\partial\theta_0}{\partial X_{COL}}(\eta) X_{COL_{max}} + \theta_{0LL,0tw}(\eta) + \theta_{0G_{max}} \tag{4.19}$$

$$\theta_{0_{min}}(\eta) = \frac{\partial\theta_0}{\partial X_{COL}}(\eta) X_{COL_{min}} + \theta_{0LL,0tw}(\eta) + \theta_{0G_{min}} \tag{4.20}$$

The results have been plotted in figure 4.6 as a function of the nacelle angle.

The collective pitch actuator is modelled with a maximum rate of $60 deg/s$ and a time constant of $0.025 s$ [17].

4.6.2. Longitudinal cyclic control

Similarly to the collective pitch control, the longitudinal cyclic control is limited. In this case the actuator positions can be modelled via:

$$\theta_{1s} = (\partial\theta_{1s}/\partial X_{LN}) X_{LN} \tag{4.21}$$

with the longitudinal stick ranging from:

$$-4.8 \leq X_{LN} \leq 4.8\, inch \tag{4.22}$$

The longitudinal stick to cyclic angle gearing ratio is phased with nacelle angle as shown in table 4.2. The upper and lower bounds of the cyclic actuator space against the nacelle angle is shown in figure 4.6. As can be seen from the figure, the cyclic control of the aircraft is completely phased out by the gearing ratio as the tiltrotor converters from helicopter to aircraft mode.

Nacelle angle, η, [deg]	**$\frac{\partial \theta_{1S}}{\partial X_{LN}}$, [deg/in]**
0 (helicopter mode)	2.1
-10	2.09
-20	1.98
-30	1.81
-40	1.60
-50	1.35
-60	1.04
-70	0.71
-80	0.362
-90 (airplane mode)	0

Table 4.2: Longitudinal cyclic gearing

4.6.3. Elevator and nacelle control

The elevator's control position limits are independent from the nacelle angle. The actuator has been modelled as an hydraulics actuator with first order lag term and a rate limit. The parameters may be found in table 4.3 [69].

Lastly the nacelle mast has also been modelled with dynamics. The parameters are also shown in table 4.3. In principle the XV-15 has two conversion rates the pilot can choose from. A slow rate of 2.5 degrees per second and a faster rate of 7.5 degrees per second [1]. No time constant is modelled since an actuator induced dynamic is considered to be much faster than the rate limit and actual nacelle travel time.

This chapter discussed the 3-DOF nonlinear tiltrotor model that will be used for the rest of this research. The trimming and linearization process was discussed as well as the progression of control derivatives throughout the flight envelope. A 1-DOF linear pitching model and a 3-DOF linear model was derived and it was shown that in the initial stages after a control input, the linear variants and their nonlinear parent behave very similar. This makes linear analysis later on possible. Lastly, physical limit actuator limits and dynamics where defined, for all four control inputs.

Control	**Min., [deg]**	**Max., [deg]**	**Rate limit, [deg/s]**	**Time constant, τ, [s]**
δ_e	-20	20	± 60	$1/20$
η	-90	5	± 2.5 /± 7.5	x

Table 4.3: Elevator and nacelle actuator parameters.

5

Incremental Nonlinear Dynamic Inversion

This chapter discusses the implementation and experimentation of INDI to the tiltrotor model. The INDI control scheme will be presented from a lower to a higher level of complexity starting with the attitude controller for a 1-DOF system. Expanding on this architecture more features will be added on the aircraft side and the controller side until the system can be evaluated against tracking performance of full envelope manoeuvres.

5.1. Incremental control applied to a single degree of freedom system

To demonstrate the fundamental architecture of incremental nonlinear dynamic inversion, the 1-DOF system from section 4.5 is used. In this case the tilrotor dynamics are linearized from a hover condition with zero velocity and with the nacelles in the upright position. Only the longitudinal cyclic is used as input to the system and the servo actuator dynamics are excluded from the evaluation.

The hover pitch dynamics are shown here again:

$$H(s) = \frac{Y(s)}{U(s)} = \frac{G}{s+F} \; where, \; \mathcal{L}^{-1}(Y(s)) = q(t) \; and \; \mathcal{L}^{-1}(U(s)) = \theta_{1s}(t) \tag{5.1}$$

Following the derivation of the INDI control laws in section 3.3, the input θ_{1s} is calculated by multiplying the desired increment in pitch acceleration with the inverse of the control effectiveness G_c and adding this to the control input of the previous timestep.

$$\theta_{1s_{des}} = \theta_{1s_0} + \Delta\theta_{1s} = G_c^{-1}(v - \dot{q}_0) \tag{5.2}$$

Where the virtual input v can be calculated via:

$$v = K_1(q_{des} - q_0) \tag{5.3}$$

The complete system is summarized in the schematic shown in figure 5.1

The scheme from figure 5.1 can be analysed analytically to determine it's stability characteristics. This is done by constructing the transfer function of the complete system. In this case, since the controller is discrete, a discrete transfer function in the z-domain has been derived. The z-domain transfer function of the complete system $sys(z)$ is presented in equation 5.4.

$$sys(z) = \frac{K_1 T_s \left(e^{FT_s} - 1\right) \frac{G}{G_c} z}{e^{FT_s} FT_s z^2 + \left(\left((K_1 T_s + 1)\frac{G}{G_c} - FT_s\right)e^{FT_s} - (K_1 T_s + 1)\frac{G}{G_c} + FT_s\right)z + \frac{G}{G_c}(1 - e^{FT_s}) + FT_s} \tag{5.4}$$

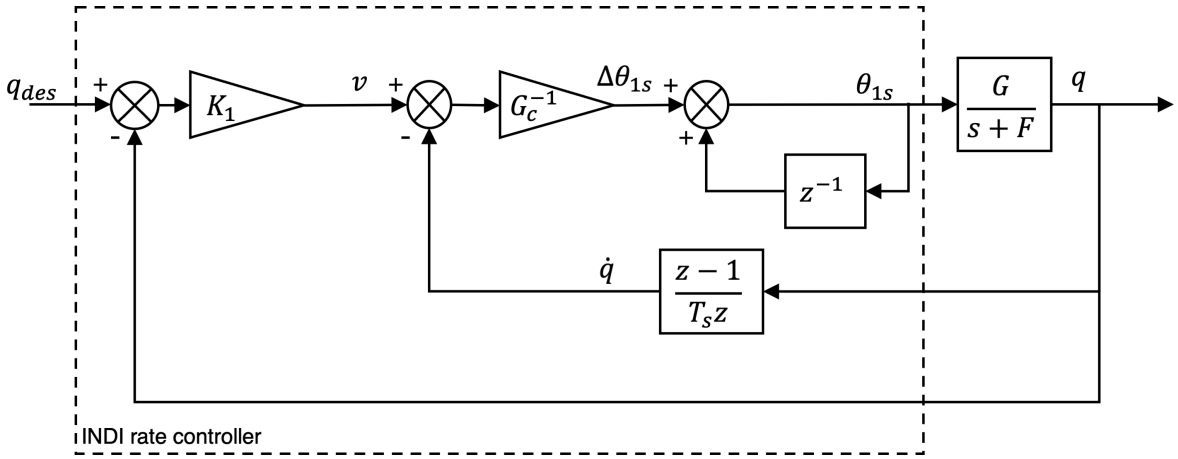

Figure 5.1: INDI rate control scheme for 1-DOF hover pitch dynamics.

F	G	T_s
1.8	-3.7	0.004

Table 5.1: System parameters of the 1-DOF pitch dynamics in hover.

To obtain the above result, the continuous time transfer function $H(s)$ has been discretized to the z-domain using a zero-order-hold transformation to simulate sampling and delay of the controller [70].

$$z.o.h.(H(s)) = (1 - z^{-1})\mathcal{Z}\left\{\frac{H(s)}{s}\right\} = \frac{Ge^{FT_s} - 1}{F(e^{FT_s}z - 1)} \tag{5.5}$$

The equation in 5.4 depends on the plant dynamics, the controller gain K_1 and the inverse of G_c, the plant dynamics and the sampling time T_s. In this case and in later simulations, the controller sampling time including computational time, T_s is equal to $1/250s$ or in other words, the run frequency of the controller is $250Hz$. A high controller frequency leaves wide frequency bandwidth for later when considering signal filtering. Notice also that the effect of the slower dynamics of F. Each time F appears in the equation it is multiplied with the sampling time T_s. In other words, the effect of F is cancelled out by the sampling frequency.

From equation 5.4, normalization between the estimated controller gain G_c and the plant's control effectiveness G is possible in multiple terms, whenever the estimated control effectiveness G_c is equal to its real counterpart. Looking at the roots of equation 5.4, the stability characteristics of the system can be determined based on the plant dynamics in F and G from $H(s)$ and the controller parameters T_s, G_c and K_1. Keeping in mind that the system is discretized, poles in the z-domain are only stable whenever their magnitude is smaller than 1. If a root of the denominator is larger than 1, the system is unstable. The numerical values of the system are summarized in table 5.1

In figure 5.2, stability characteristics of the system are plotted, together with four step responses. The plot on the left hand side graphically shows the stability trends of the roots of equation 5.4 depending on a combination of the controller gain K_1 and the ratio between the plant's control effectiveness G and the estimated controller gain G_c. The mismatch factor MF, between these two values gives an insight on how robust the controller is to modelling uncertainties. From the figure, it can be seen that the system in this configuration, remains stable whenever the gain K_1 has a positive sign and whenever the mismatch ratio remains between positive. If G_c is estimated in the order of magnitude of its real counterpart the system remains non-oscillatory for a large range of K_1. When G_c is overestimated, the system remains stable. The solution can become oscillatory as has been depicted by the light gray area. The larger overestimation of G_c(small MF), The slower the response of the system is. This is illustrated by the example shown on the right hand side of the figure. A large overestimation of G as shown in the example as $K_1 = 10$ and $MF = 0.0002$ makes the response to a step input slower than when compared to the other examples. An example of oscillatory combinations is also shown in the figure.

Practically speaking when looking at these results, one may conclude that when designing control schemes

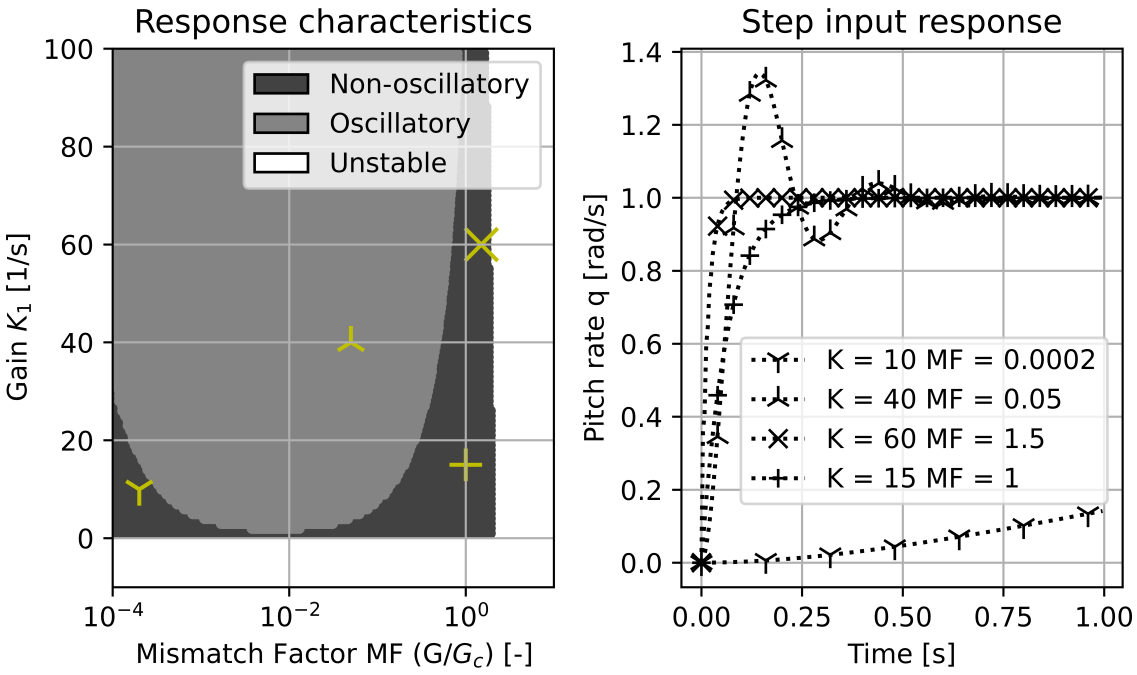

Figure 5.2: Pitch rate responses to a doublet tracking task on a INDI controller applied to 1-DOF dynamics.

like this, it may be beneficial to overestimate the control effectiveness G with a higher G_c and assign a lower value to gain K_1 to keep the system stable and non-oscillatory.

5.2. INDI applied to three degrees of freedom

The basic concept of INDI demonstrated above is now implemented on the full 3-DOF nonlinear tiltrotor model. First, an attitude controller is constructed as inner loop and later a outer loop guidance controller. The attitude controller will steer the aircraft's pitch angle with the primary longitudinal control actuators. Later, in the guidance control scheme, the inertial speeds and altitude of the aircraft are controlled by calculating the desired pitch attitude, nacelle angle and thrust increment.

5.2.1. Attitude control development

The attitude controller is based on the same principles as the INDI controller from the previous section. Control input increments of θ_{1s} and δ_e will be calculated to reach the requested fuselage pitch angle θ_f. Simultaneously, the INDI controller will solve for the desired collective θ_0 input based on the requested thrust increment ΔT. The method of deriving the fuselage pitch angle and thrust increment will be shown later when presenting the guidance/velocity part of the control scheme.

In principle the core of the INDI controller looks the same as the 1-DOF case shown earlier in section 5.1. Increments are calculated via:

$$\Delta \begin{bmatrix} \theta_0 \\ \theta_{1s} \\ \delta_e \end{bmatrix} = G_c^{-1} \begin{bmatrix} \Delta T \\ v - \dot{q}_0 \end{bmatrix} = \begin{bmatrix} G_{T,\theta_0} & G_{T,\theta_{1s}} & G_{T,\delta_e} \\ G_{q,\theta_0} & G_{q,\theta_{1s}} & G_{q,\delta_e} \end{bmatrix}^{-1} \begin{bmatrix} \Delta T \\ v - \dot{q}_0 \end{bmatrix} \tag{5.6}$$

The virtual control input v is calculated from the error between the desired pitch rate and the actual pitch rate:

$$v = K_1(q_{ref} - q_0) \tag{5.7}$$

In this case, G_c is a matrix instead of a scalar value. From the G_c entries, three important observations can be made. Conventionally, the thrust and attitude control are isolated from each-other. Collective swashplate inputs control the generated thrust while cyclic and elevator inputs control the attitude. However, as could

be seen in figure 4.1. and 4.2, there are noticeable cross-coupling effects between control inputs. Collective inputs have an unintentional influence on the pitching motion of the aircraft. The same can be said about the longitudinal cyclic. From the analyses on the control derivatives it was found that a positive cyclic increment should have a negative effect on thrust. These cross-coupling effects between the attitude actuators and the thrust actuator could make the inputs work together or against each other to achieve a desired motion.

In the case of conventional flight control, where thrust and attitude control are isolated, the joint effort is certainly not guaranteed and in the worst case actuators can clip on limits without ever reaching the requested motion or even desired direction. INDI based control can be a platform where the cross-coupling effects can help the inputs to solve the control problem as will be demonstrated later.

The second observation that can be made is that next to cross-coupling effects,, use can be made of two actuators instead of only one. Especially during transition, when the cyclic and elevator are both effective.

The third observation is that the the matrix G_c is non-square and thus is the total system is over-actuated. The matrix relates three inputs to two outputs. This causes a mathematical problem because the pure inverse of a non-square matrix is not-defined.

To solve the problems stated above (cross-coupling and over-actuation), a control allocation algorithm can be used. The purpose of the CA is to find the inverse of G_c and keep the solution within certain constraints and to prioritize control action between solutions based on tunable preferences. Two control algorithms that have been discussed in section 3.5 will be evaluated.

1. **WPI ; Weighted Pseudo Inverse Method** The first is the most simple CA and computes the inverse of G_c via a Moore-Penrose pseudoinverse operation. Next to this, weights are given to prioritize actuators that are the quickest for a specific axis. The CA calculation would look like this:

$$\Delta \begin{bmatrix} \theta_0 \\ \theta_{1s} \\ \delta_e \end{bmatrix} = W_{PIM} G_c^{\intercal} (G_c W_{PIM} G_c^{\intercal})^{+} \begin{bmatrix} \Delta T \\ \nu - \dot{q}_0 \end{bmatrix} \tag{5.8}$$

   The weighting matrix W_{PIM} is a diagonal matrix, where the weights can be chosen such to prioritize the use of an actuator. In this case, higher weights lead to higher priorization. Actuators that are prioritized are used more. Notice how the weighting matrices are arranged in equation 5.8. They are placed in such a way that no matter what the magnitude of the weights is, the magnitude of the solution is always the same.

$$W_{PIM} = \begin{bmatrix} w_{\theta_0} & 0 & 0 \\ 0 & w_{\theta_{1s}} & 0 \\ 0 & 0 & w_{\delta_e} \end{bmatrix} \tag{5.9}$$

2. **WLS ; Weighted Least Squares Method** This method is more complex in the sense that it not only takes into account the penalization or priorization of control actions like above, but can also prioritize between control axes. The control allocation problem is formulated as an optimization problem where control performance and actuator usage are evaluated.

   The general formulation of equation 3.34 can be rewritten to this specific problem as:

$$\Delta \underline{u} = \arg \min_{\Delta \underline{u}_{min} \leq \Delta \underline{u} \leq \Delta \underline{u}_{max}} \gamma \left\| W_v (G_c \Delta \underline{u} - \begin{bmatrix} \Delta T \\ \nu - \dot{q}_0 \end{bmatrix}) \right\|^2 + \left\| W_u \left(\Delta \underline{u} - \Delta \underline{u}_p \right) \right\|^2 \tag{5.10}$$

   The variable γ is a scalar gain, and W_v and W_u are diagonal matrices. With W_v control axes are prioritized relative to each other and with W_u relative use of an actuator can be weighted.

$$W_v = \begin{bmatrix} w_T & 0 \\ 0 & w_q \end{bmatrix} \tag{5.11}$$

$$W_u = \begin{bmatrix} w_{\theta_0} & 0 & 0 \\ 0 & w_{\theta_{1s}} & 0 \\ 0 & 0 & w_{\delta_e} \end{bmatrix} \tag{5.12}$$

The variable $\underline{u}$ is the vector $[\theta_0, \theta_{1s}, \delta_e]^T$ and the subscript p indicates the preferred increment of $\underline{u}$ and is set by the designer. The preferred actuator increment is non-trivial. The result of the choice leads to a preferred actuator state. The preferred actuator state can be different for each actuator.

This state can be based on the minimizing drag, aeroelastic stability or other structural or flight mechanical considerations. In this situation, the choice was made to prefer a neutral deflection (= $0deg$) for the elevator and longitudinal cyclic control. To conserve as much control authority as possible for both actuators, the preferred state should be neutral. Neutral in this sense means, no positive and no negative deflection. In other words $\theta_{1s} = 0$ and $\delta_e = 0$. For the collective control the preferred actuator state is the lower limit of the actuator space as shown in figure 4.6. Choosing the lower limit as preferred state would be an attempt to decrease required engine power.

$$\Delta \begin{bmatrix} \theta_0 \\ \theta_{1s} \\ \delta_e \end{bmatrix}_p = \begin{bmatrix} \theta_{0,min} - \theta_{0,0} \\ -1 \cdot \theta_{1s,0} \\ -1 \cdot \delta_{e,0} \end{bmatrix} \tag{5.13}$$

The subscripts zero in equation 5.13 mean that these value are from the previous timestep. The upper and lower limit $\underline{u}$ increments are calculated based on the total available actuator space and the actuator state of the previous timestep via:

$$\Delta \underline{u}_{max} = \underline{u}_{max} - \underline{u}_0 \tag{5.14}$$

$$\Delta \underline{u}_{min} = \underline{u}_{min} - \underline{u}_0 \tag{5.15}$$

From section 5.1 it could be seen that the match between the controller online or offline estimated value of the true actuator effectiveness G matters with regards of stability and oscillatory behaviour of the complete system. Although in general, the estimated value is never actually the same as it's real counterpart. The entries of G_c are in this case estimated by the control derivatives that were taken from trimmed states throughout the flight envelope. The results were already presented in section 4.4. Because large deviations exists depending on the nacelle angle and flight speed, two cases will be evaluated. In one scenario, the entries in G_c will be fixed while flying through the transition. In the other scenario, the entries will be updated from a lookup table.

Because the 3-DOF nonlinear model takes into account actuator dynamics, these need to be accounted for in the controller design. Actuator states measurements are assumed to be available. I.e. the swashplate angels θ_{1s} and θ_0 and the elevator deflection angle. Alternatively to measuring actuator states, these can also be modelled by the controller.

The controller is based on rotational accelerations of the aircraft. Normally, aircraft flight control systems only measure rotational rates using gyroscope. Gyroscope measurements can be very noisy signals so estimating rotational accelerations can become a problem since the noise is amplified when differentiating. To smooth the measurement signal, a low-pass second order filter is used. The structure of the low-pass filter is presented in the laplace domain in equation 5.16.

$$H_s(s) = \frac{\omega_n^2}{s^2 + 2\zeta\omega_n s + \omega_n^2} \tag{5.16}$$

The filter H_s has is defined with two parameters, the natural frequency ω_n and the damping ratio ζ. With these parameters the cut-off frequency can be set. The cut-off frequency is the frequency at which the input signal is attenuated by -3dB, and slopes down for higher frequencies with -20dB per decade.

To estimate the pitch acceleration, the filtered pitch rate signal q_f is differentiated via:

$$D(z) = \frac{z-1}{T_s z} \rightarrow y(k) = \frac{x(k) - x(k-1)}{T_s} \tag{5.17}$$

$$\dot{q} = D(z)H(z) \cdot q_{meas} \tag{5.18}$$

The phase lag that is introduced by the filter of equation 5.16 must be compensated for in the INDI-controller as was shown in section 3.3. In this scenario this means that the feedback signal from the actuator

measurements must be synchronized with the filter lag imposed on $\dot{q}$. This means that measurements of u_{lon} will be filtered with the same filter. The apparent signal of u_{lon} for the INDI-scheme will thus be:

$$u_f = H(z) \cdot u_{meas} \tag{5.19}$$

The outer loop of the attitude indicator steers the requested fuselage attitude. Because this scenario only includes the three longitudinal degrees of freedom, rolling and yawing angles and rates are set to zero. This means that the progression of the Euler angle θ_f with respect to the inertial plane is always linearly dependent on the pitch rate. This modeling simplification also simplifies the controller complexity effort. Normally, geometric relations are required to find the required pitch rate to reach a desired attitude. In this case however, a simple constant proportional gain will also suffice. The reference pitch rate can therefore be calculate by:

$$q_{ref} = K_2(\theta_{ref} - \theta_{meas}) \tag{5.20}$$

Lastly, the complete INDI-attitude controller is summarized by a block diagram shown in figure 5.3. The diagram shows the inner INDI-loop with control allocation and actuator measurements, middle loop for rate-control and the outer loop that controls the pitch angle.

5.3. Incremental based velocity control

The fundamental advantage of the tiltrotor is that the aircraft can hover and land vertically without needing a runway. At the same time the aircraft can cruise at high speeds with relatively efficient winglift. The transition from hover to fixed-wing flight and conversion from fixed-wing to hover is complex. The airframe configuration changes when proprotors tilt 90 degrees forward or backwards and the dynamic pressure changes significantly. These aircraft properties introduce complex nonlinearities especially when considering velocity or guidance control. For example, when the tiltrotor is in hover configuration and is hovering still, an increase in thrust means that the aircraft will primarily climb (disregarding secondary cross-coupling effects). When the tiltrotor is in airplane configuration, the proprotors have tilted and an increase in thrust primarily means an increase in velocity. In another scenario, when in hover-mode and the tiltrotor wants to fly forwards, the guidance controller needs to compute a nose-down pitching attitude. In airplane-mode however, commanding a nose-down pitching attitude will induce a descent. To cope with the aircraft configuration changes and aerodynamic nonlinearities, a cascaded INDI-velocity controller is designed. The approach used is based on the methods presented in the work of [45] and [42]. In both of these works, the cascaded design has proven to provide robust guidance for airframe configurations that need to transition from hovering to forward flight. Incremental based velocity control has the advantage that it can be explicitly designed for thrust vectoring, while taking into account aerodynamic lifting forces as well.

In this case, the cascaded design will compute reference signals for the attitude controller, namely the $\theta_{f_{ref}}$ and ΔT. Additionally, to steer through to the transition, the nacelle angle control will be integrated as well. Velocity/Position will be controlled from an inertial reference frame North-East-Down (NED) frame.

The principle of the cascased INDI velocity controller is the same as shown previously. Based on the assumption of timescale separation between the inputs and system states, slower dynamics are being disregarded and incremental control efforts are computed based on instantaneously achievable accelerations. The following main forces have been identified and will be discussed in short. Note that the design of the control law will be based on approximations of forces that act on the aircraft. This will certainly not be an accurate model, but a simple one. The goal is to find relevant dependencies between forces (accelerations) and inputs and with that their order of magnitude and direction.

- **Weight** : A constant force that does not change direction in the inertial frame. Modelled as $W = mg$
- **Wing lift** : The lift generated by the wing as a function of the velocity and the relative angle to the wind.
- **Rotor thrust** : Thrust generated by the two proprotors. Accurate modelling of the proprotor thrust is complex. An approximation is proposed that will predict the order of magnitude of the thrust depending on the nacelle angle.

- **Drag** : Drag of the aircraft as a function of velocity and relative angle to the wind. The drag force in this model mainly concerns the wing induced and wing profile drag. The drag force depends on the velocity of the aircraft and its relative angle to the wind.

- **H-force** : Typically a small force that originates from aerodynamic drag from the blades. When the tiltrotor is flying forward with high mast angles, the retreating blades of the proprotors have airspeed subtracted form the rotational speed and so increase their angle of attack. The profile drag will be reduced while the induced drag will increase. Conversely the advancing blades will will experience higher airspeeds and thus suffer more profile drag, but the induced drag will fall because of the reduced angle of attack. The overall effect of profile drag and induced drag does not balance each other out between the advancing and retreating blades the resultant is rearward facing force acting as drag.

Now that the main forces that govern the linear motions of the aircraft have been identified they can be summarized the form of Newton's second law of motion:

$$\ddot{\underline{\chi}} = \underline{f}(\underline{\chi}, \underline{u}) = \underline{g} + \frac{1}{m}\underline{L}(\dot{\underline{\chi}}, \underline{u}) + \frac{1}{m}\underline{T}(\dot{\underline{\chi}}, \underline{u}) + \frac{1}{m}\underline{D}(\dot{\underline{\chi}}, \underline{u}) + \frac{1}{m}\underline{H}(\dot{\underline{\chi}}, \underline{u}) \tag{5.21}$$

In which $\underline{\chi}$ is the position vector $[\chi_x, \chi_y, \chi_z]^T$ in the inertial NED frame, $\underline{u}$ are the control inputs, g is the gravitational acceleration, m is the vehicle's mass, T is the thrust force of the proprotors, L is the lift force of the wing and D the aircraft drag and H the H-force. All the vectors in the above equation are referenced to the right hand North-East-Down frame. This means that all the forces need to be transformed to the NED frame using the appropriate matrices. By using an inertial frame to control linear motions it makes it easier to follow up with navigation/transition control at a later stage. From equation 5.21 it appears as if this system only depends on its linear motions and the control inputs. All dynamics such as rotor dynamics or pitching dynamics have been disregarded and are only viewed as internal dynamics for this control law.

To control the longitudinal linear motion of the aircraft, three control inputs are identified. Two conventional inputs: the pitch attitude and the proprotor thrust level and one unconventional airframe specific input, the nacelle angle. By controlling the nacelle angle, the rotordiscs can be tilted with respect to the fuselage and induce forwards or backwards motions. Pilots of the V-22 tiltrotor aircraft use this technique to accelerate forward from hover condition and transition into fixed wing flight while maintaining a level pitch attitude. Alternatively, the aircraft can transition forward and backwards using a fixed nacelle angle rate. In this case the pilot controls the aircraft only via pitch attitude and thrust level. Both of these control strategies will be evaluated here. First, velocity control with access to all three inputs will be presented. This means:

$$\underline{u} = \begin{bmatrix} \theta_f & \eta & T & \end{bmatrix}^T \tag{5.22}$$

Similarly to the derivation in section 3.3, the Taylor expansion to equation 5.21 is applied. The result is shown in equation 5.23.

$$
\begin{aligned}
\ddot{\underline{\chi}} &\simeq \underline{f}(\dot{\underline{\chi}}_0, \underline{u}_0) + \left.\frac{\partial \underline{f}(\dot{\underline{\chi}}, \underline{u})}{\partial \dot{\underline{\chi}}}\right|_{\substack{\dot{\underline{\chi}}=\dot{\underline{\chi}}_0 \\ \underline{u}=\underline{u}_0}} (\dot{\underline{\chi}} - \dot{\underline{\chi}}_0) + \left.\frac{\partial \underline{f}(\dot{\underline{\chi}}, \underline{u})}{\partial \underline{u}}\right|_{\substack{\dot{\underline{\chi}}=\dot{\underline{\chi}}_0 \\ \underline{u}=\underline{u}_0}} (\underline{u} - \underline{u}_0) \\
&= \ddot{\underline{\chi}}_0 + F\left(\dot{\underline{\chi}}_0, \underline{u}_0\right)\left(\dot{\underline{\chi}} - \dot{\underline{\chi}}_0\right) + G\left(\dot{\underline{\chi}}_0, \underline{u}_0\right)\left(\underline{u} - \underline{u}_0\right) \\
&= \underline{g} + \frac{1}{m}\left.\frac{\partial \underline{L}(\dot{\underline{\chi}}, \underline{u})}{\partial \dot{\underline{\chi}}}\right|_{\substack{\dot{\underline{\chi}}=\dot{\underline{\chi}}_0 \\ \underline{u}=\underline{u}_0}} (\dot{\underline{\chi}} - \dot{\underline{\chi}}_0) \\
&+ \frac{1}{m}\left.\frac{\partial \underline{T}(\dot{\underline{\chi}}, \underline{u})}{\partial \dot{\underline{\chi}}}\right|_{\substack{\dot{\underline{\chi}}=\dot{\underline{\chi}}_0 \\ \underline{u}=\underline{u}_0}} (\dot{\underline{\chi}} - \dot{\underline{\chi}}_0) \\
&+ \frac{1}{m}\left.\frac{\partial \underline{D}(\dot{\underline{\chi}}, \underline{u})}{\partial \dot{\underline{\chi}}}\right|_{\substack{\dot{\underline{\chi}}=\dot{\underline{\chi}}_0 \\ \underline{u}=\underline{u}_0}} (\dot{\underline{\chi}} - \dot{\underline{\chi}}_0) \\
&+ \frac{1}{m}\left.\frac{\partial \underline{H}(\dot{\underline{\chi}}, \underline{u})}{\partial \dot{\underline{\chi}}}\right|_{\substack{\dot{\underline{\chi}}=\dot{\underline{\chi}}_0 \\ \underline{u}=\underline{u}_0}} (\dot{\underline{\chi}} - \dot{\underline{\chi}}_0) \\
&+ \frac{1}{m}\left.\frac{\partial \underline{L}(\dot{\underline{\chi}}, \underline{u})}{\partial \underline{u}}\right|_{\substack{\dot{\underline{\chi}}=\dot{\underline{\chi}}_0 \\ \underline{u}=\underline{u}_0}} (\underline{u} - \underline{u}_0) \\
&+ \frac{1}{m}\left.\frac{\partial \underline{T}(\dot{\underline{\chi}}, \underline{u})}{\partial \underline{u}}\right|_{\substack{\dot{\underline{\chi}}=\dot{\underline{\chi}}_0 \\ \underline{u}=\underline{u}_0}} (\underline{u} - \underline{u}_0) \\
&+ \frac{1}{m}\left.\frac{\partial \underline{D}(\dot{\underline{\chi}}, \underline{u})}{\partial \underline{u}}\right|_{\substack{\dot{\underline{\chi}}=\dot{\underline{\chi}}_0 \\ \underline{u}=\underline{u}_0}} (\underline{u} - \underline{u}_0) \\
&+ \frac{1}{m}\left.\frac{\partial \underline{H}(\dot{\underline{\chi}}, \underline{u})}{\partial \underline{u}}\right|_{\substack{\dot{\underline{\chi}}=\dot{\underline{\chi}}_0 \\ \underline{u}=\underline{u}_0}} (\underline{u} - \underline{u}_0)
\end{aligned}
\tag{5.23}
$$

With very small time increments (for example when implemented on a flight controller with high sampling frequencies), equation 5.23 can be simplified further when the considering time-scale separation assumption. If the input $\underline{u}$ can change significantly faster than $\dot{\underline{\chi}}$ can progress, so that in one timestep, $\dot{\underline{\chi}} \approx \dot{\underline{\chi}}_0$ even when $\underline{u} \neq \underline{u}_0$, it can be assumed that $\dot{\underline{\chi}} - \dot{\underline{\chi}}_0 = 0$. This means practically that $F\left(\dot{\underline{\chi}} - \dot{\underline{\chi}}_0\right) << G\left(\underline{u} - \underline{u}_0\right)$ and that $F\left(\dot{\underline{\chi}} - \dot{\underline{\chi}}_0\right)$ can be omitted from the equation. This leaves

$$\ddot{\underline{\chi}} = \ddot{\underline{\chi}}_0 + \frac{1}{m} G_v(\underline{x}, \underline{u})(\underline{u} - \underline{u}_0) \tag{5.24}$$

The G_v matrix is an effectiveness matrix that relates increments in $\underline{u}$ with the inertial linear accelerations $\ddot{\underline{\chi}}$. In the case of equation 5.23, there are four forces to be considered. Thrust, lift, drag and H-force. In this derivation only the thrust and lift force will be considered to derive the INDI control law. This decision is made on the basis that the H-force is relatively small and difficult to model. The drag force is also relatively small compared to the lift force.

Note that the forces that are not included in the control law derivation are not disregarded. The effects of these forces are still measured by the acceleration feedback signals and will be dealt with accordingly as long as the effectiveness of G_v permits (in magnitude and direction). The only decision that has been made at this point is that only the lift and thrust force by means of very simple approximations will be used to actively steer the aircraft.

Now, with this in mind, the required control action can thus be calculated via an incremental way and the INDI control law can be formulated as:

$$\underline{u} = (\ddot{\underline{\chi}}_{ref} - \ddot{\underline{\chi}}_0) m G_v^{-1} + \underline{u_0} \tag{5.25}$$

The entries of the matrix in G_v are needed to complete the calculation. This means the control derivatives of the lift and thrust force with respect to the input variables in $\underline{u}$. I.e. θ_f, η and T. To find these entries, the forces will be formulated in simple relationship. Then, the forces need to be rewritten in the inertial frame. Lastly, the forces in the inertial frame need to be differentiated with respect to u. First the lift force is discussed. Later the thrust force.

The lift force which is generated by the wing and is approximated in the aerodynamic frame based on equation 5.26.

$$L(\theta_f, V_\infty) = \frac{1}{2}\rho V_\infty^2 S C_{l_\alpha}(\alpha - \alpha_0) \tag{5.26}$$

The lift force is a function of aircraft and wing parameters but also on the flight mechanical aircraft states α and V_∞. Both the angle of attack and free stream velocity are assumed to be available data from either state reconstruction or directly from sensors. However, because this is an effort to search for control derivatives for the inputs in $\underline{u}$, i.e. θ_f, T and η, the lift force needs to be expressed in one or more of these states. Otherwise, the control derivative of the lift force with respect to $\underline{u}$ is in principle zero. To fix this, the angle of attack is written in terms of the flight path angle γ and θ via the relationship:

$$\alpha = \theta_f - \gamma \tag{5.27}$$

and then, assuming that also the flight path angle γ can be reconstructed, equation 5.26 be written as:

$$L(\theta_f, V_\infty) = K_l(\theta_f - \gamma - \alpha_0) \tag{5.28}$$

Including the simplification in notation where $K_l = \frac{1}{2}\rho V_\infty^2 S C_{l_\alpha}$. Presented in vector form in the aerodynamic frame the lift force looks like shown in equation 5.29. In which the lift force point in the negative z axis of the aerodynamic frame.

$$\underline{L}^a = \begin{bmatrix} 0 \\ 0 \\ -1 \cdot K_l(\theta_f - \gamma - \alpha_0) \end{bmatrix} \tag{5.29}$$

To represent the lift force in the NED inertial frame two frame transformations need to take place. One from aerodynamic to the body frame and from the body to the inertial frame. These transformation matrices are shown below. The transformation matrices are presented as if also lateral motions are considered here, but this is not the case. The matrices are shown for complete tree-dimensional transformations for sake of being familiar to the reader. The transformation from body to inertial frame can be extended to include the two lateral Euler angles as well. For a full overview of body-inertial transformation sequences in Euler and quaternion representation the reader is referred to the work of Diebel in [49].

$$T_{BA}(\alpha) = T_y(\alpha) = \begin{bmatrix} \cos(\alpha) & 0 & -\sin(\alpha) \\ 0 & 1 & 0 \\ \sin(\alpha) & 0 & \cos(\alpha) \end{bmatrix} \tag{5.30}$$

$$T_{EB}(\theta_f) = T_y(\theta_f) \begin{bmatrix} \cos(\theta_f) & 0 & \sin(\theta_f) \\ 0 & 1 & 0 \\ -\sin(\theta_f) & 0 & \cos(\theta_f) \end{bmatrix} \tag{5.31}$$

$$T_{EA} = T_{EB} \cdot T_{BA} = \begin{bmatrix} c(\alpha - \theta_f) & 0 & -s(\alpha - \theta_f) \\ 0 & 1 & 0 \\ s(\alpha - \theta_f) & 0 & c(\alpha - \theta_f) \end{bmatrix} \tag{5.32}$$

Carrying out the frame transformation of the lift force from the aerodynamic to the inertial frame, the lift force looks like:

$$\underline{L}^E = T_{EA}\underline{L}^a \begin{bmatrix} K_l(\theta_f - \gamma - \alpha_0)s(\alpha - \theta_f) \\ 0 \\ -K_l(\theta_f - \gamma - \alpha_0)c(\alpha - \theta_f) \end{bmatrix} \tag{5.33}$$

From there, the control derivatives of the lift force with respect to $\underline{u}$ can be found.

$$G_{lift} = \begin{bmatrix} \frac{\partial \underline{L}^E}{\partial \theta_f} & \frac{\partial \underline{L}^E}{\partial \eta} & \frac{\partial \underline{L}^E}{\partial T} \end{bmatrix} = \begin{bmatrix} K_l((\gamma + \alpha_0 - \theta_f)c(\alpha - \theta_f) + s(\alpha - \theta_f)) & 0 & 0 \\ 0 & 0 & 0 \\ K_l((\gamma + \alpha_0 - \theta_f)s(\alpha - \theta_f) - c(\alpha - \theta_f)) & 0 & 0 \end{bmatrix} \tag{5.34}$$

Then, assuming the tiltrotor is not an aerobatics aircraft and the flight path angle remains small compared to the angle of attack and pitch angle, the angle of attack can be expressed only by the pitch angle.

$$\gamma \approx 0 \rightarrow \alpha = \theta_f \tag{5.35}$$

The control derivatives with respect to the lift force can then finally be written as:

$$G_{lift} = \begin{bmatrix} K_l(\alpha_0 - \theta_f) & 0 & 0 \\ 0 & 0 & 0 \\ -K_l & 0 & 0 \end{bmatrix} \tag{5.36}$$

The thrust force was based on the assumption that in hover the thrust equals the weight of the aircraft and in fixed wing flight, the thrust equals about 20% of the weight of the aircraft. This is of course a crude approximation but as long as the direction and order of magnitude of the derivative is correct, it should be okay.

$$T = gm\left(1.2 - \frac{1}{10}\left(\frac{8}{90}\eta + 2\right)\right) \tag{5.37}$$

The thrust force in vector form is initially presented in the nacelle frame. The thrust thrust points in the negative z-axis of the nacelle frame.

$$\underline{T}^N = \begin{bmatrix} 0 & 0 & -T \end{bmatrix}^T \tag{5.38}$$

The thrust force as modelled in equation 5.37 is not substituted in equation 5.38 because this would introduce a dependency of the magnitude of the thrust with respect to nacelle angle changes in the control derivatives. The relationship as described in equation 5.37 does not actually exists, there is no strict dependency of the thrust on the nacelle angle. This relationship as formulated by equation 5.37 is only used to estimate the order of magnitude of the thrust in a more simpler (than something else). Using the relationship in the derivation of the control derivatives may imply to the controller that if there would be a nacelle angle change, the magnitude of the thrust would also change.

To implement the thrust force in the INDI law, this force also needs to be represented in the inertial NED frame. First the thrust vector is transformed from the nacelle frame to the body frame with T_{BN}, and then from the body frame to the inertial representation with T_{EN}. Again the matrix formulations are kept in 3D including the lateral axis for the familiarity of the reader and also demonstrate that expanding the method to six degrees of freedom is possible.

$$T_{BN}(\eta) = \begin{bmatrix} cos(\eta) & 0 & -sin(\eta) \\ 0 & 1 & 0 \\ -sin(\eta) & 0 & cos(\eta) \end{bmatrix} \tag{5.39}$$

$$T_{EN} = T_{EB} \cdot T_{BN} = \begin{bmatrix} c(\theta_f + \eta) & 0 & s(\theta_f + \eta) \\ 0 & 1 & 0 \\ -s(\theta_f + \eta) & 0 & c(\theta_f + \eta) \end{bmatrix} \tag{5.40}$$

$$\underline{T}^E = T_{EN}\underline{T}^N = \begin{bmatrix} -Ts(\theta_f + \eta) \\ 0 \\ -Tc(\theta_f + \eta) \end{bmatrix} \tag{5.41}$$

$$G_{thrust} = \begin{bmatrix} \frac{\partial \underline{T}^E}{\partial \theta_f} & \frac{\partial \underline{T}^E}{\partial \eta} & \frac{\partial \underline{T}^E}{\partial T} \end{bmatrix} = \begin{bmatrix} -Tc(\theta_f + \eta) & -Tc(\theta_f + \eta) & -s(\theta_f + \eta) \\ 0 & 0 & 0 \\ Ts(\theta_f + \eta) & Ts(\theta_f + \eta) & -c(\theta_f + \eta) \end{bmatrix} \tag{5.42}$$

Finally the complete control effectiveness matrix G_v can be constructed by summing G_{lift} and G_{thrust} together.

$$G_v = G_{lift} + G_{thrust} = \begin{bmatrix} -Tc(\theta_f + \eta) + K_l(-\theta_f + \alpha_0) & -Tc(\theta_f + \eta) & -s(\theta_f + \eta) \\ 0 & 0 & 0 \\ Ts(\theta_f + \eta) - K_l & Ts(\theta_f + \eta) & -c(\theta_f + \eta) \end{bmatrix} \tag{5.43}$$

The matrix G_v relates the change of u with the change of the lift and thrust force in the (X, Y, Z) inertial frame. Because in this case only the longitudinal motions are considered, the middle row can be deleted:

$$G_v = G_{lift} + G_{thrust} = \begin{bmatrix} -Tc(\theta_f + \eta) + K_l(-\theta_f + \alpha_0) & -Tc(\theta_f + \eta) & -s(\theta_f + \eta) \\ Ts(\theta_f + \eta) - K_l & Ts(\theta_f + \eta) & -c(\theta_f + \eta) \end{bmatrix} \tag{5.44}$$

Equation 5.24 can now be rearanged and fitted with the above result to come to the final indi-control law:

$$\begin{bmatrix} \theta_f \\ \eta \\ T \end{bmatrix}_{ref} = \left(\begin{bmatrix} \ddot{\chi}_x \\ \ddot{\chi}_z \end{bmatrix}_{ref} - \begin{bmatrix} \ddot{\chi}_x \\ \ddot{\chi}_z \end{bmatrix}_0 \right) m G_v^{-1} + \begin{bmatrix} \theta_f \\ \eta \\ T \end{bmatrix}_0 \tag{5.45}$$

A measurement of the thrust force T is in practice difficult to obtain, so T_0 must be treated as an unknown. This is not a problem because the attitude controller was already setup to only require thrust increments ΔT instead of a thrust-level. Measurements of the fuselage pitch angle and nacelle angle are assumed to be available. Measurements of the accelerations are also available from an onboard IMU, however similar to the gyroscope sensor, these can be noisy and must therefore be filtered with a low-pass filter, just as was shown before with the filter in equation 5.16. Furthermore, the measurements of the IMU are in the body frame and must be transformed to the inertial frame. This can be done with the same transformation as shown in equation 5.31. Similarly to the one presented in equation 5.16. And analogous to the attitude controller, synchronization is required between the accelerations measurements $\underline{\ddot{\chi}}$ and the actuator measurements $u = [T, \theta_f, \eta]^T$. Synchronization can be performed by filtering the actuator measurements as well. Note that only the actuator feedback measurements need to be synchronized. The measurements that are required for the entries in the effectiveness matrix (equation 5.44 do not require synchronization and can be used as is. Again, leaving:

$$\begin{bmatrix} \theta_f \\ \eta \\ \Delta T \end{bmatrix}_{ref} = m G_v^{-1} \left(\begin{bmatrix} \ddot{\chi}_x \\ \ddot{\chi}_z \end{bmatrix}_{ref} - \begin{bmatrix} \ddot{\chi}_x \\ \ddot{\chi}_z \end{bmatrix}_f \right) + \begin{bmatrix} \theta_f \\ \eta \\ 0 \end{bmatrix}_f \tag{5.46}$$

This is a incremental control law that controls linear accelerations in the inertial NED-frame. From here, similar to what was shown in the attitude controller design, outer-loops can be integrated to also steer velocities and to maintain altitude and position(when in hover mode.)

The velocity control law is given by:

$$\begin{bmatrix} \ddot{\chi}_x \\ \ddot{\chi}_z \end{bmatrix}_{ref} = K_3 \cdot \underline{\dot{\chi}}_{error} = K_3 \left(\begin{bmatrix} \dot{\chi}_x \\ \dot{\chi}_z \end{bmatrix}_{ref} - \begin{bmatrix} \dot{\chi}_x \\ \dot{\chi}_z \end{bmatrix}_0 \right) \tag{5.47}$$

When transitioning from hover to airplane mode, or converting back, the differences between commanded input and measured feedback can be very large ($|\underline{\dot{\chi}}_{error}| \approx 150kts$). Large errors like this generate large acceleration reference signals that are physically impossible to reach causing the incremental control law to wind up. To fix this, the acceleration reference signals can be bounded by upper and lower limits. These are defined separately for vertical and horizontal motions (χ_i, with $i = [x, z]$)

$$\ddot{\chi}_{i_{ref}} = \begin{cases} \ddot{\chi}_{i_{max}} & \text{if } K_3 \cdot \dot{\chi}_{i_{error}} \geq \ddot{\chi}_{i_{max}} \\ K_3 \cdot \dot{\chi}_{i_{error}} & \text{if } \ddot{\chi}_{i_{max}} > K_3 \cdot \dot{\chi}_{i_{error}} > \ddot{\chi}_{i_{min}} \\ \ddot{\chi}_{i_{min}} & \text{if } K_3 \cdot \dot{\chi}_{i_{error}} \leq \ddot{\chi}_{i_{min}} \end{cases} \tag{5.48}$$

The velocity control law does not include explicit filtering of the velocity feedback signals. In real world applications these signals have to be reconstructed anyway via appropriate state estimation techniques such as Kalman filtering. In this report, these feedback signals ($\underline{\dot{\chi}}_0 = [\dot{\chi}_x, \dot{\chi}_z]_0^T$) are extracted directly from the model.

Note on velocity control. The velocities that are calculated and commanded in this scheme are referenced to the inertial frame. From an aerodynamic point of view, these are less meaningful. Aerodynamic lifting and propulsive forces created by the wing and rotors depend on speed of the relative airflow which they encounter. In that sense, the free stream velocity V_∞ of the aircraft maybe a more logical choice for speed control. On the other hand, when in hover mode, and accurate positioning is required a controller referenced to the inertial frame may be better suited, even when there is wind present. As long as there is no wind, the inertial speeds can construct the aerodynamic free stream velocity.

Lastly, the most outer-loop of the velocity controller can be designed. This loop calculates the velocity reference signals based on commanded position and altitude setpoints. The position control law is given by:

$$\begin{bmatrix}\dot{\chi}_x\\ \dot{\chi}_z\end{bmatrix}_{ref} = K_4 \cdot \underline{\chi}_{error} = K_4\left(\begin{bmatrix}\chi_x\\ \chi_z\end{bmatrix}_{ref} - \begin{bmatrix}\chi_x\\ \chi_z\end{bmatrix}_0\right) \tag{5.49}$$

Velocity references are also limited and must be changed according to flight envelope or conversion corridor limits. These are also defined separately for x and z directions.

$$\dot{\chi}_{i_{ref}} = \begin{cases}\dot{\chi}_{i_{max}} & \text{if } K_4 \cdot \chi_{i_{error}} \geq \dot{\chi}_{i_{max}}\\ K_4 \cdot \chi_{i_{error}} & \text{if } \dot{\chi}_{i_{max}} > K_4 \cdot \chi_{i_{error}} > \dot{\chi}_{i_{min}}\\ \dot{\chi}_{i_{min}} & \text{if } K_4 \cdot \chi_{i_{error}} \leq \dot{\chi}_{i_{min}}\end{cases} \tag{5.50}$$

5.3.1. Over-actuation

The result of the previous section introduces a problem. The matrix G_v from equation 5.44 is not square and can therefore not be inverted in a standard way. The over-actuated system is the result of the fact that both the nacelle angle and the fuselage pitch angle can vector the thrust around the pitch angle. With both the similar effect on accelerations. To solve this issue, two methods will be proposed. The first will consider the nacelle system separate and outside of the velocity controller and without integrating the nacelle feedback with the rest of the velocity control scheme. The second method will be solving the over-actuated system via the Weighted Least Squares control allocation scheme that has been presented and used for the attitude controller.

Isolate nacelle control

Excluding the nacelle control from the velocity control solves the overactuated system because the middle column in matrix G_v can be removed. By removing the control derivatives with respect to the nacelle angle, the incremental control law does not compute nacelle angle changes to achieve a requested linear acceleration. In this sense, nacelle control is excluded from the velocity controller and the actuator vector $\underline{u}$ becomes $[\theta_f, T]^T$. and thus the control effectiveness matrix can be written as:

$$G_v = \begin{bmatrix}-Tc(\theta_f+\eta) + K_l(-\theta_f+\alpha_0) & -s(\theta_f+\eta)\\ Ts(\theta_f+\eta) - K_l & -c(\theta_f+\eta)\end{bmatrix} \tag{5.51}$$

The matrix from equation 5.51 is square and can therefore be inverted in a standard way to solve the incremental control law:

$$\begin{bmatrix}\theta_f\\ \Delta T\end{bmatrix}_{ref} = mG_v^{-1}\left(\begin{bmatrix}\ddot{\chi}_x\\ \ddot{\chi}_z\end{bmatrix}_{ref} - \begin{bmatrix}\ddot{\chi}_x\\ \ddot{\chi}_z\end{bmatrix}_f\right) + \begin{bmatrix}\theta_f\\ 0\end{bmatrix}_f \tag{5.52}$$

Note however, that nacelle angle information is still required to compute the entries in G_v. This is because the thrust orientation depends on the angle of the nacelle. The result of equation 5.51 leaves an incremental acceleration controller without integrated nacelle control. The aircraft is able to hover and cruise and fly at set nacelle angles in the conversion envelope, but not coordinated with the mast angle. To transition from hover mode to airplane mode the nacelle angle has to be changed separately. In this method this is done via a feed-forward signal. When the transition is initiated, two commands are given:

1. Aircraft speed is set for cruise speed.
2. Nacelle angle is set for -90 degrees. Commanded rates can be set at 2.5$[deg/s]$ or 7.5$[deg/s]$.

Integrated nacelle control

The following method builds further on the result that was obtained in equation 5.44. The control allocation problem of the non-square control effectiveness problem can be solved by using the Weighted Least Squares method. The objective function is now formulated as follows:

$$\Delta \underline{u} = \arg \min_{\Delta \underline{u}_{min} \leq \Delta \underline{u} \leq \Delta \underline{u}_{max}} \gamma \left\| W_v \left(\frac{1}{m} G_v \Delta \underline{u} - \left(\underline{\ddot{\chi}}_{ref} - \underline{\ddot{\chi}}_f \right) \right) \right\|^2 + \left\| W_u \left(\Delta \underline{u} - \Delta \underline{u}_p \right) \right\|^2 \tag{5.53}$$

In this scheme the control goals and efforts are again optimized. With $u = [\theta_f, \eta, T]^T$. The scalar gain γ prioritizes the control goal over the control effort The weighting matrices W_v and W_u can be written as:

$$W_v = \begin{bmatrix} w_x & 0 \\ 0 & w_z \end{bmatrix} \tag{5.54}$$

$$W_u = \begin{bmatrix} w_{\theta_f} & 0 & 0 \\ 0 & w_\eta & 0 \\ 0 & 0 & w_T \end{bmatrix} \tag{5.55}$$

The weight w_T should be set zero since the max and minimum thrust values are not well defined. Therefore also preferred increments in thrust is not well defined. Although less thrust may lead to a more efficient flight. Moreover, the thrust is effectively limited by the collective swashplate limits in the attitude controller. The goal of the coordinated transition maneuver is to fly through the conversion corridor. That means within the limits of nacelle angle vs airspeed. The increment limits can be set so that they reflect the conversion envelope. The fuselage pitch limits can be set by the designer at his discretion. The maximum and minimum increments are defined by the current state of the pitch angle and nacelle angle and their limits:

$$\Delta \begin{bmatrix} \theta_f \\ \eta \end{bmatrix}_{max} = \begin{bmatrix} \theta_f \\ \eta \end{bmatrix}_{max} - \begin{bmatrix} \theta_f \\ \eta \end{bmatrix}_0 \tag{5.56}$$

$$\Delta \begin{bmatrix} \theta_f \\ \eta \end{bmatrix}_{min} = \begin{bmatrix} \theta_f \\ \eta \end{bmatrix}_{min} - \begin{bmatrix} \theta_f \\ \eta \end{bmatrix}_0 \tag{5.57}$$

The preferred actuator increments in $\Delta \underline{u}_p$ are defined as:

$$\Delta \begin{bmatrix} \theta_f \\ \eta \\ T \end{bmatrix}_p = \begin{bmatrix} -1 \cdot \theta_f \\ \Delta\eta_{max} \vee \Delta\eta_{min} \\ 0 \end{bmatrix} \tag{5.58}$$

The preferred direction of η depends on whether the aicraft is transitioning to airplane mode ($\Delta\eta_{min}$)or converting back to hover mode ($\Delta\eta_{max}$). Keeping in mind that the tiltrotor is in airplane mode when the mast angle is at $-90deg$. The complete controller scheme of the velocity controller is shown in figures 5.4 and 5.5.

This chapter discussed the design of an INDI attitude and velocity controller for XV-15 tiltrotor configuration. First, a short anaylsis was performed on a 1-DOF system to demonstrate to an extent the robustness characteristics of INDI. Next the attitude controller was designed for the full 3-DOF nonlinear model. A control allocation problem was identified and two methods were presented to solve the over-actuated system. Next, incremental based velocity controller was designed based on linear acceleration measurements and a simple model for the lift and thrust controlling forces. The WLS control allocation solver was introduced to the velocity controller in order to integrate nacelle control. In the end a global velocity controller was designed to steer the aircraft from helicopter mode to fixed wing mode and back.

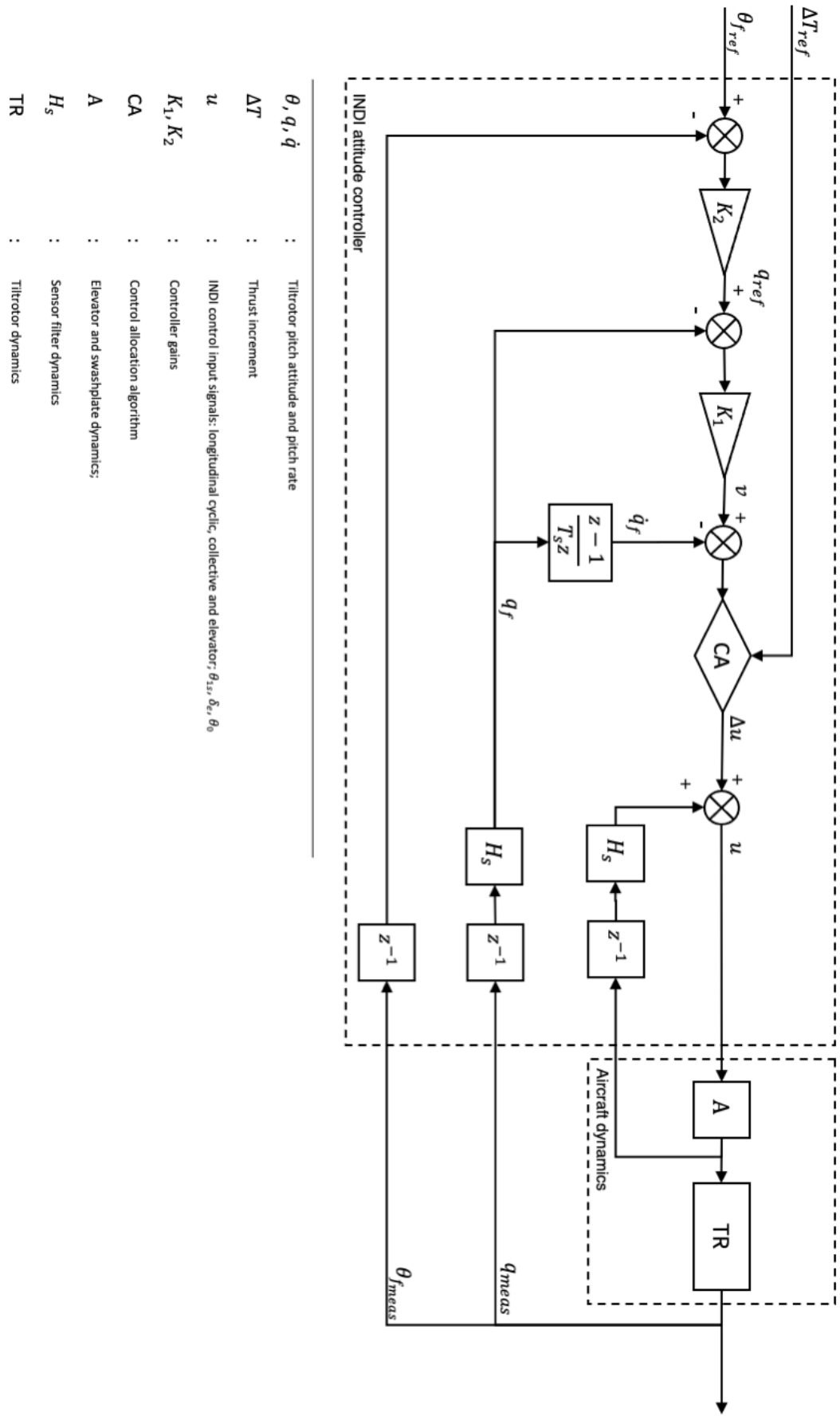

Figure 5.3: INDI attitude controller scheme for 3-DOF.

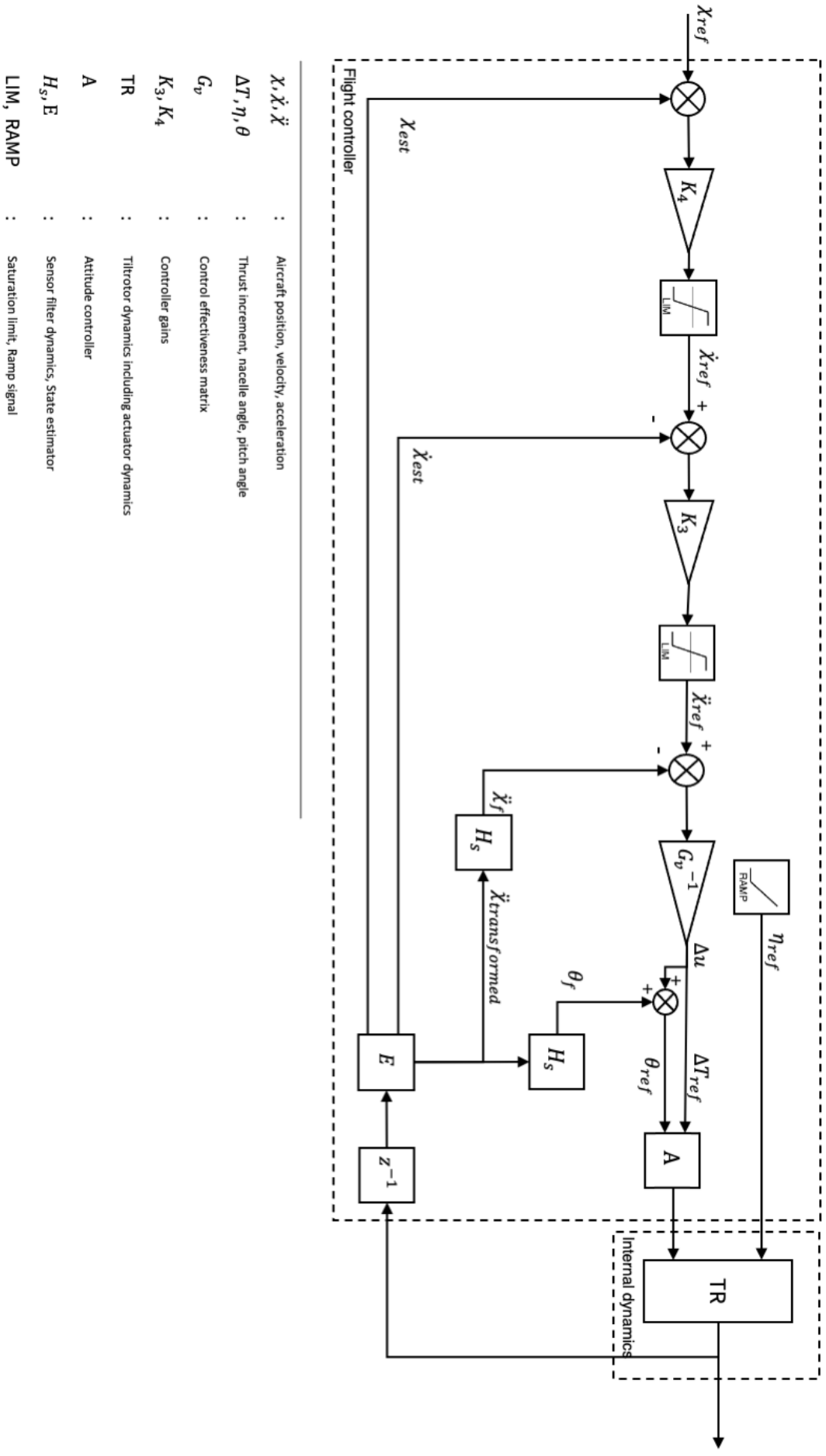

$\chi, \dot{\chi}, \ddot{\chi}$	:	Aircraft position, velocity, acceleration
$\Delta T, \eta, \theta$	:	Thrust increment, nacelle angle, pitch angle
G_v	:	Control effectiveness matrix
K_3, K_4	:	Controller gains
TR	:	Tiltrotor dynamics including actuator dynamics
A	:	Attitude controller
H_s, E	:	Sensor filter dynamics, State estimator
LIM, RAMP	:	Saturation limit, Ramp signal

Figure 5.4: INDI velocity controller with isolated Nacelle control.

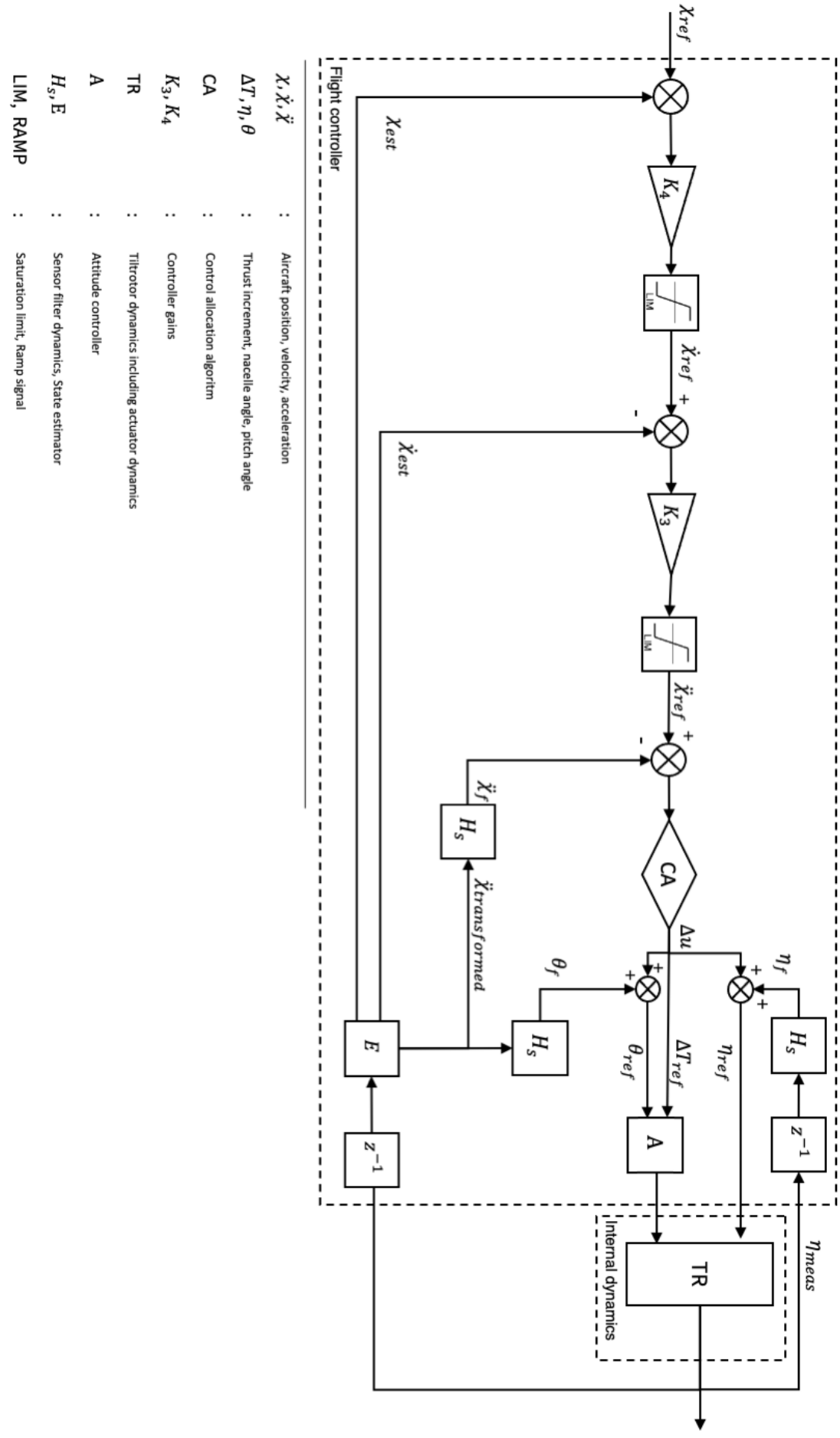

$\chi, \dot{\chi}, \ddot{\chi}$	:	Aircraft position, velocity, acceleration
$\Delta T, \eta, \theta$	:	Thrust increment, nacelle angle, pitch angle
CA	:	Control allocation algoritm
K_3, K_4	:	Controller gains
TR	:	Tiltrotor dynamics including actuator dynamics
A	:	Attitude controller
H_s, E	:	Sensor filter dynamics, State estimator
LIM, RAMP	:	Saturation limit, Ramp signal

Figure 5.5: INDI velocity controller with integrated Nacelle control.

6

Incremental Backstepping

This chapter discusses the derivation and design of an incremental backstepping attitude controller. First, the control laws are derived using a system of equations describing the plant behaviour together with Control Lyapunov Functions. Second, command filters are introduced to simplify the analytic expressions of the control laws. Next the control scheme is specified in detail, describing how it is implemented in the case of the 3-DOF tiltrotor model. Lastly, the attitude controller is expanded to also take into account thrust increment inputs and the control allocation problem is shortly discussed.

6.1. Control law derivation

By defining the system of equations governing the behaviour of the plant, the backstepping control laws can be derived in a recursive manner. The derivation relies a detailed mathematical proof concerning the stability characteristics of dynamical systems. This is explained extensively in the work of [30] and is for now left out of the current description.

$$\underline{\dot{x}}_1 = f_1(\underline{x}) + g_1(\underline{x})\underline{x}_2 \tag{6.1}$$

$$\underline{\dot{x}}_2 = f_2(\underline{x}) + g_2(\underline{x})\underline{u} \tag{6.2}$$

The goal is to design an attitude controller. The first equation will describe the kinematic relations between the body rates and the inertial Euler angles. This 3-DOF model only describes longitudinal motions. This means that $\underline{x}_1 = [\theta_f]$. The second equation describes the dynamics of the aircraft and relates control inputs of $\underline{u} = [\theta_0, \theta_{1s}, \delta_e]^T$ to the rotational rate $\underline{x}_2 = q$. To design an incremental controller, similarly to what was done in the previous chapter, the second equation needs to be reformulated by performing a Taylor series expansion operation.

$$\begin{aligned}\underline{\dot{x}}_2 =& f_2(\underline{x}) + g_2(\underline{x})\underline{u} \\ =& \underline{\dot{x}}_0 + F_2\left(\underline{x}_0, \underline{u}_0\right)\left(\underline{x} - \underline{x}_0\right) + G\left(\underline{x}_0, \underline{u}_0\right)\left(\underline{u} - \underline{u}_0\right) \\ =& \underline{\dot{x}}_{2,0} + F_2(\underline{x} - \underline{x}_0) + G_c\Delta\underline{u}\end{aligned} \tag{6.3}$$

In the above formulation, the higher order terms of the Taylor series expansion are ignored. The subscript zero indicates states of the previous timestep. F is the linearized term with respect to x and G_c is the linearized term with respect to u using the same notation as the previous chapter. Because x_1 and x_2 are both scalars, the vector notation will be dropped from here on:

The following error states z_1 and z_2 are introduced:

$$z_1 = x_1 - x_{1,des} \tag{6.4}$$

and

$$z_2 = x_2 - x_{2,des} \tag{6.5}$$

The goal behind the derivation of the first control law α is to force the error z_1 to zero by making the system of equation 6.4 asymptotically stable. This is done with via the Control Lyapunov Function (CLF). The CLF for this subsystem is defined as:

$$V_1 = \frac{1}{2} z_1 z_1 \tag{6.6}$$

with its time-derivative defined as:

$$\dot{V}_1 = z_1 \dot{z}_1 \tag{6.7}$$

and the derivative of the error $\dot{z}_1$ is:

$$\dot{z}_1 = f_1(x) + g_1(x) x_2 - \dot{x}_{1,des} \tag{6.8}$$

To guarantee asymptotic stability of the error z_1, the derivative of V_1 must be made non-positive when $x_2 = \alpha$. This means:

$$\dot{V}_1 = z_1 \left(f_1(x) + g_1(x)\alpha - \dot{x}_{1,des} \right) \leq 0 \tag{6.9}$$

Now using the above inequality as design constraint, the control law for α can be designed. One solution for α is if the term in brackets equals $-c_1 z_1$ with the gain $c_1 > 0$. This would render the complete expression globally negative. Carrying out the algebra, α must be:

$$\alpha = \frac{1}{g_1} \left(-c_1 z_1 - f_1(x) + \dot{x}_{1,des} \right) \tag{6.10}$$

This is not the only solution for α. More optimal solutions may exist and depend on the dynamics in $f_1(x)$ and $g_1(x)$ but also on the choice of V_1 as the CLF. The control law of equation 6.10 is dependent on the kinematic relations, and on the derivative of the control signal $x_{1,des}$. This signal has to be derived at some point.

Now that the first control law has been derived, the controller can be expended to take into account the dynamics of equation 6.2. Similarly to the first stage, a CLF is constructed to take into account the error dynamics of z_2 and render these to zero. The task is now to find a control law for Δu that ensures that z_2 converges to zero. Remembering that $x_{2,des}$ is actually the previously calculated control signal α, this means that x_2 converges to its desired value α. To find the stabilizing function of Δu a CLF for the entire system (i.e. equation 6.4 and 6.5) is needed. The CLF of the previous stage is used and amended to also penalize the error z_2 like so:

$$V_2 = V_1 + \frac{1}{2} z_2 z_2 \tag{6.11}$$

The error dynamics of z_2 are defined as:

$$\begin{aligned} \dot{z}_2 =& \dot{x}_2 - \dot{x}_{2,des} \\ =& f_2(x) + G_c(x) u - \dot{\alpha} \end{aligned} \tag{6.12}$$

The derivative of α with respect to time is defined as:

$$\begin{aligned} \dot{\alpha} =& \frac{\partial \alpha}{\partial x_1} \dot{x}_1 + \frac{\partial \alpha}{\partial x_{1,des}} \dot{x}_{1,des} + \frac{\partial \alpha}{\partial \dot{x}_{1,des}} \ddot{x}_{1,des} \\ =& -\frac{c_1}{g_1} \dot{x}_1 + \frac{c_1}{g_1} \dot{x}_{1,des} + \frac{1}{g_1} \ddot{x}_{1,des} \\ =& -\frac{c_1}{g_1} \left(f_1 + g_1 (z_2 + \alpha) \right) + \frac{c_1}{g_1} \dot{x}_{1,des} + \frac{1}{g_1} \ddot{x}_{1,des} \end{aligned} \tag{6.13}$$

Now that the dynamics of z_2 have been defined, the CLF of equation 6.11 can be used to find the constraints on the design of the control law for u. Just as with the previous design stage, Again, the derivative of the CLF must be negative to ensure asymptotic stability of z_1 and z_2.

$$\begin{aligned}\dot{V}_2 =& \dot{V}_1 + z_2\dot{z}_2 \\ =& \dot{V}_1 + z_2\left[\dot{x}_2 - \dot{\alpha}\right] \\ =& \dot{V}_1 + z_2\left[\dot{x}_{2,0} + F_2(x - x_0) + G_c\Delta u - \dot{\alpha}\right] \\ =& \frac{\partial V_1}{\partial z_1}z_1 + z_2\left[\dot{x}_{2,0} + F_2(x - x_0) + G_c\Delta u - \dot{\alpha}\right] \\ =& \frac{\partial V_1}{\partial z_1}\left(f_1(x) + g_1(z_2 + \alpha) - \dot{x}_{1,des}\right) + z_2\left[\dot{x}_{2,0} + F_2(x - x_0) + G_c\Delta u - \dot{\alpha}\right] \\ =& z_1\left(f_1(x) + g_1\alpha - \dot{x}_{1,des}\right) + z_2\left[z_1g_1 + +F_2(x) + G_c\Delta u - \dot{\alpha}\right]\end{aligned} \tag{6.14}$$

The first term of $\dot{V}_2$ is already negative by the choice of α (See equation 6.9). The second term can be made negative with the appropriate choice for Δu. For example, if the part within square brackets equals $-c_2z_2$, with $c_2 > 0$, the second term is forced negative. Carrying out the algebra, Δu becomes:

$$\Delta u = \frac{1}{G_2}\left(-c_2z_2 - g_1z_1 - \dot{x}_{2,0} - F_2(x - x_0) + \dot{\alpha}\right) \tag{6.15}$$

At this point, the timescale separation assumption can be made. When assuming that the states in x progress slower than u and the effect of F_2 is much smaller than of G_c, the slower dynamics can be disregarded ($F_2(x - x_0) \approx 0$) [6]. The result of the assumption is the final control law for Δu as shown in equation 6.16.

$$\Delta u = \frac{1}{G_c}\left(-c_2z_2 - g_1z_1 - \dot{x}_{2,0} + \dot{\alpha}\right) \tag{6.16}$$

The final control input u can then be calculated via:

$$u = u_0 + \Delta u \tag{6.17}$$

The result from equation 6.16 is no longer dependent on complex aerodynamic effects in F_2 but only on the measured acceleration $\dot{x}_{2,0}$ and depends only on the control effectiveness in G_c and kinematic relations from equation 6.1. The dependency is not only directly noticeable via the term g_1z_1 but also indirectly via the derivative of the previous control law α (see equation 6.13). The signal $\dot{\alpha}$ complicates the expression for Δu by not only being dependent on kinematics, but even more on the first and second derivative of $x_{1,des}$.

6.2. Command filtering

To alleviate the need to differentiate the command signal $x_{1,des}$ two times. A command filter (single-input-multi-output) will be used to obtain $\dot{x}_{1,des}$ and $\dot{\alpha}$. Instead of differentiating the command signal which makes the controller susceptible to noise, a filter structure is more robust since it only performs integration. Similar to the implementation as shown in [51], the control signal α will be filtered and the effect of the filter will be compensated such that the stability properties of the backstepping control laws are maintained. Two extra variables are defined to calculate the compensated signal:

$$\bar{z}_1 = z_1 - \chi_1 \tag{6.18}$$

with,

$$\dot{\chi}_1 = -c_1\chi_1 + g_1\left(x_{2,c} - \alpha\right) + g_1\chi_2 \tag{6.19}$$

$$\dot{\chi}_2 = -c_2\chi_2 + g_2\left(u_{pred} - u_{des}\right) + g_1\chi_2 \tag{6.20}$$

The variable $\bar{z}_1$ is the compensated tracking error and is obtained by removing the filtered unachieved portion of α. The unachieved portion of α is estimated with the filter of equation 6.19. The actuator dynamics and actuator limits are also considered a filter and are used to derive the compensator χ_2. In this case Δu_{pred} refers to the predicted increment of the actuator (due to actuator dynamics) and Δu_{des} is the intended actuator increment. A graphic overview of the compensation estimator is provided in figure 6.2.

Now, instead of using only z_1 in the calculation of the increment in u, the filter corrected value $\bar{z}_1$ from equation 6.18 is taken into account as well:

$$\Delta u = G_c^{-1}\left(-c_2 z_2 - g_1 \bar{z}_1 - \dot{x}_{2,0} + \dot{x}_{2,c}\right) \tag{6.21}$$

Notice here that the analytically derived expression of $\dot{\alpha}$ is replaced by $\dot{x}_{2,c}$ which is one of the two outputs of the command filter that filters α.

The structure of the command filter is as follows:

$$\begin{bmatrix} \dot{q}_1 \\ \dot{q}_2 \end{bmatrix} = \begin{bmatrix} q_2 \\ 2\zeta\omega_n\left(S_R\left\{\frac{\omega_n^2}{2\zeta\omega_n}\left[S_M\left(x_c^o\right) - q_1\right]\right\} - q_2\right) \end{bmatrix} \tag{6.22}$$

$$\begin{bmatrix} x_c \\ \dot{x}_c \end{bmatrix} = \begin{bmatrix} q_1 \\ q_2 \end{bmatrix} \tag{6.23}$$

where $S_M()$ and $S_R()$ are magnitude and rate limit functions and both behave like:

$$S_M(x) = \begin{cases} M & \text{if} \quad x \geq M \\ x & \text{if} \quad |x| < M \\ -M & \text{if} \quad x \leq -M \end{cases} \tag{6.24}$$

If the input signal x_c^0 is bounded, then x_c and $\dot{x}_c$ are bounded and continuous as well. Notice again that $\dot{x}_c$ is obtained without differentiation. When it is desired to limit the state x_c within some envelope defined by S_M and/or S_R the command filter ensures that these constraints will be met. If the objective of the command filter is only to compute x_c and $\dot{x}_c$, then M and R can be set infinitely large and are therefore not effective. When the command filter is operating in the linear range, the dynamics represented in state space are:

$$\begin{bmatrix} \dot{q}_1 \\ \dot{q}_2 \end{bmatrix} = \begin{bmatrix} 0 & 1 \\ -\omega_n^2 & -2\zeta\omega_n \end{bmatrix}\begin{bmatrix} q_1 \\ q_2 \end{bmatrix} + \begin{bmatrix} 0 \\ \omega_n^2 \end{bmatrix} x_c^o \tag{6.25}$$

In the form of a transfer function the command filter becomes familiar again:

$$\frac{X_c(s)}{X_c^o(s)} = \frac{\omega_n^2}{s^2 + 2\zeta\omega_n s + \omega_n^2} \tag{6.26}$$

The structure of the command filter is of a second order low-pass filter when command limiting is not in effect. The error $x_c - x_c^o$ can be made arbitrarily small by selecting a ω_n sufficiently larger than the bandwidth of the signal x_c^o [71]. A graphic overview of the command filter structure is provided in figure 6.1.

6.3. Implementation on nonlinear model

Now that the structure of the incremental backstepping controller has been derived, it can be applied to the specific case of attitude control for the 3-DOF model. Starting with the kinematic equation from 6.1. These kinematics are deterministic and fully known and can be written quite simply as a scalar unitary gain since the motion is only longitudinal and fuselage pitch angle progresses linearly with the body pitch rate q. They can thus be written as:

$$\dot{\theta}_f = 0 + 1 \cdot q \tag{6.27}$$

The dynamics of the aircraft have been written in Taylor series form in equation 6.3. Where x_2 is the pitch rate q and $\underline{u} = [\theta_0, \theta_{1s}, \delta_e]^T$. The parameters in F_2 are disregarded at this point since they are not required for calculating the control inputs.

$$\dot{q} = \dot{q}_0 + F_2(x - x_0) + G_c\Delta\begin{bmatrix} \theta_0 \\ \theta_{1s} \\ \delta_e \end{bmatrix} \tag{6.28}$$

The first control law α is specified like so:

$$\begin{aligned}\alpha =& \frac{1}{g_1}\left(-c_1 z_1 - f_1(x) + \dot{x}_{1,des}\right)\\ =& -c_1(\theta_f - \theta_{f,c}) + \dot{\theta}_{f,c}\end{aligned} \tag{6.29}$$

Where the subscript $_c$ indicates that these command signals are derived from a command filter. The second control law Δu was derived in equation 6.16 can be specified like:

$$\begin{aligned}\Delta u =& G_c^{-1}\left(-c_2 z_2 - g_1 \bar{z}_1 - \dot{x}_{2,0} + \dot{x}_{2,c}\right)\\ =& G_c^{-1}\left(-c_2\left(q - q_c\right) - \bar{z}_1 - \dot{q} + \dot{q}_c\right)\end{aligned} \tag{6.30}$$

The compensated tracking error $\bar{z}_1$ can be calculated via:

$$\bar{z}_1 = \theta_f - theta_{f,c} - \chi_1 \tag{6.31}$$

The unachieved portion of α is found by integrating the next signal:

$$\dot{\chi}_1 = -c_1\chi_1 + (q_c - \alpha) + \chi_2 \tag{6.32}$$

$$\dot{\chi}_2 = -c_2\chi_2 + G_c\left(\Delta u_{pred} - \Delta u_{des}\right) \tag{6.33}$$

Because this is an incremental method based pitch accelerations in stead of complex model information, the pitch accelerations need to be derived from pitch rate measurements. Just as with the INDI-control scheme, the pitch accelerations are derived by first filtering the pitch rate measurements with a low-pass second order filter after which the signal is differentiated with a two-point backward difference method as was presented in equation 5.17. The lag that is introduced by these two operations needs to be accounted for in the incremental control law. This means that just as with the INDI-controller, the actuator position feedback needs to be synchronized with the lag that has been introduced elsewhere in the system.

6.4. Thrust integration and control allocation

Up to this point the design only concerned the control of the attitude of the aircraft. However as with the INDI control scheme, the thrust also needs to be controlled. This is done at the same place as was done before, since the velocity controller outputs are unchanged and still request ΔT.

$$\Delta\begin{bmatrix}\theta_0\\ \theta_{1s}\\ \delta_e\end{bmatrix} = G_c^{-1}\begin{bmatrix}\Delta T\\ \left(-c_2\left(q - q_c\right) - \bar{z}_1 - \dot{q} + \dot{q}_c\right)\end{bmatrix} \tag{6.34}$$

The matrix G_c has the same entries as equation 5.6 and is repeated here for simplicity:

$$G_c = \begin{bmatrix}G_{T,\theta_0} & G_{T,\theta_{1s}} & G_{T,\delta_e}\\ G_{q,\theta_0} & G_{q,\theta_{1s}} & G_{q,\delta_e}\end{bmatrix} \tag{5.6}$$

Again the same problem arises as with the INDI-controller. The matrix G_c is not square and can therefore not be inverted in a trivial way. Control allocation is thus required to coordinate the control efforts between the the actuators. The same algorithms can be considered here. The weighted pseudo-inverese method (**WIP**) and the Weighted Least Squares method (**WLS**) are both applicable and allow the over-actuated system to find a solution within constraints and preferences (priorities). When the desired control increments are calculated via the CA the control inputs signal are found via in the same way as before:

$$\begin{bmatrix}\theta_0\\ \theta_{1s}\\ \delta_e\end{bmatrix} = \begin{bmatrix}\theta_0\\ \theta_{1s}\\ \delta_e\end{bmatrix}_0 + \Delta\begin{bmatrix}\theta_0\\ \theta_{1s}\\ \delta_e\end{bmatrix} \tag{6.35}$$

A complete scheme is presented in figure 6.3.

In this chapter an incremental backstepping attitude controller was derive for the XV-15 tiltrotor configuration. Command filters were implemented to simplify the analytic expressions of the control law. Two control allocation algorithms were proposed to solve the over-actuated system.

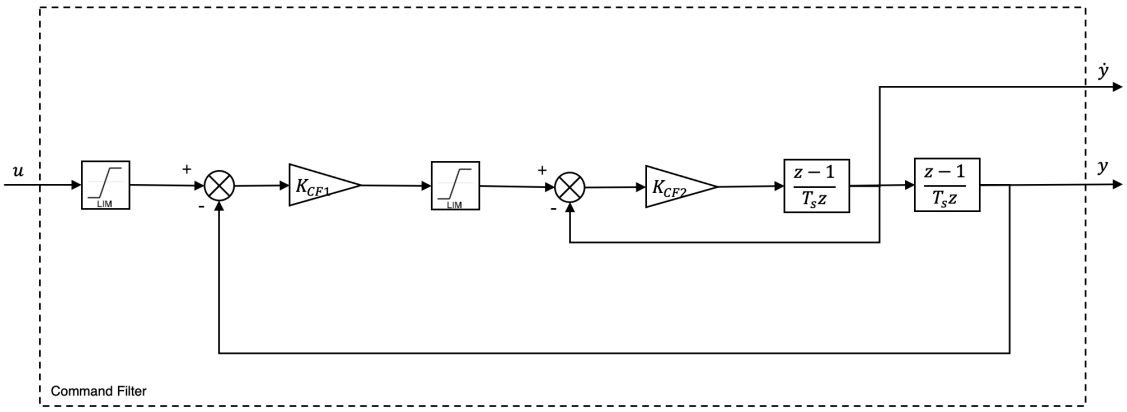

$u, y, \dot{y}$	:	Filter input, filtered output, filtered derivative
K_{CF1}	:	$2\zeta\omega_n$
K_{CF2}	:	$\frac{\omega_n^2}{2\zeta\omega_n}$
ζ, ω_n	:	Filter parameters
LIM	:	Magnitude and rate limits

Figure 6.1: IBKS command filter structure

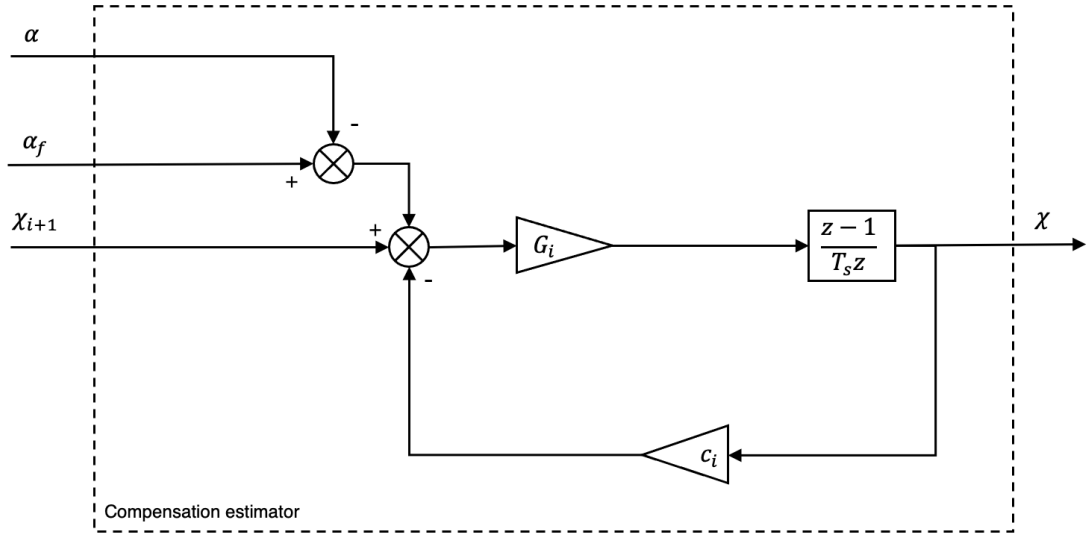

α, a_f	:	True command signal, Filtered command signal
G_i	:	Control derivative of the ith system
c_i	:	Controller gain for the ith system
χ	:	Compensation estimate

Figure 6.2: IBKS compensation estimator

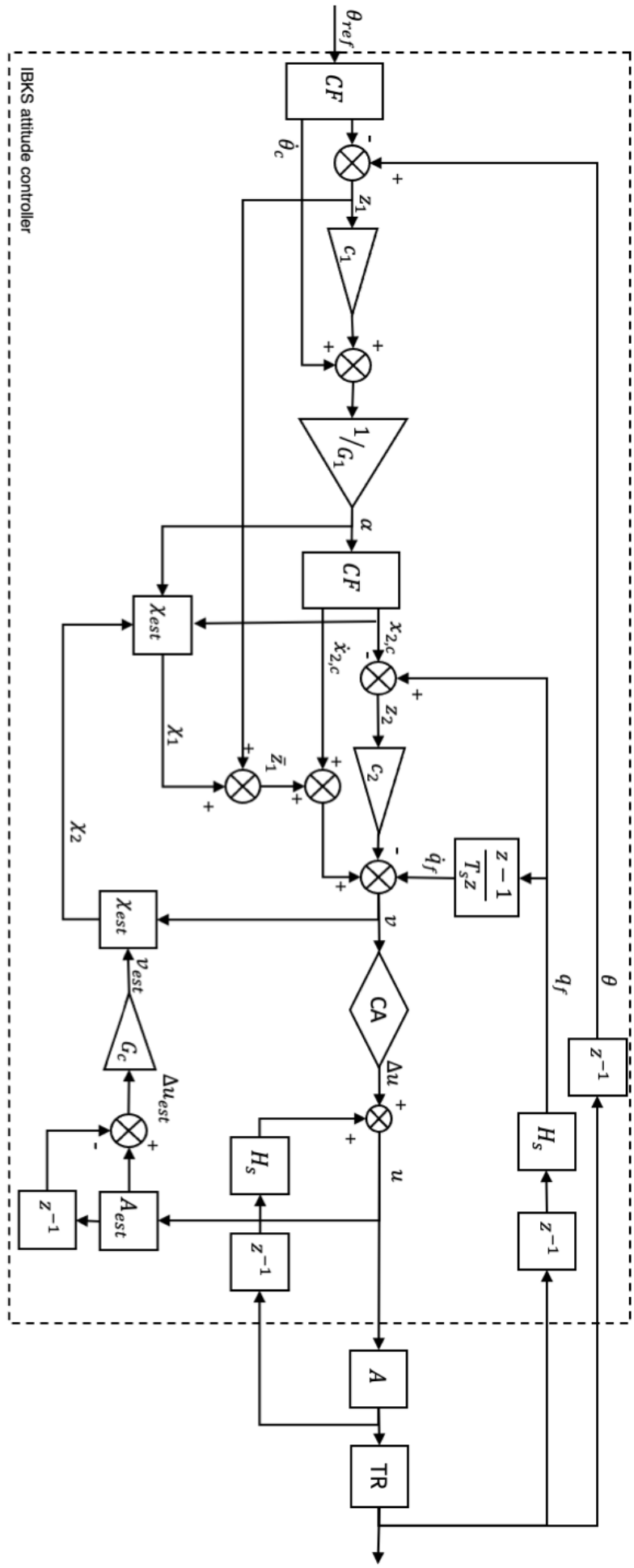

θ, q	:	Aircraft pitch attitude, pitch rate	CA	:	Control allocation algorithm		
u, u_{est}	:	IBKS control inputs, longitudinal cyclic, collective and elevator; θ_{1s}, δ_e, θ_0, Estimated control inputs	G_i	:	Control effectiveness of the ith system	c_1, c_2	: IBKS gains
χ_{est}	:	Compensation estimator	v, v_{est}	:	Virtual input, Estimated virtual input	H_s	: Sensor filter
χ_i	:	Compensation estimate for the ith system	$z_i, \bar{z}_i$	:	Error states, Compensated error states	A, A_{es}	: Actuator dynamics, Estimated actuator dynamics

Figure 6.3: IBKS attitude controller scheme for 3-DOF

7

Tuning and testing

The control methods that were derived in the previous chapters have been implemented on the longitudinal nonlinear model. In this chapter, the performance of the different controllers will be evaluated.

First, the attitude control allocation algorithms will be tuned, compared and tested in different flight conditions. Second, the INDI and IBKS attitude controllers are compared. Finally, the velocity controller will be tested in different flight conditions and with different transition strategies.

7.1. Attitude control allocation

The previous chapters have presented two methods to solve the control problem of the over-actuated system. To control the two axis of the attitude controller, namely the thrust ΔT and the pitch dynamics of q there are three actuators available, resulting in a non-square control effectiveness matrix as was shown in equation 5.6.

$$G_c = \begin{bmatrix} G_{T,\theta_0} & G_{T,\theta_{1s}} & 0 \\ G_{q,\theta_0} & G_{q,\theta_{1s}} & G_{q,\delta_e} \end{bmatrix} \tag{5.6}$$

In this section the Weighted Least Squares (WLS) allocation algorithm is tuned and tested and compared against Weighted Pseudo Inverse method (WPIM) which is regarded as a baseline. The WLS algorithm allows tuning via the cost function of equation 5.10. The algorithm can prioritize a specific axis over another with the weights in W_v and it can prioritize the use of a specific actuator over others with the weights in W_u.

The matrix of equation 5.6 is populated with the control derivatives from the linearization results of section 4.4. For the tuning of the control allocation algorithm, the entries in the matrix G_c are scheduled using flight speed V_∞ and the mast angle η.

The focus of the tuning effort of the WLS solver is on the control of the pitch axis. The thought behind this is that in the case of actuator saturation, it is more desirable to remain in control over the attitude of the aircraft then in control over the thrust. In both hover and fixed wing flight, control over the attitude of the aircraft is crucial to remain stable and it may therefore be beneficial to give up in exchange propulsive control.

In general, the controllability of the pitch axis is in hands of the longitudinal cyclic and elevator for which they have been designed. However, in section 4.4 it was noticed that the effectiveness of the longitudinal cyclic control is very weak and could even cross over (control reversal) in the middle of the conversion corridor as can be seen in figure 4.1. At low airspeeds, the elevator is also less effective due to the low dynamic pressure. When the control effect of an actuator is low, the risk of saturation becomes higher which can lead to loss of control. In such a situation it can thus be beneficial to coordinate the control effort and also use the collective input to remain in control. In the case of incremental control this means that the required action on the pitch acceleration or virtual control v should be distributed over all three actuators in stead of only θ_{1s} and δ_e. This can be forced or "tuned" via the matrix W_v and the structure of G_c.

When tuning for prioritization of axes, the dynamics of the solver have to be taken into account. The objective of the solver is to minimize the cost function of equation 5.10. When considering $W_v = I$, the control part of the objective function is minimized based only on the control derivatives in G_c. However,

the order of magnitude of the thrust derivatives compared to pitch derivatives is very large. $T_{\theta_{1s}}$ and $T_{\theta_0} \approx 5 \cdot 10^5$ while M_{θ_0}, $M_{\theta_{1s}}$ and $M_{\delta_e} \approx 5$ as can be seen from figures 4.1, 4.2 and 4.3. This means that the cost function in this configuration is relatively sensitive to changes in Δu on the thrust axis. A unit increment of the collective or longitudinal cyclic costs in the order of 10^5 in the thrust axis. The same unit increment may only decrease the cost in the order of 10^0 on the pitch axis. Basically, with a weighting matrix of equal weights ($W_v = I$), the WLS algorithm will find a solution to satisfy the requested control action on ΔT first and only then solve for q even if the required effort in v is not reached and actuators are clipped.

$$\Delta \underline{u} = \arg \min_{\Delta \underline{u}_{min} \leq \Delta \underline{u} \leq \Delta \underline{u}_{max}} \gamma \left\| W_v (G_c \Delta \underline{u} - \begin{bmatrix} \Delta T \\ v - \dot{q}_0 \end{bmatrix}) \right\|^2 + \left\| W_u \left(\Delta \underline{u} - \Delta \underline{u}_p \right) \right\|^2 \tag{5.10}$$

The sensitivity to these aircraft dynamics can be adjusted with the W_v matrix and can be tuned by observing that the derivative of the objective function with respect to Δu is dependent on the product of $W_v \cdot G_c$ as shown in equation 7.1. To equalize or prioritize the sensitivity of the two axis, the ratio of control effectiveness per actuator should be equal. A unit increment in collective should change the cost of the objective function based on the ΔT error with the same speed as it would change the cost based on the error in pitch.

$$\frac{\partial cost}{\partial \Delta u} \propto W_v \cdot G_c = \begin{bmatrix} w_T & 0 \\ 0 & w_q \end{bmatrix} \cdot \begin{bmatrix} G_{T,\theta_0} & G_{T,\theta_{1s}} & 0 \\ G_{q,\theta_0} & G_{q,\theta_{1s}} & G_{q,\delta_e} \end{bmatrix} = \begin{bmatrix} w_T G_{T,\theta_0} & w_T G_{T,\theta_{1s}} & 0 \\ w_q G_{q,\theta_0} & w_q G_{q,\theta_{1s}} & w_q G_{q,\delta_e} \end{bmatrix} \tag{7.1}$$

The entries w_T and w_q are coupled when the goal is to achieve a certain sensitivity ratio across the collective and cyclic actuators. This means one weight can be fixed to 1. In this case w_q is set to 1. The sensitivity ratio is expressed as the weight on thrust and pitch as $\frac{p_T}{p_q}$.

$$\frac{p_T}{p_q} = w_T \left| \frac{G_{T,\theta_0}}{G_{q,\theta_0}} \right| \tag{7.2}$$

$$\frac{p_T}{p_q} = w_T \left| \frac{G_{T,\theta_{1s}}}{G_{q,\theta_{1s}}} \right| \tag{7.3}$$

Because the sensitivity is a ratio, one parameter can be set equal to one. In this case p_T is set equal to 1. For the tuning process, only the absolute value of the control effectiveness ratios is used. This is because the individual sign of the control effectiveness entries does not matter at this stage. First of all, because the weighting factors in W_v cannot be negative and second of all because the direction of individual entries does not matter as long as the rate of change with respect to Δu reflects the ratio of p_T/p_q. Solving the set of two equations for w_T leaves:

$$w_T = \begin{bmatrix} \frac{G_{T,\theta_0}}{G_{q,\theta_0}} \\ \frac{G_{T,\theta_{1s}}}{G_{q,\theta_{1s}}} \end{bmatrix}^+ \frac{1}{p_q} \begin{bmatrix} 1 \\ 1 \end{bmatrix} \tag{7.4}$$

Where the none-square matrix is inverted with a pseudo-inverse. The entries in G_c are scheduled with look-up tables so they may change throughout the flight. This means that to maintain the required sensitivity, w_T needs to be recalculated each timestep. To test what the effect is of the proposed tuning strategy based on sensitivity, four different configurations will be evaluated here. The normal sensitivity of $W_v = I$ and tuned version with $p_q = 1, 2$ and 4. Higher values of p_q implicate a higher sensitivity for the pitch axis which thus means that the pitch axis is prioritized when solving the allocation problem perhaps at the cost of thrust.

Another way of controlling the sensitivity of the algorithm is by changing the configuration of the control effectiveness matrix G_c. The matrix as shown in equation 5.6 is set up in such a way that the control allocation algorithm can coordinate a control effort using all available control power. However, a control effort does not have to be fully coordinated across all three actuators and it may be beneficial to disregard certain actuators for specific axes. For example, in the matrix G_c the control effectiveness of θ_{1s} on thrust, $G_{T,\theta_{1s}}$, could be set to zero. This would mean that the solver does not take this contribution into account when calculating actuator increments. However, leaving such information out of the matrix G_c may lead

to actuators working against each other in stead of cooperating. Different configuration of G_c that will be tested are presented in table 7.1.

G_c **ID**	**Configuration**
M1	$\begin{bmatrix} G_{T,\theta_0} & G_{T,\theta_{1s}} & 0 \\ G_{q,\theta_0} & G_{q,\theta_{1s}} & G_{q,\delta_e} \end{bmatrix}$
M2	$\begin{bmatrix} G_{T,\theta_0} & 0 & 0 \\ G_{q,\theta_0} & G_{q,\theta_{1s}} & G_{q,\delta_e} \end{bmatrix}$
M3	$\begin{bmatrix} G_{T,\theta_0} & 0 & 0 \\ 0 & G_{q,\theta_{1s}} & G_{q,\delta_e} \end{bmatrix}$
M4	$\begin{bmatrix} G_{T,\theta_0} & G_{T,\theta_{1s}} & 0 \\ 0 & G_{q,\theta_{1s}} & G_{q,\delta_e} \end{bmatrix}$

Table 7.1: Different configurations of the control effectiveness matrix that will be evaluated.

To test these two tuning methods and their combinations, a doublet pitch rate manoeuvre is simulated at the flight conditions of $V = 60m/s$ and $\eta = -60deg$. The linearization results from section 4.4 indicated that in the region of this point, there may relatively weak longitudinal cyclic and elevator control effectiveness on the pitch axis. This would therefore be an interesting scenario to test this method of prioritization.

For the simulations, the INDI controller from figure 5.3 is used with the parameters as shown in table 7.3. The attitude controller calculates a required action on pitch (v) and thrust (ΔT) to be solved by the control allocation algorithm. To evaluate the performance of the control allocation algorithm, the requested control action from the attitude controller is compared to the assigned control action by the CA solver. The comparison does not take into account the actual response of the aircraft. This deviation can then be used to compare the different controller configurations. The calculation of this metric is shown in equation 7.5 and shown graphically in figure 7.1. Notice already that with the WPIM method, the deviations between the requested effort and assigned effort will always be zero. With WPIM the actuator increment solutions are not constraint by the maximum and minimum actuator limits opposed to the WLS algorithm. So for WPIM, the requested effort is always achieved. As would be the case with the inversion of a square effectiveness matrix. Note that when the requested effort is assigned in this way, it may not be achieved because actuators may saturate before reaching their desired position.

Next to the deviation on control effort, the error in pitch rate is also evaluated to see what the eventual overall controller performance would be (See equation 7.6). The controller gain K_1 that sets the stiffness of the attitude controller on the pitch rate control, has been tuned with $G_c = M1$ and is kept the same for all evaluations.

$$\begin{bmatrix} \Delta T \\ v - \dot{q} \end{bmatrix}_{error} = \begin{bmatrix} \Delta T \\ v - \dot{q} \end{bmatrix}_{request} - \begin{bmatrix} \Delta T \\ v - \dot{q} \end{bmatrix}_{assigned} = \begin{bmatrix} \Delta T \\ v - \dot{q} \end{bmatrix}_{request} - G_c \Delta \begin{bmatrix} \theta_0 \\ \theta_{1s} \\ \delta_e \end{bmatrix} \tag{7.5}$$

$$q_{error} = q_{ref} - q \tag{7.6}$$

To test the performance a doublet maneuver is used. It starts of from a trimmed state at $V = 60m/s$ and $\eta = -60deg$ and concerns two reference signals for the controller to solve. A pitch rate signal (q_{ref}) and a thrust increment signal ΔT_{ref}. The pitch rate signal is a doublet of $25deg/s$ with a step time of $1.5sec$. The thrust increment signal is a sinusoidal signal with a frequency of $1Hz$ and an amplitude of 10^4N to simulate thrust increment request from the velocity controller. Combinations of different G_c matrices are tested against four different sensitivity parameters. The G_c configuration of M3 is only evaluated against $W_v = I$ because as shown in table 7.1, this configuration only has isolated controls of thrust and pitch, so tuning here would not make a difference. Furthermore, the sensitivity gains p_q have been chosen by initial

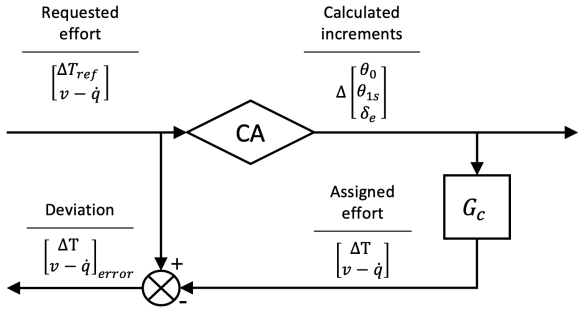

Figure 7.1: Calculation of the control deviation from the control allocation solver

.

trial and error to identify a space where there is any significant visible difference between performance. The configurations that have been evaluated are identified by the letter S and a corresponding number. They can be referenced in table 7.2.

Figure 7.2 shows the results of the pitching maneuver for configurations S1 to S4. These configurations all have the same structure of G_c but vary in their sensitivity parameter p_q. Looking at the pitch rate rates only, a difference can be observed between configuration S1 and the others. S1 is the configuration with $W_v = I$ and cannot sustain the pitch rate demand in the first step, while the rest is still able to converge to the reference signal.

Looking at the efforts of the control allocation configuration specifically, the assigned effort as calculated via equation 7.5 are shown in figures 7.3 and 7.4. Straight away it is visible that in the case of S1, the CA configuration does not fully assign the requested pitch effort to actuators. At the moment the pitch rate diverges from the reference signal in figure 7.3, the CA deviates from the requested signal. At the same time for S1, the thrust signal is followed without deviation. When the sensitivity on pitch in increases, as shown for configurations S2, S3 and S4, with $p_q = [\frac{1}{2}, 1, 5]$, the deviations in pitch decrease and the CA follows the requested effort more closesly. On the other hand as was predicted earlier, this is at the cost of the thrust deviations. The plots in figure 7.4 show that that for increasing pitch sensitiviy, the deviations on thrust increase as well. With $W_v = I$ the thrust assigned matched 100% with the requested effort, while with $p_q = 5$ in S4, large errors are visible.

Figure 7.5 shows the actual control inputs that are send to the control actuators. The plots show that in the case of configuration S1 , the pitching request indeed clips the longitudinal cyclic and elevator which causes the aircraft to deviate from the pitch rate reference signal. The CA solution deviates from the requested effort because it cannot assign anymore increments to θ_{1s} or δ_e because the constraints of the objective function are reached. The collective input for S1 appears to be unaffected by the pitch deviation. When the sensitivity on pitch is in increased, the cyclic and elevator remain clipped but the collective input signal does change in the attempt to solve the pitch request.

The analysis on pitching and thrust performance includes all configurations from table 7.2. The results are summarized in the bar chart of figures 7.6 and figure 7.7. Figure 7.6 shows the root mean square of the error over time between the requested pitch and thrust effort and the actual assigned pitch and thrust effort as calculated via equation 7.5. Figure y shows the root mean square of the error between the pitch rate reference signal q_{ref} and the actual measured aircraft pitch rated q.

From figure 7.6 it can be seen that increasing the pitch sensitivity can indeed decrease the assigning error. This trend holds for the configurations of $G_c = M1$ and $M2$, where the entry G_{q,θ_0} is included. Simultaneously, for these configurations, the thrust deviation increases when with increasing values of p_q. For the configurations where G_{q,θ_0} is not included, the pitching deviation does not become smaller or change with increasing pitch sensitivity. For the set configurations S14 to S15 no deviations are registered. This is expected since the WPIM method does include actuator constraints and thus the requested solution is always provided despite the fact that the solution over all may not be physically feasible. The WPIM configurations are included in the analysis to compare there performance when it comes to the pitch rate error.

The results from figure 7.6 indicate that there may be an optimal configuration when it comes to minimizing both the pitch deviation and thrust deviation. In this specific scenario this optimum may be the configuration of S2, where the G_c matrix is fully populated and the pitch sensitivity $p_q = 0.5$. Configuration S2 has the most information in G_c to fully coordinate the pitch and thrust effort among the three actuators.

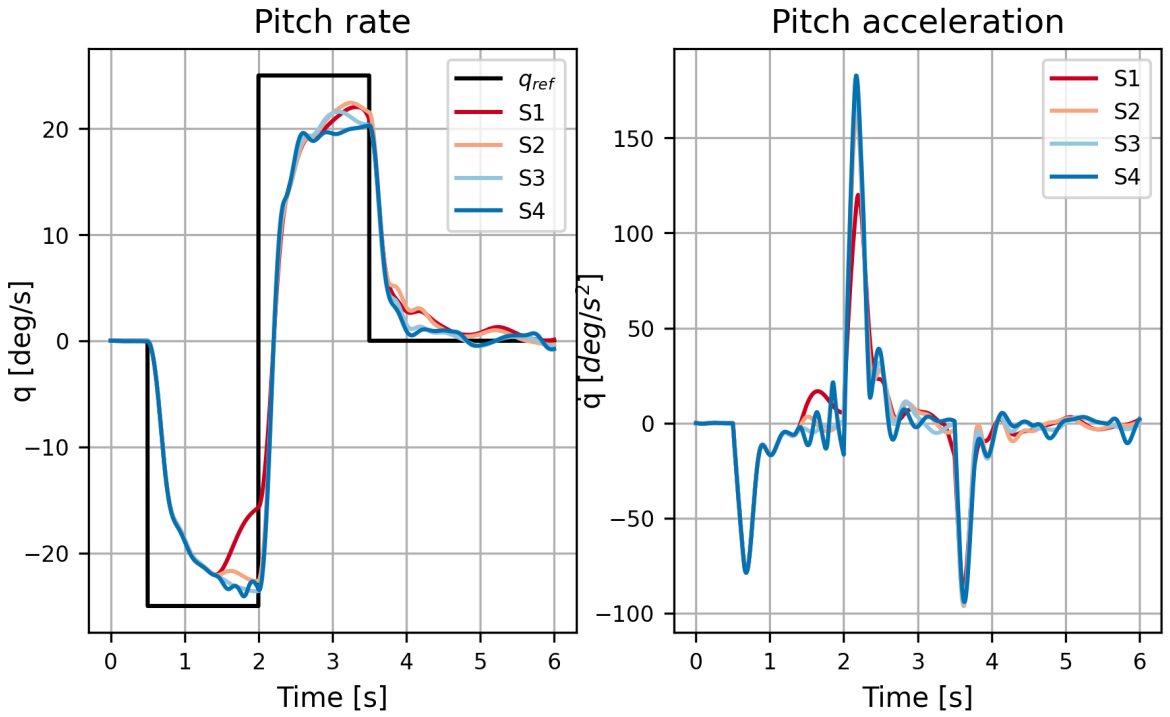

Figure 7.2: Pitching maneuver with configurations S1, S2, S3 and S4. at $V = 60m/s$ and $\eta = -60deg$

.

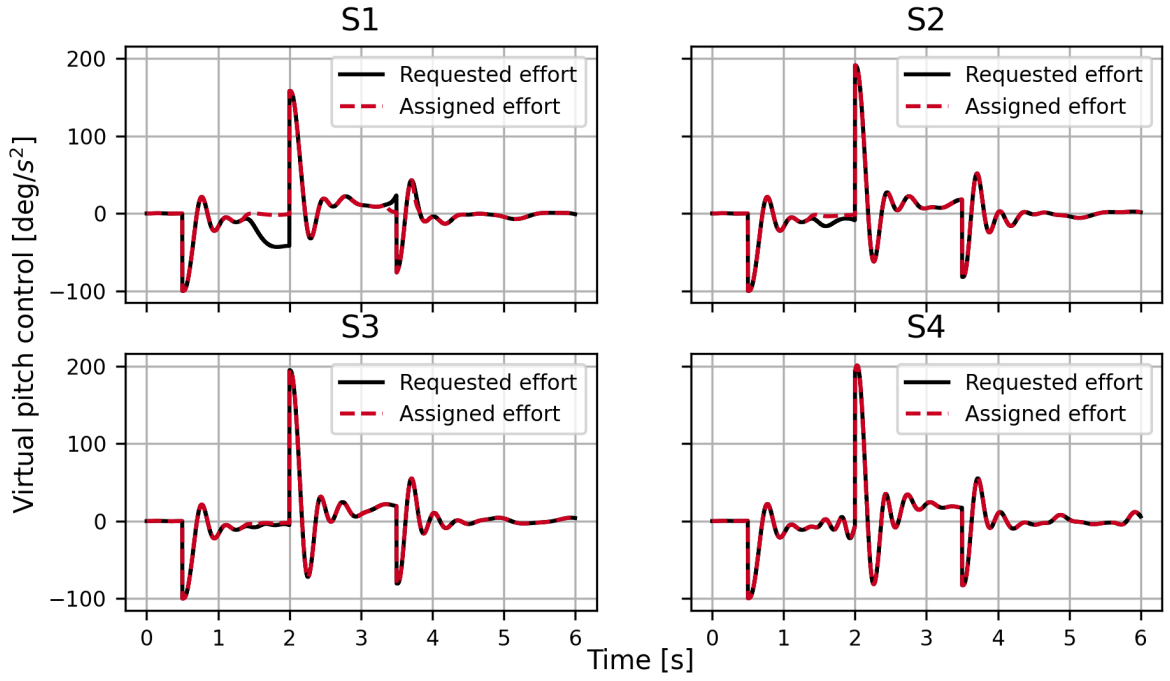

Figure 7.3: Pitching maneuver with configurations S1, S2, S3 and S4. at $V = 60m/s$ and $\eta = -60deg$

.

Configuration ID	**CA solver**	p_q	W_v	G_c **configuration**
S1	WLS	N/A	$\begin{bmatrix}1 & 0\\0 & 1\end{bmatrix}$	M1
S2	WLS	0.5	w_T see eq. 7.4 ; $w_q = 1$	M1
S3	WLS	1	w_T see eq. 7.4 ; $w_q = 1$	M1
S4	WLS	5	w_T see eq. 7.4 ; $w_q = 1$	M1
S5	WLS	N/A	$\begin{bmatrix}1 & 0\\0 & 1\end{bmatrix}$	M2
S6	WLS	0.5	w_T see eq. 7.4 ; $w_q = 1$	M2
S7	WLS	1	w_T see eq. 7.4 ; $w_q = 1$	M2
S8	WLS	5	w_T see eq. 7.4 ; $w_q = 1$	M2
S9	WLS	N/A	$\begin{bmatrix}1 & 0\\0 & 1\end{bmatrix}$	M3
S10	WLS	N/A	$\begin{bmatrix}1 & 0\\0 & 1\end{bmatrix}$	M4
S11	WLS	0.5	w_T see eq. 7.4 ; $w_q = 1$	M4
S12	WLS	1	w_T see eq. 7.4 ; $w_q = 1$	M4
S13	WLS	5	w_T see eq. 7.4 ; $w_q = 1$	M4
S14	WPIM	N/A	N/A	M1
S15	WPIM	N/A	N/A	M2
S16	WPIM	N/A	N/A	M3
S17	WPIM	N/A	N/A	M4

Table 7.2: The different control allocation configurations are considered for tuning.

The impact this has on the actual pitch rate q is shown in figure 7.7.

From figure 7.7 it can be seen that the actual differences in pitch rate error between the different configurations is not significant. Small improvements over the result of S1 can be found when increasing sensitivity for $G_c = M1$ and $M2$. Overall, the maximum difference between results is 9%. Moreover, the WLS solver does not appear to be better performing then the WPIM solver.

From the results from figure 7.1 it was chosen to test how the configuration of S2 would perform at different flight conditions. These are in hover at ($V = 0m/s$, $\eta = 0deg$), in the corridor at ($V = 45m/s$, $\eta = -10deg$), and in fixed wing flight at ($V = 90m/s$, $\eta = -90deg$). These points are highlighted in the conversion corridor shown in figure 7.8.

The same maneuver from the CA tuning process is used to evaluate the controller performance at the specified flight conditions. The same controller parameters have been used as presented in table 7.3. The results of these tests are shown in figure 7.9.

The results from figure 7.9 are twofold. At the flight conditions $V = 60m/s$ and $V = 90m/s$, the reference signal is followed reasonably. For the case at $V = 60m/s$ this is is expected since the CA has been tuned at this point. At $V = 90m/s, \eta = -90deg$, the cyclic actuator has been phased out completely and only the collective and elevator remain to control the pitch axis. Both responses clearly converge to the reference signal.

On the other hand, the responses at $V = 0$ and $V = 45$ are not as expected. For both cases the initial response to the reference signal is even in the opposite direction after which the aircraft steers in the correct direction again. The response is oscillatory and it is not clear if the response will eventually converge back

Controller parameter	Setting	Remark
Controller run frequency	250 Hz	
Attitude controller	INDI	See figure 5.3
K_1	4 s^{-1}	
G_c entries	Scheduled	As a function of (V, η), see figures 4.1, 4.2 and 4.3
ω_s	$25s^{-1}$	
ζ_s	0.55	
γ	1000	
w_{θ_0}	1	
$w_{\theta_{1s}}$	1	
w_{δ_e}	1/5	

Table 7.3: Attitude control parameter settings that remain constant during the control allocation evaluation.

to the reference signal. To find out what may be the cause of this, the hover case of $V = 0m/s, \eta = 0deg$ is somethign someting.

The control effectiveness of the collective input to pitch is not well defined in hover. As shown in figure 4.3 the value is relatively small. To test what the influence of the collective is on the pitching dyanmics with an incremental controller a special matrix G_c is defined. In this control effectiveness matrix only the collective actuator is used to control the pitching motion of the aircraft. The matrix is shown in equation 7.7 and is referred to as CA configuration S18.

$$G_c|_{S18} = \begin{bmatrix} 0 & 0 & 0 \\ G_{q,\theta_0} & 0 & 0 \end{bmatrix} \tag{7.7}$$

Figure 7.10 shows pitch rate responses of configurations S1, S2, S9 and S18. It is clearly visible that when the pitch and thrust axis are decoupled (S1,S9), the response converges without oscillations in a predicable way. As discussed earlier, the configuration of S1 can be viewed as having decoupled control of pitch and thrust. Since the weighting matrix $W_v = I$ the sensitivities per axis are so far apart that thrust will always be solved first and only then pitch. The response of S2 is known and does not behave well. The S18 response is striking in that it does not at all appear to follow the reference signal. This may be expected since the control effectiveness is very weak. At the same time, the use of collective does influence the pitching motion. This may indicate that the control effectiveness crosses over and becomes negative in some stages. From the previous analysis in section 4.5 it was shown that if the sign between the actual aircraft's control effectiveness and the controller's estimated value is opposite, the system becomes uncontrollable. In this case. The control effectiveness of the collective has been estimated by linearizing the dynamics and looking at the control derivatives. The estimated values are then scheduled by (V and η). Although incremental control is robust against modelling mismatches, the controller in this scenario is not able to follow the reference signal.

To cope with this behaviour, for the rest of the controller evaluation in this chapter, a decoupled CA configuration is chosen. In this case the most simple configuration is chosen, namely S9 (See table 7.2). The pitch motion is only controlled with cyclic and elevator and thrust is only controlled with the collective actuator. This means that no cooperative control is applied anymore and possibly control actuators may work against each other. On the other hand, the control effectiveness for these relations are better defined.

7.2. Attitude controller

In chapters 5 and chapter 6, two attitude controllers were designed. Using the control allocation algorithm that was chosen from the previous section, these two attitude controllers are now tuned and evaluated against each other at different flight conditions.

Both the INDI controller and the IBKS controller have been tuned in hover from a trimmed state ($V = 0m/s$ and $\eta = 0deg$) against a doublet pitch maneuver without thrust commands. First the rate gains were tuned, then the outer attitude gains. The IBKS command filters have been set such that the phase lag is minimized while remaining stable at the controller run frequency of $250Hz$. The tuned parameters for

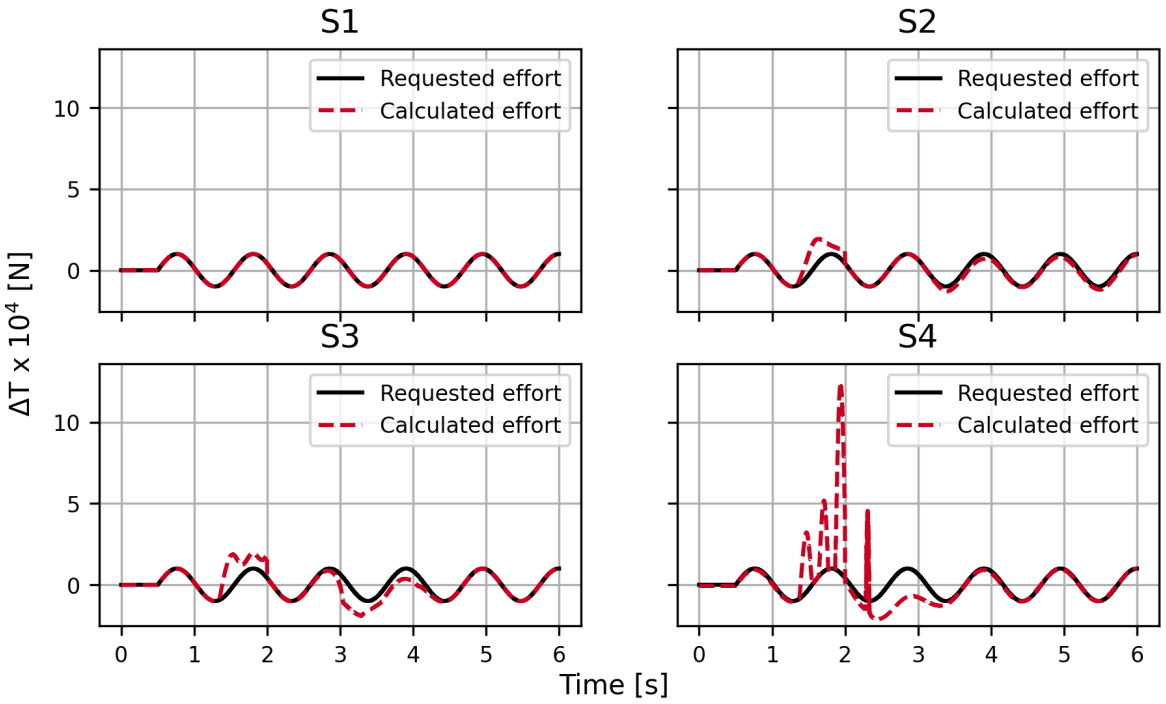

Figure 7.4: Pitching maneuver with configurations S1, S2, S3 and S4. at $V = 60m/s$ and $\eta = -60deg$

.

both controllers are presented in table 7.4. The control schemes for the INDI controller is shown in figure 5.3 and the scheme for the IBKS controller is shown in figure 6.3.

As a baseline, a standard PID controller was designed tuned and tested in hover and fixed wing flight to compare its performance to the incremental methods. The schematics of this controller are shown in figure 7.26. The hover PID controller only controls the longitudinal cyclic θ_{1s}, while the fixed wing PID controller only controls the elevator. No mixing has been implemented so these have not been applied in the conversion corridor. Tuning of the controller parameters has been done against a pitch doublet in hover.

Figure 7.11 shows the response on a pitch doublet after the three controllers have been tuned. All three have been tuned such that their pitch attitude response appear critically damped. The pitch attitude response for all three is very similar. In the pitch rate response, small overshoot is visible from the IBKS. The PID controller is more oscillatory in its rate response. The effect is also visible in the control inputs shown in figure 7.12. Both the IBKS and PID controller inputs are oscillatory while the INDI inputs remain steady.

Figures 7.13 and 7.14 show the behaviour of the controllers in the conversion corridor at ($V = 60m/s$ and $\eta = -60deg$). Only the INDI and IBKS controllers are shown since the PID controller was designed without a mixer and can therefore be used in fixed wing and helicopter mode only. Note that the controller parameters are the same as were in the previous maneuver and are shown in table 7.4. The pitch down motion is achievable by both controllers and the IBKS shows the least overshoot. The pitch up motion is unachievable by both controllers however. As can be seen from figure 7.14 the input signals to the elevator and longitudinal cyclic control are clipped and the actuators cannot provide anymore control force. Although the inputs are clipped the aircraft does move in the correct direction.

In fixed wing mode ($\eta = -90deg$), the longitudinal cylic control is completely phased out and cannot be used. This only leaves the elevator to control the pitch axis of the aircraft. Figures 7.15 and figure 7.16 show the response of the aircraft at $V = 150m/s$ and $\eta = -90$. The parameters for all three controllers are still the same as before and are shown in table 7.4.

All three controllers are able to track the reference signal. Notice especially that although the gains of the PID controller have not changed, the linear controller is still well capable of the tracking task and may even outperform the incremental controllers.

The INDI controller shows the most overshoot in both directions. Comparing this to figure 7.16, the

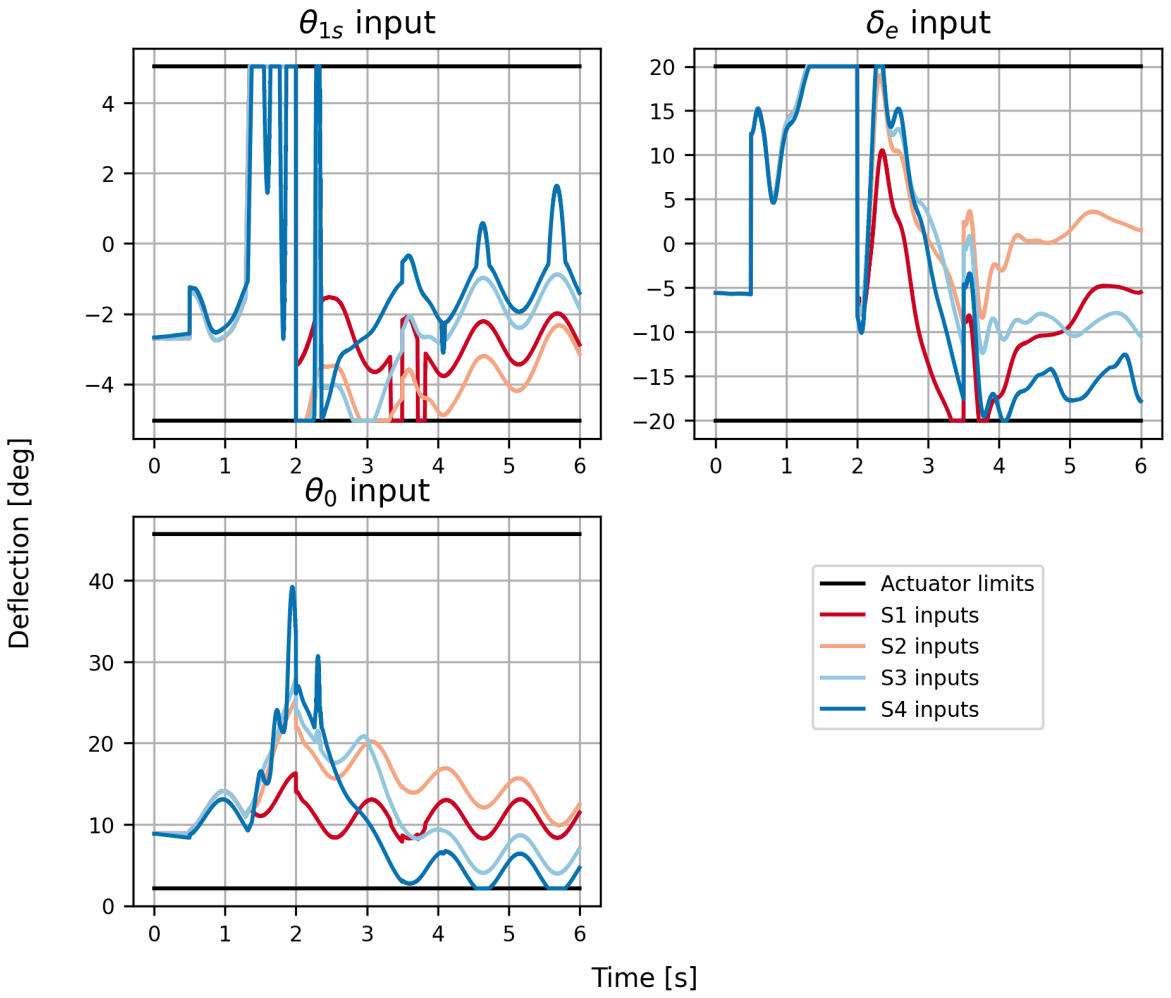

Figure 7.5: Actuator control inputs calculated for the pitching maneuver with configurations S1, S2, S3 and S4. At $V = 60m/s$ and $\eta = -60deg$

.

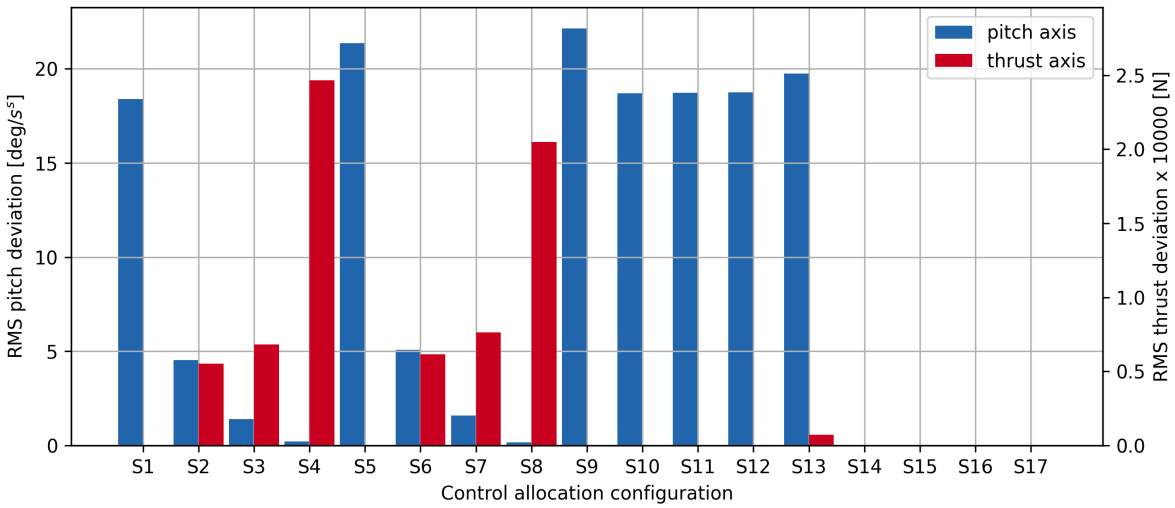

Figure 7.6: RMS of pitch and thrust assigning deviation of all controller configurations. At $V = 60m/s$ and $\eta = -60deg$

.

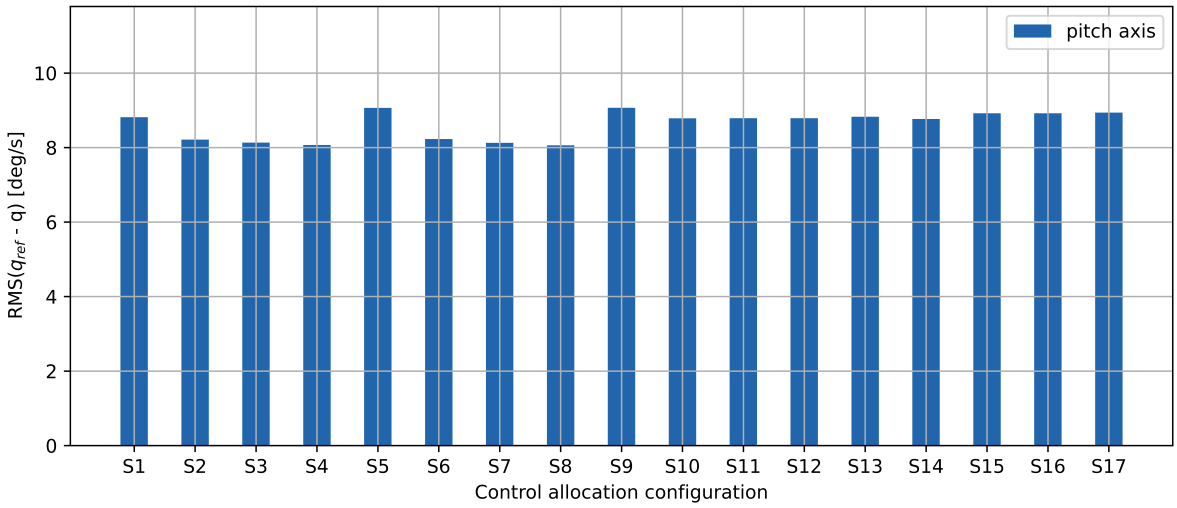

Figure 7.7: RMS of pitch rate error of all controller configurations. At $V = 60m/s$ and $\eta = -60deg$.

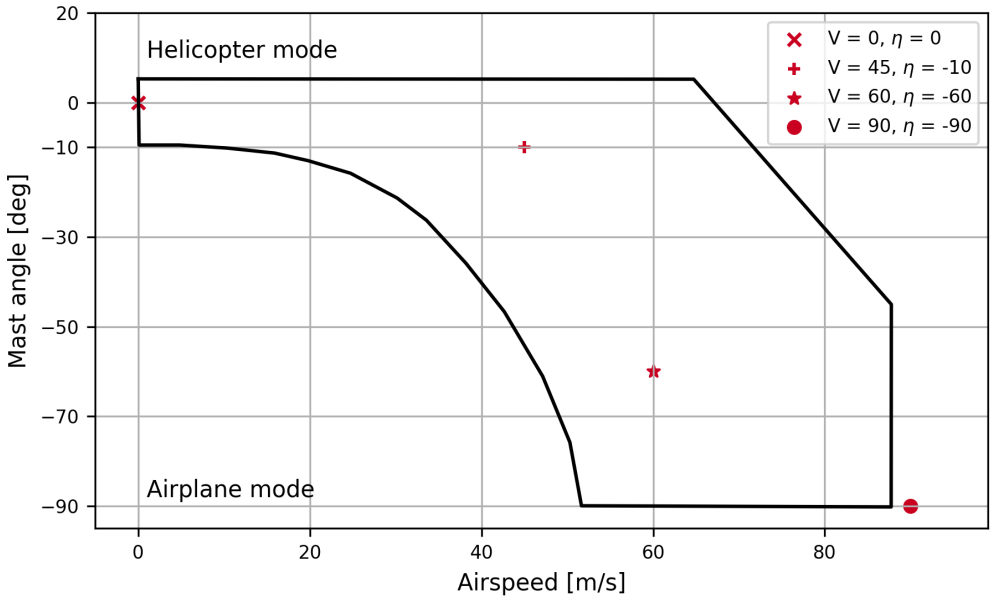

Figure 7.8: Flight evaluation points for the S2 control allocation configuration.

.

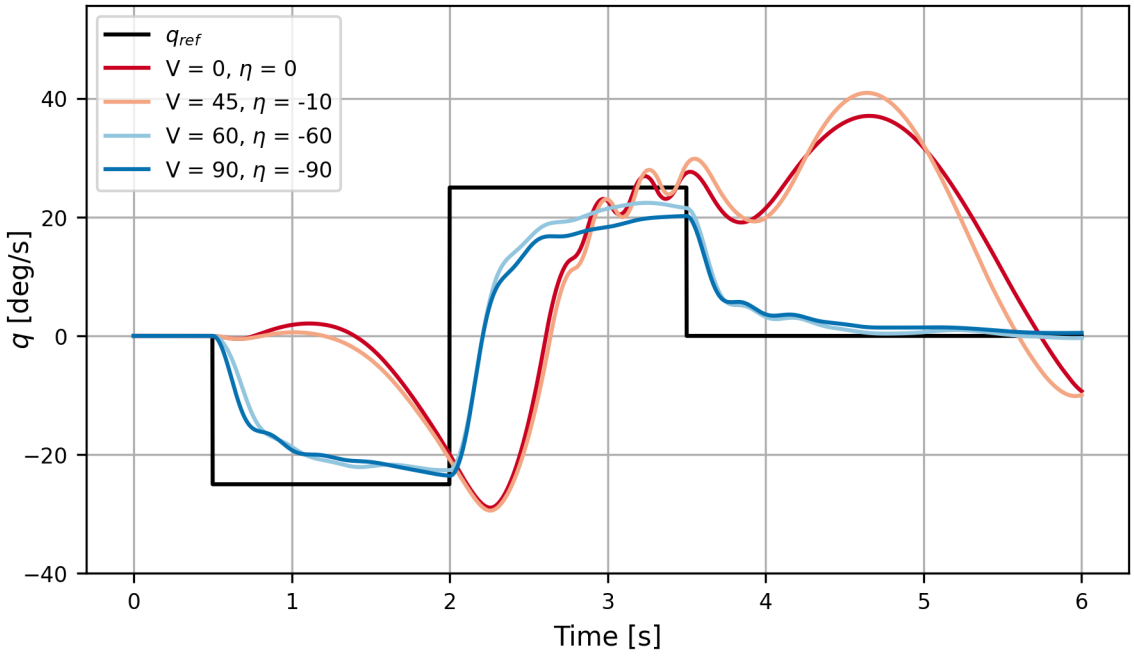

Figure 7.9: Pitch rate response at multiple points in the flight envelope with the control allocation solver configured as S2.

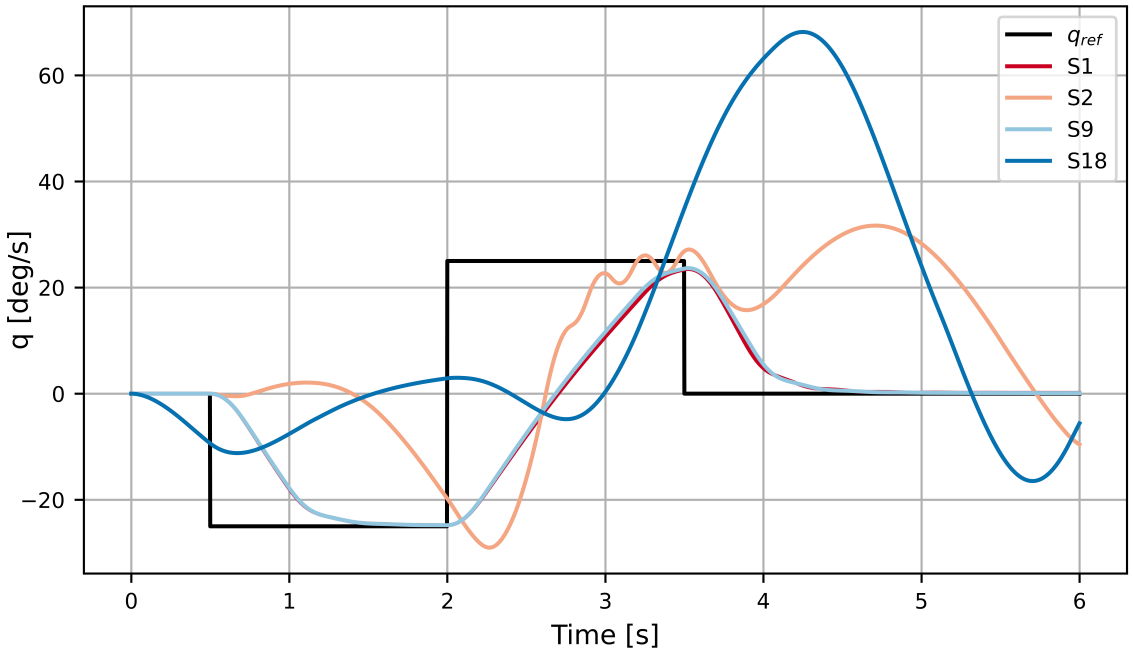

Figure 7.10: Pitch rate response in hover ($V = 0m/s$ and $\eta = 0deg$)with CA configurations S1, S2, S9, S18.

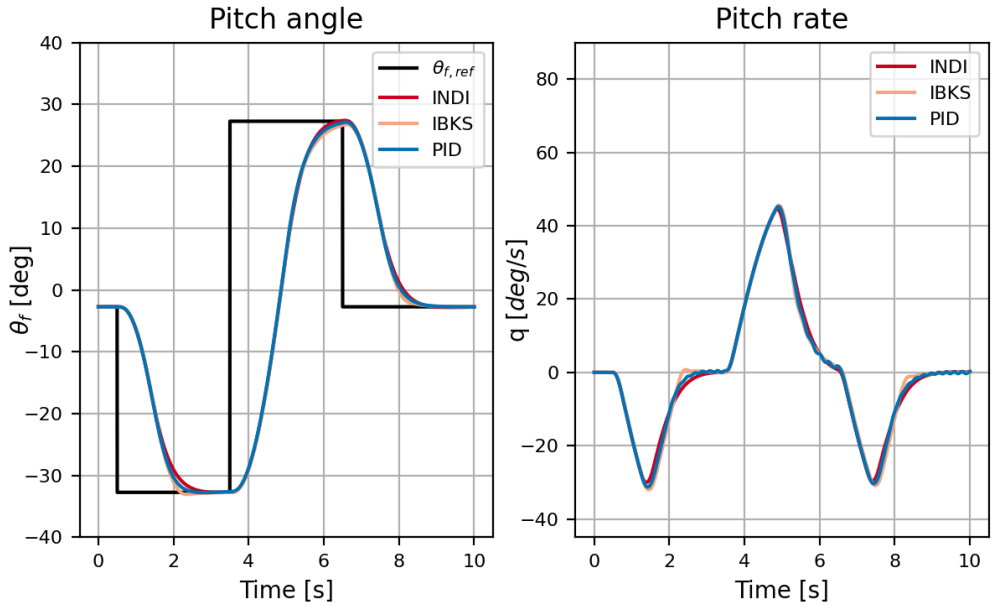

Figure 7.11: Pitch angle and rate responses to pitch angle doublet tracking task in hover (helicopter mode) of the INDI, IBKS and PID attitude controllers.

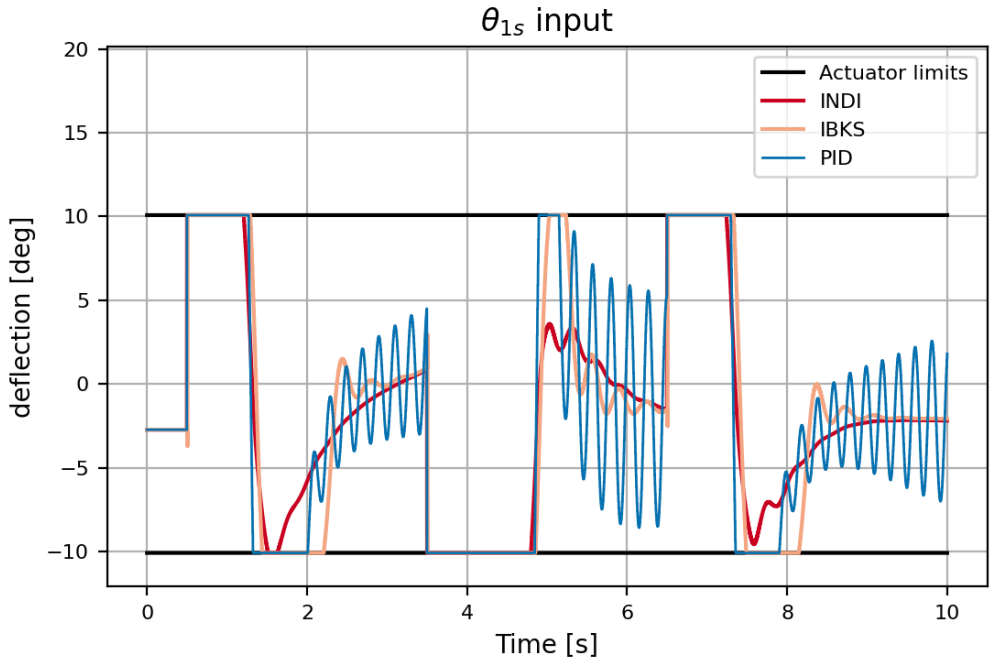

Figure 7.12: Actuator control inputs after pitch angle doublet tracking task in hover (helicopter mode) calculated by the INDI, IBKS and PID attitude controllers.

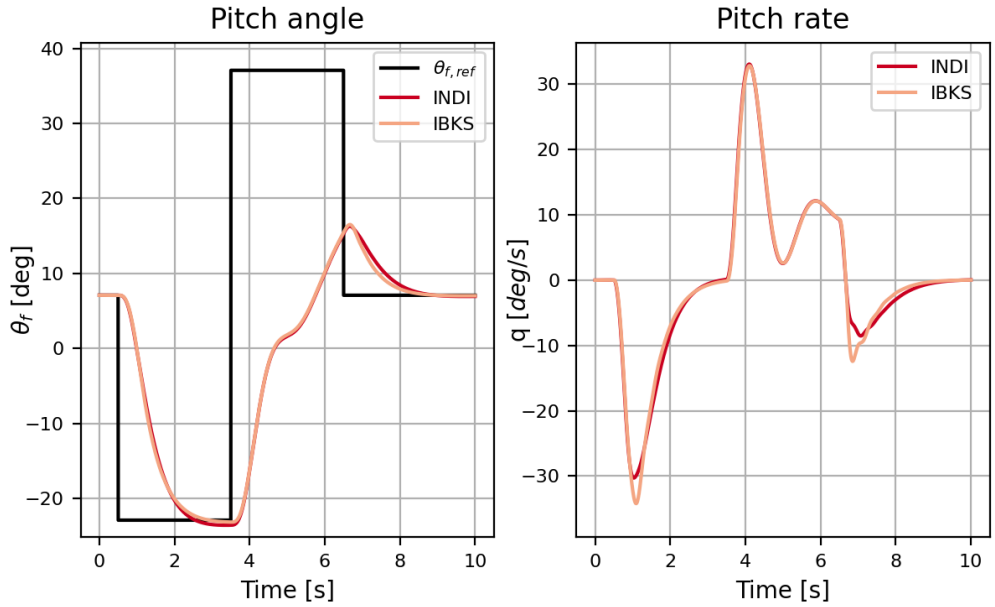

Figure 7.13: Pitch angle and rate responses to a pitch angle doublet tracking task at $60m/s$ and $\eta = -60deg$ of the INDI, IBKS and PID attitude controllers.

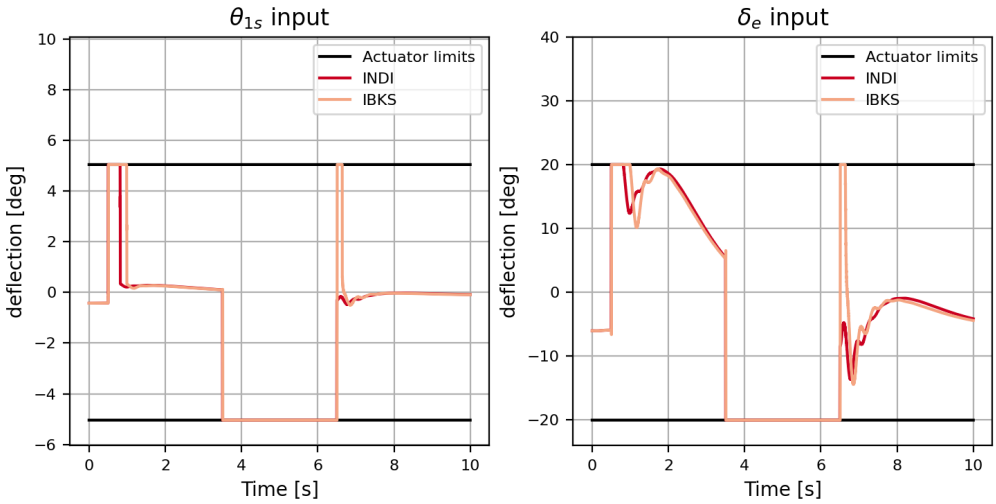

Figure 7.14: Actuator control inputs after to a pitch angle doublet tracking task at $60m/s$ and $\eta = -60deg$ calculated by the INDI, IBKS and PID attitude controllers.

Controller parameter	Setting	Unit	Remark
Run frequency	250	Hz	
ω_s	25	$1/s$	
ζ_s	0.55		
CA solver	WLS		
G_c	M3		See table 7.1
G_c entries	Scheduled		as a function of (V, η) see figures 4.1, 4.2 and 4.3
W_v	I		
γ	1000		
w_{θ_0}	1		
$w_{\theta_{1s}}$	1		
w_{δ_e}	$1/5$		
INDI			See figure 5.3
K_1	4	$1/s$	
K_2	1.55	$1/s$	
IBKS			See figure 6.3
c_1	2.4		
c_2	4		
$\omega_{cf,1}$	125	$1/s$	
$\zeta_{cf,1}$	$\sqrt{2}$		
$S_{M,1}$	30	deg	
$S_{R,1}$	∞	deg/s	
$\omega_{cf,2}$	125	$1/s$	
$\zeta_{cf,2}$	$\sqrt{2}$		
$S_{M,2}$	$S_{R,1}$	deg/s	
$S_{R,2}$	10	deg/s^2	
PID			See figure 7.26
K_P	-3.15	s	
K_I	-0.85	s	
K_D	-0.65	s	
Anti-windup method	clamping		
K_2	2.7	$1/s$	

Table 7.4: Attitude controller parameter settings

INDI controller does not clip the elevator input when the aircraft overshoots. The elevator dynamics are faster ($100deg/s$) than the maximum deflection rate of the longitudinal cyclic ($60deg/s$). Because the INDI controller is sensitive to actuator dynamics, the controller could have been tuned stiffer for fixed wing flight. On the other hand, this may would have caused oscillatory responses back in hover mode.

7.3. Velocity controller

In this section, the velocity controller that was designed in section 5.3 will be tuned and tested. First the velocity controller in hover is demonstrated. Then transition manoeuvres are shown using an integrated nacelle control versus a feed forward nacelle control approach.

7.3.1. Velocity control in helicopter mode

In hover the nacelle angle remains in the upright position and the linear velocities are controlled only by the thrust of the proprotors and the orientation of the fuselage. For the incremental control law this means that the matrix G_v which was derived in equation 5.51 can be used. The matrix is square and can be inverted in a standard manner. The diagram of the complete controller is shown in figure 5.4.

To test the velocity controller in helicopter mode a horizontal speed profile was designed. The profile is

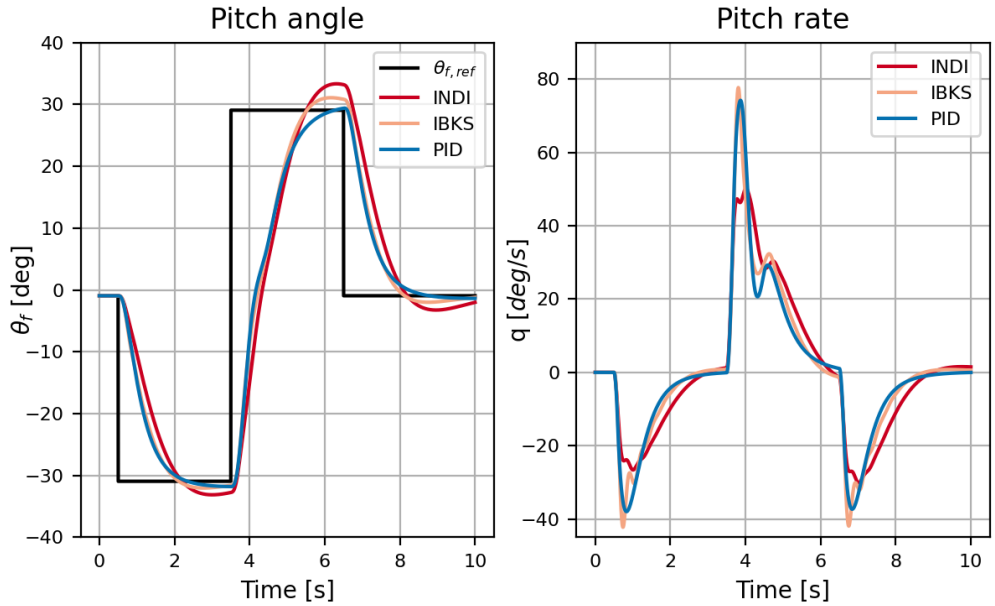

Figure 7.15: Pitch attitude response of a doublet pitch reference input for different attitude controllers. ($V = 150m/s, \eta = 0deg$)

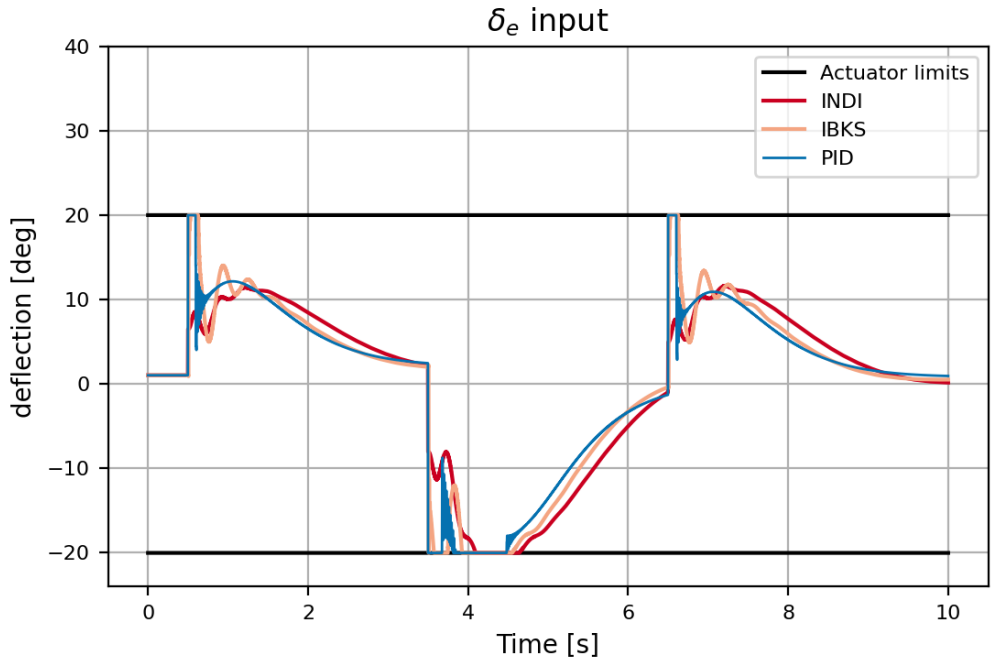

Figure 7.16: Actuator control inputs calculated by different attitude controllers tracking a doublet pitch attitude reference signal. ($V = 150m/s, \eta = 0deg$)

Controller parameter	Setting	Unit	Remark
Run frequency	250	Hz	
Attitude controller	INDI		
K_3	2	$1/s$	
K_4	0.5	$1/s$	
$\ddot{\chi}_{max}$	5	m/s^2	
$\ddot{\chi}_{min}$	-5	m/s^2	
$\dot{\chi}_{max}$	∞	m/s	
$\dot{\chi}_{min}$	$-\infty$	m/s	
$\omega_{n,lin}$	25	$1/s$	linear acceleration filter
ζ_{lin}	0.55		
Ex. nacelle control			See figure 5.4
G_v	see eq. 5.51		Recalculated each timestep
Inc. nacelle control			See figure 5.5
CA solver	WLS	N/A	
G_v	see eq. 5.44		Recalculated each timestep
W_v	I		
W_u	$I \cdot [10, 1, 1]$		
γ	1000		

Table 7.5: Velocity controller parameter settings.

shown in figure 7.17. The aircraft starts-off from a trimmed hover state. Then the aircraft accelerates to $20m/s$. At $20m/s$ the aircraft is commanded to speed up and slow down following a sinusoidal signal. After this, the aircraft is commanded to accelerate to $40m/s$. Lastly, the aircraft slows down again to $20m/s$ and again to a hover. Simultaneous to the horizontal speed profile, the aircraft is commanded to hold it current altitude. The parameters which have been used to test the velocity controller are summarized in table 7.5

Looking at figure 7.17, the aircraft can follow the horizontal speed commanded signal without overshoot. The vertical speed response does show some overshoot. However, the entire profile has been flown with a maximum altitude loss of 2 meters. In figure 7.18, the calculated attitude and thrust commands are shown. As expected, the attitude commands can be tracked by the INDI controller. The maximum thrust command is in the order of $15 \cdot 10^3 N$, but most commands remain smaller than $3 \cdot 10^3 N$.

7.3.2. Velocity control through transition and fixed wing flight

The incremental velocity controller has shown to be functional. Now the controller is tested against transition through the conversion corridor and in fixed wing flight. For the transition two configurations are tested. One is the helicopter configuration as tested in the previous sections. In this configuration there is no active control of the mast angle. The mast angle is simply commanded to lower at a constant rate. This configuration is shown in figure 5.4. The parameters are shown in table 7.5. The mast angle rate can be set at two values a slow rate of $2.5deg/s$ and a fast rate of $7.5deg/s$. Both cases will be evaluated.

The other configuration that will be tested is an incremental velocity controller, which has mast angle control integrated. The controller was derived in section 5.3 and its main control law is shown in equation 5.45. The scheme is summarized in figure 5.5.

To solve the over-actuated system, i.e., the non-square G_v matrix, the WLS solver is used. The WLS solver was chosen over the ordinary pseudo-inverse method because the solver can take into account constraints of actuator limits. In this case all "actuators" ($[\theta_f, \eta, T]$) are limited in their operational space. Especially in this, the limits of η are interesting. The WLS solver can limit the movement of the nacelle angle to keep the aircraft within the conversion envelope. Because this is an incremental controller, the limits are formulated as increments. The maximum and minimum increments are calculated from the current position in the flight envelope to the maximum and minimum allowable mast angles at the current speed. If the aircraft is accelerating faster than the nacelle angle rate, the aircraft could still end up outside the conversion envelope. The aircraft's acceleration can be considered but has not been implemented at this stage. The

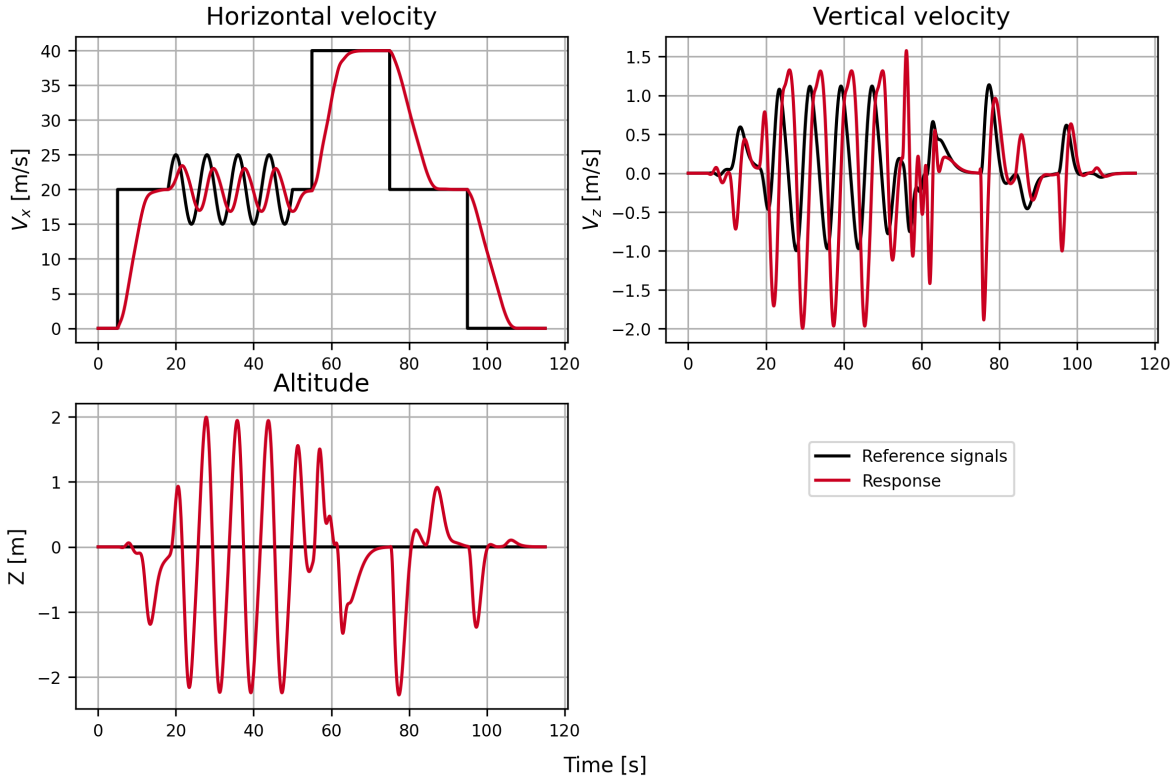

Figure 7.17: Vertical and horizontal inertial velocities of the tiltrotor in helicopter mode tracking a horizontal speed profile while holding altitude.

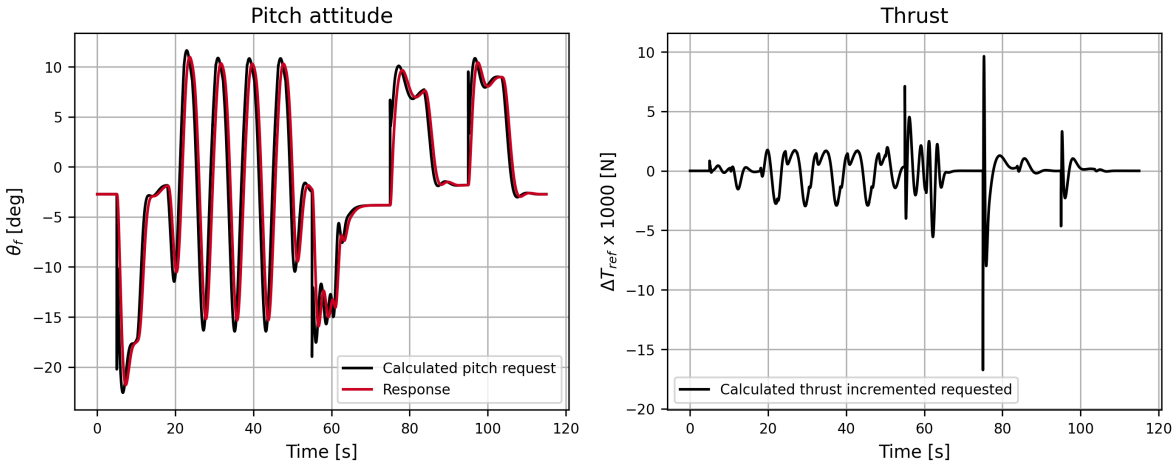

Figure 7.18: Commanded pitch and thrust signals calculated by the velocity controller while following a horizontal tracking and altitude hold task in hover mode.

nacelle increment limits are calculated as:

$$\Delta\eta_{max} = \eta_{max}|_{V_0} - \eta_0 \tag{7.8}$$

$$\Delta\eta_{min} = \eta_{min}|_{V_0} - \eta_0 \tag{7.9}$$

The subscript 0 indicates the current state of the aircraft.

Regarding the weighting matrices, the order of magnitude of the control derivatives in both axes (χ_x and χ_z) are the same. This is not surprising since the same forces are used to control vertical and horizontal velocities. After initial testing it was found that the weighting matrix W_v could remain equal to I. For the weighting matrix W_u, the choice was made to prioritize the pitch control. The preferred increments of θ_f where set to maintain a nose level attitude as shown in equation 5.58. So when this output is prioritized via W_u, the WLS algorithm will solve for the requested response while favoring a nose level attitude vs a change in nacelle angle or thrust force increment. The numerical values are presented in table 7.5.

Both configurations are tested with a slow and fast nacelle angle rate. In figure 7.19 the speed profile and the responses of all four configurations are shown. The maneuver consists of 3 steps. In the first step, the nacelle angle is still upright and does not move. At $20m/s$, the aircraft accelerates forwards again and starts tilting the nacelles. Next, the aircraft accelerates for $80m/s$ to remain in the corridor. The last step is accelerating to a higher cruising speed to demonstrate the controller performance in fixed wing flight. Next to the horizontal speed profile, the aircraft is commanded to hold its current altitude. The responses of the four controllers are similar considering the horizontal speed profile, except for the configuration with a slow nacelle rate and integrated nacelle control. The vertical speed responses appear noisy for all configurations. At the same time, the maximum altitude deviation is 6 meters above the starting height. The maximum altitude loss is 2 meters.

Figure 7.20 shows the nacelle progression over time. The controllers without integrated nacelle control move their nacelles at a constant rate as can be seen clearly from the graph.

Finally the flights are plotted against each other in the conversion corridor. This is shown in figure 7.20. Three of the four controllers are transitioning with relatively slow speeds. while the controller with isolated nacelle control and a slow nacelle rate flies through the conversion faster. This is a combination of the feed forward control of the nacelle angle change and the slow tilt-rate. In this scenario the aircraft is faster accelerating than the nacelle's are tilting. This not necessarily a problem since the commanded speed was set at $80m/s$ and which is still in the flight envelope.

During the tuning process it was found that the limits on the reference signals $\dot{\chi}_{ref}$ are important to keep the system stable. If the limits of commanded reference signals are set to high, the system becomes unstable. This affects the agility of the aircraft and may be undesirable. The cause of the instability may be because of the assumptions made during the derivation of the incremental control law. Specifically the modelling of the lift and thrust control forces.

Another reason for the instability could be that the time-scale separation assumption that was used to derive the control law, does not hold. Compared to the attitude controller, the actuators of the velocity controller are slower (excluding the thrust commands). The pitch attitude and nacelle change relatively slowely compared to the linear accelerations. It could be that the actuators (θ_f, η,ΔT), move so slowely that the dynamics of the system cannot be disregarded anymore.

The last maneuver presented in this evaluation is a full flight from a hover, an acceleration in helicopter mode, transition to fixed wing flight, acceleration to cruise flight. Deceleration back to the conversion corridor and a conversion back to helicopter mode and a still hover. For this maneuver the integrated nacelle control is used together with the fast nacelle tiltrate. Figure 7.22 shows the horizontal speed profile and the response of the aircraft. During this flight the aircraft was commanded to maintain its current altitude. From the speed profile it can be seen that the aircraft can indeed follow the tracking tasks and can accelerate to $130m/s$ and also decelerate with a maximum altitude deviation of $6m$ and a maximum altitude loss of $2m$.

Figure 7.23 shows the command signals that have been calculated by the velocity controller. As can be seen, the commanded pitch attitude remains between 20 degrees up and down and the aircraft is able to follow the pitch commands. In figure 7.24 the flight path is shown against the conversion corridor. Similarly to the previous transitions with fast nacelle tiltrates, the transition is flown relatively slow. Looking back at the results from section 7.1, and figure 4.1, the flight passes straight through the region where there is less

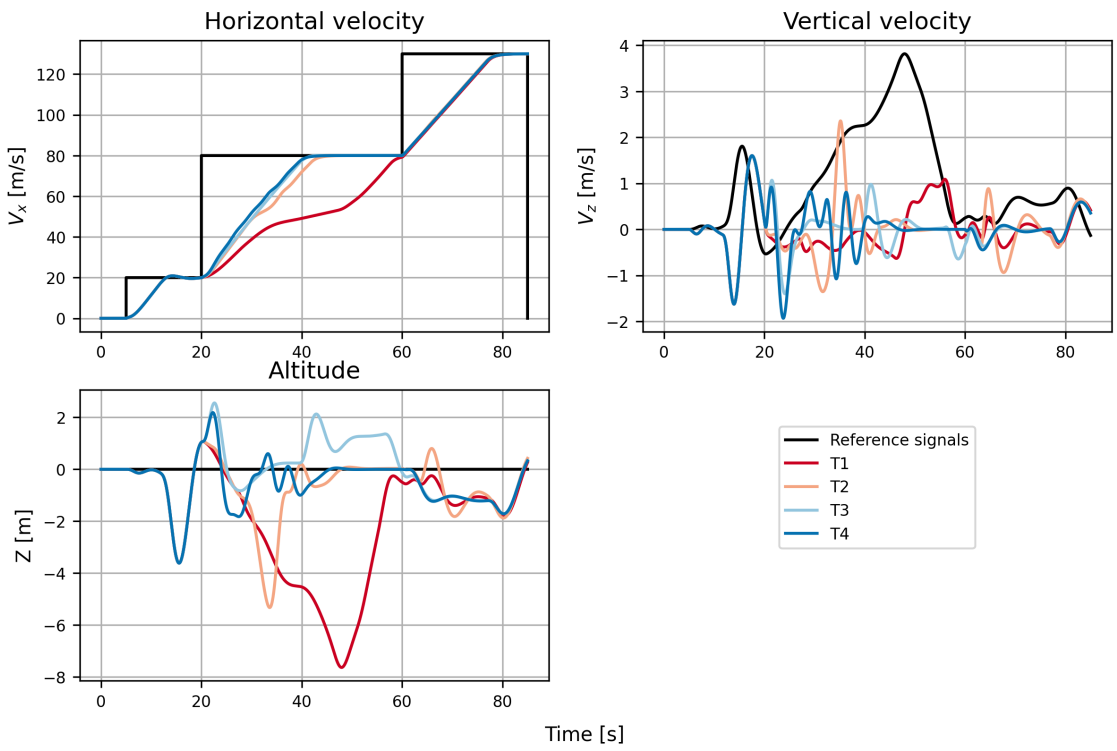

Figure 7.19: Horizontal speed profile from hover in helicopter mode to cruise speed in fixed wing mode. T1 = slow nacelle rate, integrated nacelle control , T2= fast nacelle rate, integrated nacelle control, T3= slow nacelle rate, separate nacelle control, T4= fast nacelle rate, separate nacelle control.

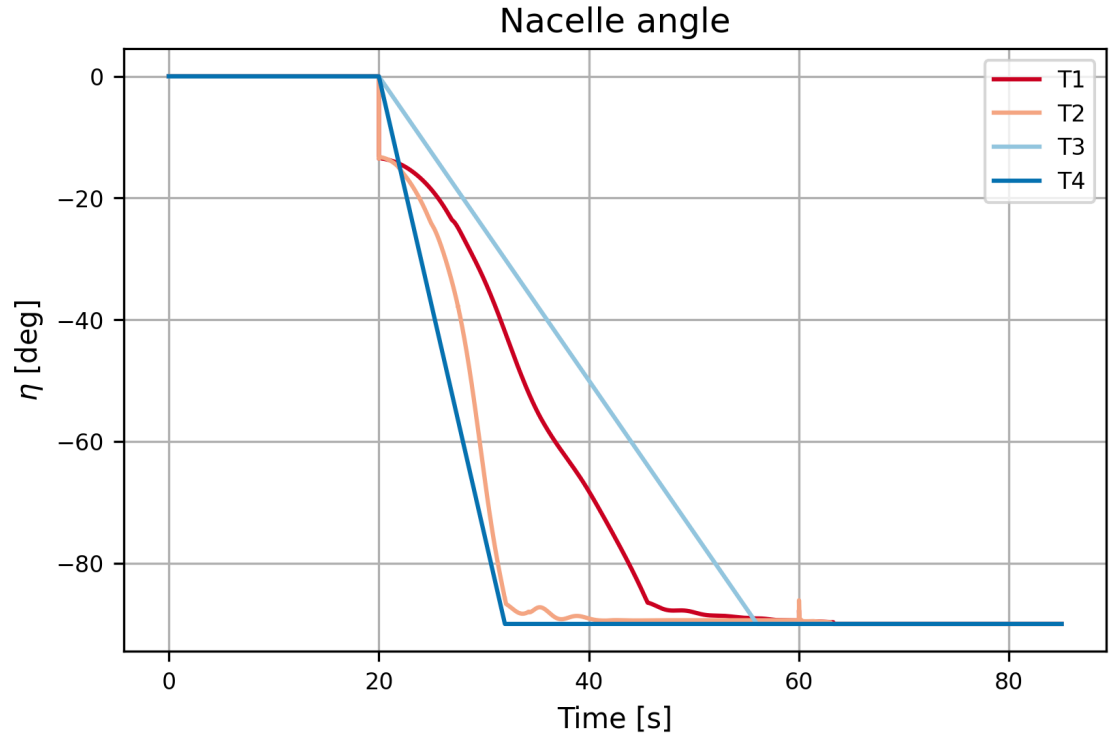

Figure 7.20: Nacelle angle command with respect tot time. T1 = slow nacelle rate, integrated nacelle control , T2= fast nacelle rate, integrated nacelle control, T3= slow nacelle rate, separate nacelle control, T4= fast nacelle rate, separate nacelle control.

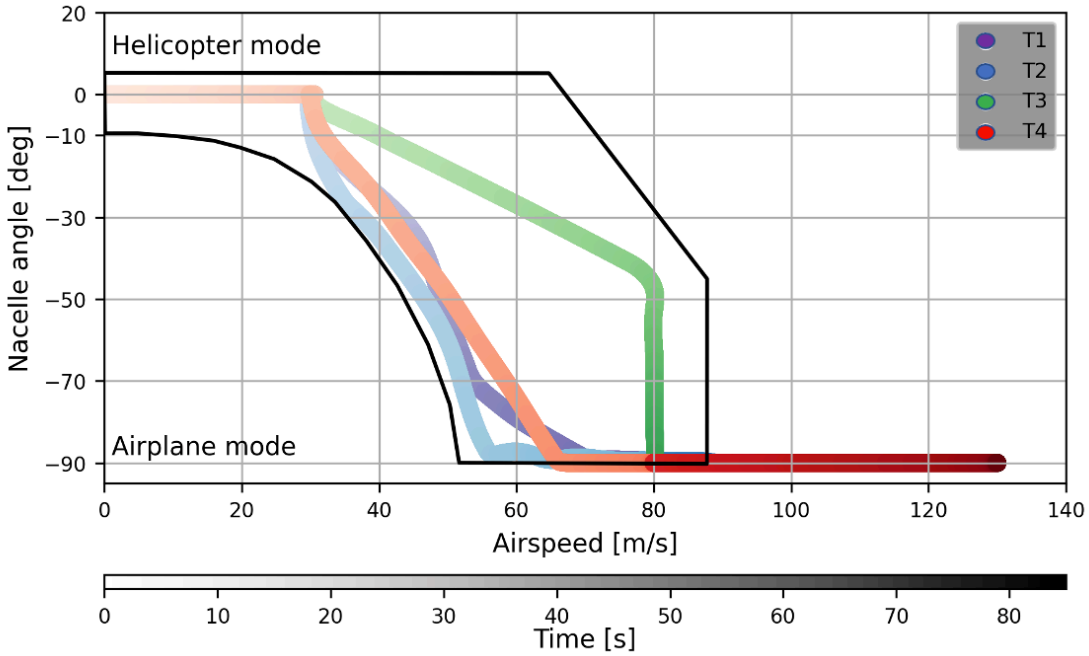

Figure 7.21: Flight path of the different controller configurations shown against the conversion corridor. T1 = slow nacelle rate, integrated nacelle control , T2= fast nacelle rate, integrated nacelle control, T3= slow nacelle rate, separate nacelle control, T4= fast nacelle rate, separate nacelle control.

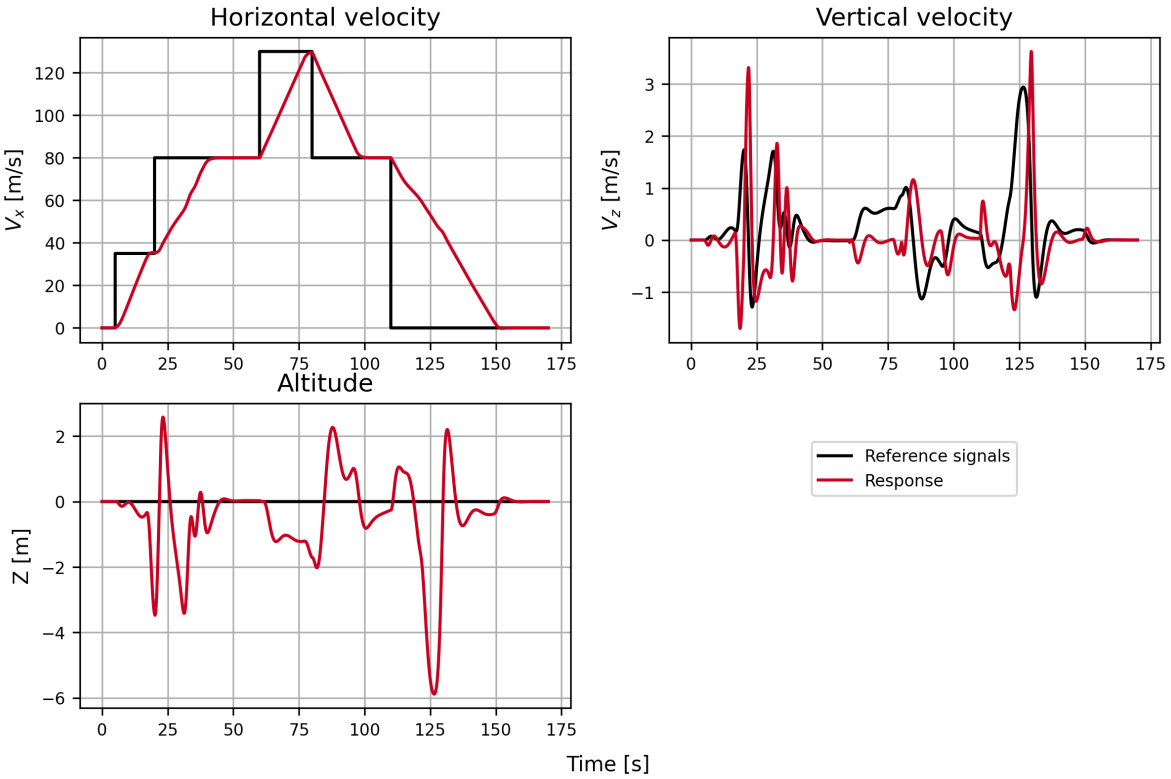

Figure 7.22: Horizontal and vertical inertial velocity response of the tiltrotor with integrated nacelle control following "full flight" speed tracking and altitude hold task from a standing hover to fixed-wing cruising speed and back to hover. With fast nacelle rate.

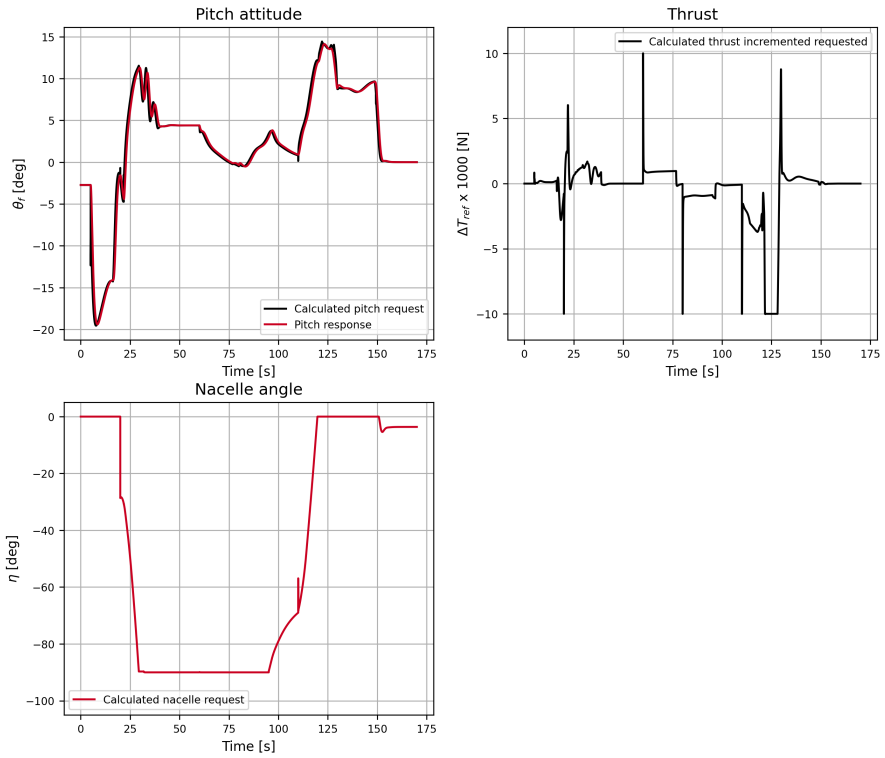

Figure 7.23: Velocity controller outputs during a full flight maneuver with integrated nacelle control and a fast nacelle rate.

pitch authority. Figure 7.23 does not reveal any loss of pitch control and the attitude controller is able to track the pitch command during the entire flight.

In figure 7.25, the actuator commands are shown. Notice the control phasing of the longitudinal cyclic control which is completely disabled during fixed wing flight. The collective limits are also phased to provide more pitch for efficient propulsion and during cruis flight. From the perspective of the actuators the aircraft remains controllable since the control signals are almost never clipped.

This chapter discussed the tuning and testing of the control methods that were derived in this research. First the control allocation algorithms were tested and tuned to find the optimal performance configuration for this application. Next the INDI and IBKS attitude controllers were compared to each-other and a conventional PID scheme. Later, the INDI attitude controller was applied as in the tests of the velocity controller. The velocity controller was tested by following tracking tasks in hover and through the conversion corridor and in fixed wing mode.

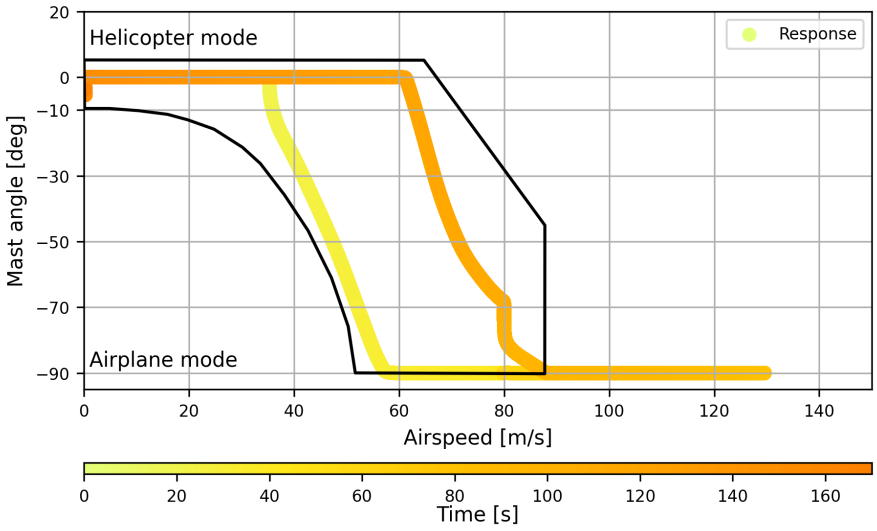

Figure 7.24: Full flight maneuver with integrated nacelle control shown against the conversion corridor.

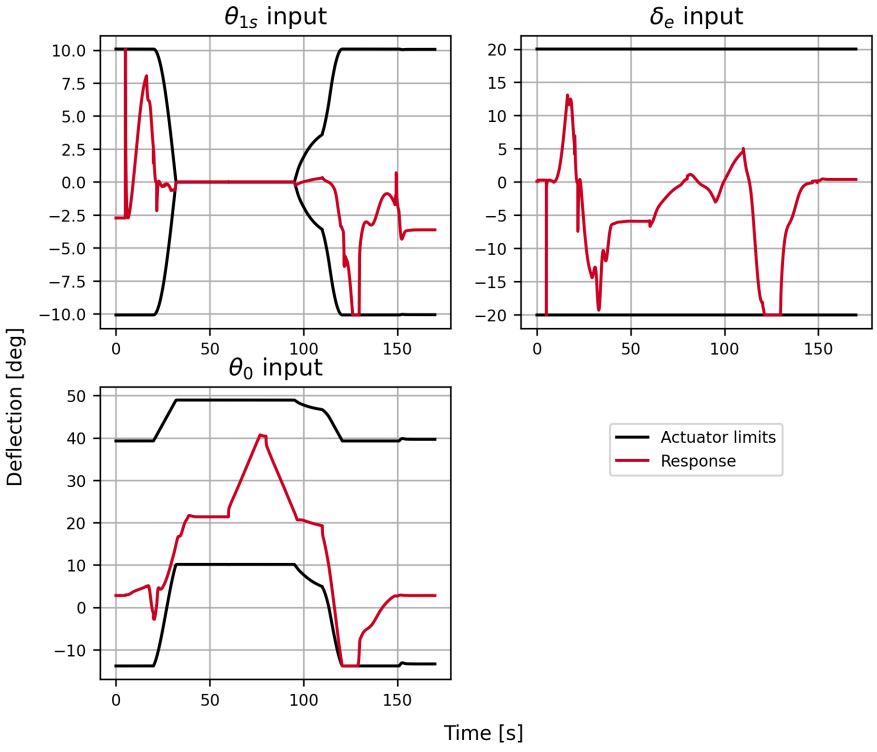

Figure 7.25: Actuator control inputs during a full flight maneuver with integrated nacelle control.

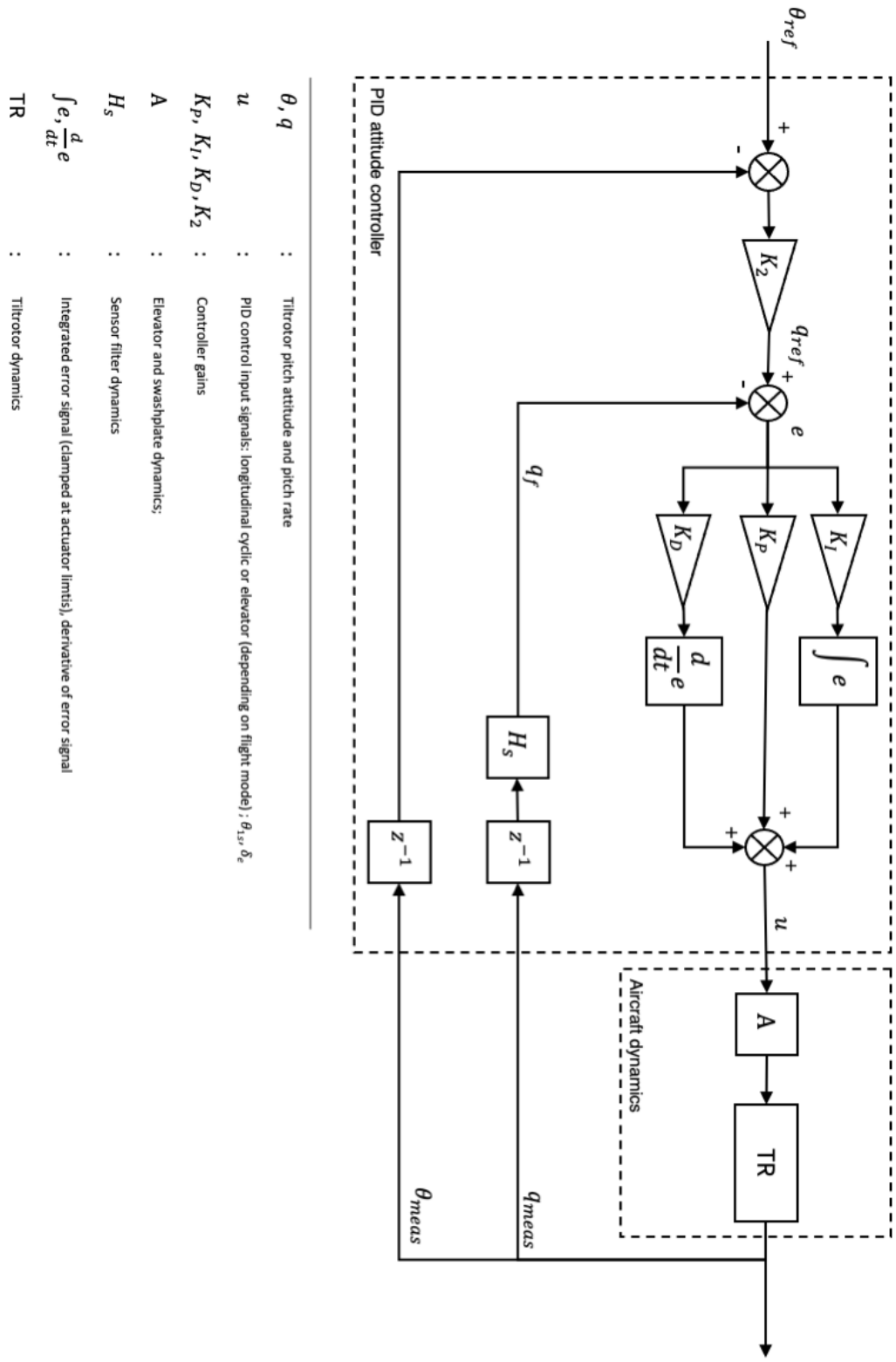

θ, q	:	Tiltrotor pitch atttitude and pitch rate
u	:	PID control input signals: longitudinal cyclic or elevator (depending on flight mode); θ_{1s}, δ_e
K_P, K_I, K_D, K_2	:	Controller gains
A	:	Elevator and swashplate dynamics;
H_s	:	Sensor filter dynamics
$\int e, \frac{d}{dt}e$	:	Integrated error signal (clamped at actuator limtis), derivative of error signal
TR	:	Tiltrotor dynamics

Figure 7.26: PID attitude controller for helicopter and fixed-wing mode.

Part IV

Wrap-up

8

Conclusions and recommendations for future research

In this final part, the thesis is concluded. The most important findings of the report are summarized and discussed. Whenever applicable, recommendations for future research are provided.

This research addressed the question of how incremental nonlinear control can be applied to tiltrotor aircraft, with particular attention to the design of the attitude controller in combination with a control allocation solver and a global velocity controller, which can steer the aircraft through a transition and conversion based on incremental logic. In the attempt to answer the research question, the following steps were taken.

A three-degree of freedom nonlinear model of the XV-15 was implemented and linearized to find the pitch and thrust control derivatives. The actuator limits and dynamics were defined and added to the nonlinear model.

A brief analysis in the z-domain was presented on the performance of an INDI controller applied to the one degree of freedom linearized pitch dynamics of the tiltrotor model. The z-domain transfer function was analyzed for different gains and model mismatches to get an idea of how robust incremental control can be against model mismatches between the plant's control effectiveness and the estimated control effectiveness of the controller. In this simple case, it was shown that INDI can remain stable and non-oscillatory for a large set of model mismatches and gains. When the control effectiveness is not exactly known it may be beneficial to overestimate the value. Furthermore, it was found that if the control effectiveness estimated value is of the opposite sign, the controller becomes unstable. For future analyses, it would be interesting to add the phase lag introduced by the sensor filter, actuator dynamics, and possibly rotor dynamics.

In the next part, an INDI controller was designed for the complete 3-DOF nonlinear model. The controller was designed to receive pitch angle and thrust increment requests and calculate the required positions of the longitudinal cyclic, collective, and elevator. A control allocation problem was formulated, and two different strategies were proposed as a solution. The Weighted Least Squares method solved by the active set method and a Weighted pseudo Inverse method. Both methods were adapted for this specific use case.

Next, an attitude controller was designed based on incremental nonlinear backstepping. The controller was derived from the equations of motion of the aircraft and the control Lyapunov function to guarantee positive stability and convergence properties. To minimize the mathematical complexity of the control laws, command filters were introduced to derive command signals numerically that would otherwise have to be determined via mathematical expressions. Thrust control and control allocation were integrated in the design as well.

An integrated incremental velocity controller was designed to fly through the conversion corridor. The control laws were derived from the linear equations of motion expressed in the form of Newton's second law of motion. The controller computes thrust increments, pitch attitude, and nacelle angles to achieve a desired linear acceleration. The controller forces that are used are the thrust force and the lift generated by the wings. The desired accelerations are derived from a cascaded P-loop structure. The velocity controller was derived with respect to the north-east-down inertial frame. For helicopter control, this may be a logical frame of reference. For fixed-wing aircraft, however, ground speeds are not necessarily important information to keep flying. It would be interesting to find a global incremental velocity controller referenced to the aerodynamic

frame for future work. This way, in fixed wing mode, flight speeds can be controlled directly, as well as angle of attack and sideslip.

In the next part of the report, the WLS control allocation algorithm was tested with different configurations of control effectiveness and weighting matrices. The attempt was to find a configuration with which the collective, longitudinal cyclic, and elevator could cooperatively control the pitch axis such that the risk of control saturation was minimized while maintaining control of the pitch axis. It was found that the joint effort of all three actuators via the WLS algorithm could lead to better performing rate tracking in the region of the conversion corridor where cyclic and elevator effectiveness' are weak. However, when the same configuration was tested in hover, the system was unstable. The performance degradation could be explained by the control effectiveness of the collective input which may not be estimated well enough by only looking at the linearized control derivatives. For future research it would be interesting to evaluate how much more a-priori model knowledge of the collective is required to estimate the control effectiveness well enough for coordinated collective control efforts. Alternatively, one could also look into online learning algorithms that could determine the control effectiveness values during the flight. Care must be taken to choose an algorithm that would converge relatively fast as some of the actuators cross-over and become the opposite sign in the conversion corridor.

The backstepping controller was compared to the INDI controller and as a baseline with a standard PID controller against a pitch attitude tracking tasks at multiple points in the flight envelope. All three controllers were able to converge to the reference signal. The INDI controller showed some overshoot in fixed wing mode, which could be explained by the faster actuator dynamics compared to helicopter mode. Changing actuator dynamics has an effect on the INDI controller and may be resolved by gain tuning synchronous to the phasing of the cyclic control. The PID controller showed the best response.

Lastly, the velocity controller was demonstrated. First in helicopter mode only. The helicopter mode proved able to follow a horizontal speed tracking task with accelerations and decelerations. The vertical deviation was a maximum of 2 meters. Different transition strategies with integrated and isolated nacelle control were tested, and they were all able to remain within the conversion corridor.

The velocity controller with integrated nacelle control was tested to fly from a standing hover to cruise in fixed wing mode and back. During which the aircraft was well able to follow the reference signal. The flight moved through the region of weak cyclic effectiveness without saturating the actuators. The velocity controllers included limits on the maximum and minimum commanded linear accelerations. These limits were found to be necessary to keep the system stable. This might be because the control effectiveness matrix for the velocity controller may not be an accurate enough estimation of the actual force derivatives. For future work, it would be interesting to investigate if there are other forces than the lift and thrust force that play a significant role in the linear accelerations of the aircraft and how they can be modeled in a simplified way such that they can be added to the controller.

Another reason for the required acceleration limits may be the fact that if the aircraft accelerates faster than these limits, the timescale separation principle does not hold anymore. The actuators, which in this case are the nacelle, pitch attitude and collective, react to slower than the aircraft accelerates and the controlling forces may not be the dominating forces in the equations of motion.

The incremental control structure that has been presented in this work allows relatively easy adaptation to control more degrees of freedom. It would therefore be interesting to expand the current controllers to also include the lateral axis. Additionally, the rotor dynamics have been disregarded for most of this work. Similarly to filter-induced phase lag, synchronization of rotor phase lag can be important to remain stable when the aircraft relies on the rotor controls.

Bibliography

[1] M. Maisel, D. J. Giulianetti, and D. C. Dugan, *The History of the XV-15 Tilt Rotor Research Aircraft from Concept to Flight* (NASA, Washington D.C., 2000).

[2] B. Boeing, *A New Era In Vertical Flight,* (2020).

[3] K. W. Goldstein and L. W. Dooley, *V-22 Control Law Development,* in *42nd Annual Forum of the American Helicopter Society* (Washington D.C., 1986) pp. 673–684.

[4] M. B. Tischler, *Stanford University*, Ph.D. thesis, Stanford University (1987).

[5] T. van Holten, J. Melkert, B. Marrant, and M. D. Pavel, *Helicopter Performance, Stability, and Control (AE4314 Diktaat)*, November (TU Delft, Delft, 2002).

[6] B. P. Acquatella, W. Falkena, E. J. van Kampen, and Q. P. Chu, *Robust nonlinear spacecraft attitude control using incremental nonlinear dynamic inversion,* AIAA Guidance, Navigation, and Control Conference 2012 (2012), 10.2514/6.2012-4623.

[7] M. Maisel, *Tilt rotor research aircraft familiarization document*, Tech. Rep. (NASA Aimes Research Center, Moutain View, 1975).

[8] P. Sokolowski, *Liturature study: Flight Dynamics Modelling of a Tiltrotor Aircraft,* (2020).

[9] S. W. Ferguson, *Nasa Cr-166537*, Tech. Rep. (NASA Ames Research Center, 1989).

[10] E. E. Blount, *Airplane-Helicopter,* (1933).

[11] J. M. Drees, *Expanding Tilt Rotor Capabilities,* in *Twelfth European Rotorcraft Forum* (ERF, Garmish - Partenkirchen, 1986) pp. 13–1.

[12] B. L. McManus, *V-22 Tiltrotor Fly-By-Wire Flight Control System,* in *Eleventh European Rotorcraft Forum* (European Rotorcraft Forum, London, 1985) pp. 57–1.

[13] Augusta Westland, *The Game Changer,* (2016).

[14] W. W. Chung, D. Linse, A. Paris, D. Salvano, T. Trept, T. Wood, H. Gao, D. Miller, K. Wright, R. Young, and V. Cheng, *NASA*, Tech. Rep. October (NASA Ames Research Center, Moutain View, 2011).

[15] US, *Addressing the future challenges of the operation of power lift category/tiltrotor class aircraft in international air navigation, ICAO AE35-WP,* (2004).

[16] C. Chalk, D. Key, J. Kroll, R. Wasserman, and R. Radford, *Background Information and User Guide for MIL-F-83300-Military Specification–Flying Qualities of Piloted V/STOL Aircraft*, Tech. Rep. (Cornell Aeronautical Laboratory Inc., New York, 1970).

[17] G. D. Padfield, *Helicopter flight dynamics : including a treatment of tiltrotor aircraft* (John Wiley & Sons Inc., 2018).

[18] R. L. Marr and G. B. Churchill, *Flight Control System Development For The XV-15 Tilt Rotor Aircraft,* in *32nd Annual National V/STOL Forum of the American Helicopter Society* (Washington D.C., 1976) pp. 1–1042.

[19] R. C. Innis, C. A. Holzbauser, and H. C. Quigley, *Airwothiness Considerations for STOL Aircraft*, Tech. Rep. January (NASA Ames, 1970).

[20] K. H. Landis and I. Glusman, *Development of ADOCS Controllers and Control Laws*, Tech. Rep. (Boeing Vertol Company, Philadelphia, 1987).

[21] B. L. Stevens, F. L. Lewis, and E. N. Johnson, *Aircraft Control and Simulation*, 3rd ed., 3 (Wiley, Hoboken, 2016) p. 55.

[22] J. Watkinson, *Art of the Helicopter* (Elsevier, Burghfield Common, 2004).

[23] R. W. Prouty, *Helicopter Performance, Stability and Control*, 2nd ed. (Krieger Publishing Company, Malabar, 2002).

[24] M. D. Pavel, P. Shanthakumaran, Q. P. Chu, O. Stroosma, M. Wolfe, and H. Cazemier, *Incremental nonlinear dynamic inversion for the apache AH-64 helicopter control,* Journal of the American Helicopter Society **65**, 1 (2020).

[25] M. Manness, J. Gribble, and D. Murray-Smith, *Multivariable Methods For Helicopter Flight Control Law Design: A Review,* in *16th European Rotorcraft Forum* (Glasgow, 1990) pp. 1–14.

[26] G. Meyer, R. L. Hunt, and R. Su, *Design of a Helicopter Autopilot by Means of Linearizing Transformations*, Tech. Rep. (NASA Ames Research Center, Moffett Field, 1982).

[27] G. Stein, D. Bugajski, R. Hendrick, and G. Stein, *Dynamic inversion: An evolving methodology for flight control design,* International Journal of Control **59**, 71 (1994).

[28] S. N. Singh and W. Rugh, *Decoupling in a class of nonlinear systems by output feedback,* Journal of Dynamic Systems, Measurement and Control **94** (1972), 10.1016/S0019-9958(74)90723-2.

[29] J.-J. E. Slotine and W. Li, *Applied nonlinear control* (Prentice Hall, 1991) p. 459.

[30] M. Krstić, I. Kanellakopoulos, and P. Kokotovic, *Nonlinear and Adaptive Control Design* (John Wiley & Sons Inc., New York, 1995).

[31] J. Doyle and G. Stein, *Multivariable Feedback Design: Concepts for a Classical/Modern Synthesis,* Journal of Process Control **1**, 55 (1991).

[32] G. J. Balas, W. Garrard, and J. Reiner, *Robust dynamic inversion control laws for aircraft control,* in *Guidance, Navigation and Control Conference* (AIAA, Hilton Head Island, 1992) pp. 192–205.

[33] A. J. Calise and R. T. Rysdyk, *Adaptive Model Inversion Flight Control for Tiltrotor Aircraft,* in *AIAA Guidance, Navigation and Control Conference* (1997).

[34] P. R. Smith and Y. Patel, *Translational motion control of VSTOL aircraft using nonlinear dynamic inversion,* in *20th Atmospheric Flight Mechanics Conference* (American Institute of Aeronautics and Astronautics Inc, AIAA, 1995) pp. 238–252.

[35] B. J. Bacon and A. J. Ostroff, *Reconfigurable flight control using nonlinear dynamic inversion with a special accelerometer implementation,* AIAA Guidance, Navigation, and Control Conference and Exhibit (2000), 10.2514/6.2000-4565.

[36] V. Saksena, J. O'Reilly, and P. Kokotovic, *Singular Perturbations and Time-scale Methods in Control Theory : Survey 1976-1983 ",* Automatica **20**, 273 (1984).

[37] S. Sieberling, Q. P. Chu, and J. A. Mulder, *Robust flight control using incremental nonlinear dynamic inversion and angular acceleration prediction,* Journal of Guidance, Control, and Dynamics **33**, 1732 (2010).

[38] P. Simplício, M. D. Pavel, E. J. van Kampen, and Q. P. Chu, *An acceleration measurements-based approach for helicopter nonlinear flight control using incremental nonlinear dynamic inversion,* Control Engineering Practice **21**, 1065 (2013).

[39] L. G. Sun, C. C. De Visser, Q. P. Chu, and J. A. Mulder, *Online aerodynamic model identification using a recursive sequential method for multivariate splines,* Journal of Guidance, Control, and Dynamics **36**, 1278 (2013).

[40] S. Haykin and B. Widrow, *Least-Mean-Square Adaptive Filters* (John Wiley & Sons Inc., New Jersey, 2003).

[41] E. J. Smeur, Q. P. Chu, and G. C. De Croon, *Adaptive incremental nonlinear dynamic inversion for attitude control of micro air vehicles,* Journal of Guidance, Control, and Dynamics **39**, 450 (2016).

[42] E. J. Smeur, *TU Delft*, Ph.D. thesis, TU Delft (2018).

[43] B. J. Bacon, A. J. Ostroff, and S. M. Joshi, *Reconfigurable NDI controller using inertial sensor failure detection & isolation,* IEEE Transactions on Aerospace and Electronic Systems **37**, 1373 (2001).

[44] M. Krstić, D. Fontaine, P. Kokotovic, and J. Paduano, *Useful Nonlinearities and Global Stabilization of Bifurcation in a Model of Jet Engine Surge and STall,* IEEE Transactions on Automatic Control **43**, 1739 (1998).

[45] E. J. Smeur, G. C. De Croon, and Q. P. Chu, *Cascaded incremental nonlinear dynamic inversion for MAV disturbance rejection,* Control Engineering Practice **73**, 79 (2018).

[46] E. R. Van Oort, *Adaptive Backstepping Control and Safety Analysis for Modern Fighter Aircraft*, Ph.D. thesis, TU Delft, Delft (2011).

[47] L. Sonneveldt, *Adaptive Backstepping Flight Control for Modern Fighter Aircraft*, Ph.D. thesis, TU Delft (2011).

[48] H. K. Khalil, *Nonlinear Systems*, 3rd ed. (Prentice Hall, Upper Saddle River, NJ, 2002).

[49] J. Diebel, *Representing attitude: Euler angles, unit quaternions, and rotation vectors*, Tech. Rep. (Stanfordr University, Stanford, 2006).

[50] Q. P. Chu, *Advanced flight control AE4311,* (2017).

[51] J. A. Farrell, M. Polycarpou, M. Sharma, and W. Dong, *Command filtered backstepping,* IEEE Transactions on Automatic Control **54**, 1391 (2009).

[52] R. Penrose, *A generalized inverse for matrices,* Mathematical Proceedings of the Cambridge Philosophical Society **51**, 406 (1955).

[53] T. Berger, M. B. Tischler, and J. F. Horn, *Outer-Loop Control Design and Simulation Handling Qualities Assessment for a Coaxial-Compound Helicopter and Tiltrotor,* in *VFF 76th Annual Forum & Technology Display*, October (2020).

[54] O. Härkegård, *Efficient active set algorithms for solving constrained least squares problems in aircraft control allocation,* Proceedings of the IEEE Conference on Decision and Control **2**, 1295 (2002).

[55] R. T. Rysdyk, A. J. Calise, and R. T. Chen, *Nonlinear adaptive control of tiltrotor aircraft using neural networks,* in *World Aviation Congress, 1997* (1997).

[56] R. T. Rysdyk and A. J. Calise, *Fault tolerant flight control via adaptive neural network augmentation,* in *1998 Guidance, Navigation, and Control Conference and Exhibit* (American Institute of Aeronautics and Astronautics Inc, AIAA, 1998) pp. 1722–1728.

[57] R. T. Rysdyk and A. J. Calise, *Adaptive model inversion flight control for tilt-rotor aircraft,* Journal of Guidance, Control, and Dynamics **22**, 402 (1999).

[58] E. N. Johnson and A. J. Calise, *Pseudo-Control Hedging: A New Method for Adaptive Control,* in *Advances in Navigation Guidance and Control Technology Workshop[*, April 2015 (Redstone Arsenal, 2000).

[59] R. K. Mehra, R. K. Prasanth, R. L. Bennett, D. Neckels, and M. Wasikowski, *Model predictive control design for XV-15 tilt rotor flight control,* in *AIAA Guidance, Navigation, and Control Conference and Exhibit* (American Institute of Aeronautics and Astronautics Inc., 2001).

[60] T. Yomchinda, J. F. Horn, and N. Cameron, *Integrated flight control design and handling qualities analysis for a tilt rotor aircraft,* AIAA Atmospheric Flight Mechanics Conference , 1 (2009).

[61] P. Krishnamurthy and F. Khorrami, *Adaptive backstepping and θ-D based controllers for a tilt-rotor aircraft,* 2011 19th Mediterranean Conference on Control and Automation, MED 2011 , 540 (2011).

[62] T. Liang, W. Wang, S. Wu, and K. Lu, *Nonlinear attitude control of tiltrotor aircraft based on dynamic surface adaptive backstepping,* Proceedings of the 29th Chinese Control and Decision Conference, CCDC 2017 , 603 (2017).

[63] J. Zhang, P. Bhardwaj, S. A. Raab, S. Saboo, and F. Holzapfel, *Control allocation framework for a tilt-rotor vertical take-off and landing transition aircraft configuration,* 2018 Applied Aerodynamics Conference , 1 (2018).

[64] J. Howitt, *Application of Non-linear Dynamic Inversion to Rotorcraft Flight Control,* in *American Helicopter Society 61st Annual Forum* (AHS, Grapevine, 2005).

[65] R. v. d. Goot, *Helicopter Control using Incremental Adaptive Backstepping*, Tech. Rep. (TU Delft, 2017).

[66] M. Arons, *Effect of Lead-Lag Dynamics on Command Filtered Incremental Adaptive Backstepping Hingeless Rotorcraft*, Tech. Rep. (TU Delft, 2020).

[67] S. W. Ferguson, *A Mathermatical Model for Real Time Flight Simulation of a Generic Tilt-Rotor Aircraft*, Tech. Rep. (NASA Ames Research Center, Moutain View, 1988).

[68] M. D. Pavel, *Prediction of the necessary degrees of freedom for helicopter real-time simulation models,* Journal of Aircraft **45**, 1256 (2008).

[69] R. S. Russell, *Non-linear F-16 Simulation using Simulink and MATLAB*, Tech. Rep. (University of Minnesota, 2003).

[70] G. F. Franklin, D. Powell, and M. L. Workman, *Digital Control of Dynamic Systems*, 3rd ed. (Ellis-Kagle Press, Half Moon Bay, 1998).

[71] J. A. Farrell, M. Sharma, and M. Polycarpou, *Backstepping-based flight control with adaptive function approximation,* Journal of Guidance, Control, and Dynamics **28**, 1089 (2005).

[72] O. Härkegård, *WLS Control allocation algorithm,* (2008).

A

EOM 3-DOF model

The table with the system of equations may be found on the next page.

Table A.1: 3-DOF system of equations.

Input parameters	
Environmental	$\rho,\ g$
Aircraft	$m,\ I_y,\ A_{eq},\ N_R$
Rotor	$m_b,\ \Omega,\ R,\ c_b,\ I_b,\ K_\beta,\ \theta_{tw},\ N_b,\ C_{l_\alpha,b},\ C_{d_0,b},\ C_{d_1,b},\ C_{d_2,b}$
Wing	$C_{l_{\alpha,w}},\ \alpha_{0L,w},\ C_{D0,w},\ c_{m_{ac},w},\ S_w,\ AR_w,\ e_w,\ i_w,\ d_{x,w},\ d_{z,w}$
Horizontal stabilizer	$C_{l_{\alpha,hs}},\ \alpha_{0L,hs},\ C_{D0,hs},\ c_{m_{ac},hs},\ S_{hs}S,\ AR_{hs},\ e_{hs},\ i_{hs},\ \frac{dCl_{hs}}{dElev},\ d_{x,hs},\ d_{z,hs}$
Nacelle	$l_n,\ d_{x,n},\ ,d_{z,n}$
Controls	$\delta_{e,min},\ \delta_{e,max},\ \delta_{e,r\,max},\ \delta_{e,\tau},\eta_{min},\ \eta_{max},\ \eta_{r\,max},\ \eta_\tau,\theta_{0,min},\ \theta_{0,max},$ $\theta_{0,r\,max},\ \theta_{0,\tau},\theta_{1s,min},\ \theta_{1s,max},\ \theta_{1s,r\,max},\ \theta_{1s,\tau}$
Control variables	$\theta_0,\ \theta_{1s},\ \delta_e,\ \eta$
State variables	$u,\ w,\ q,\ \theta_f$
Calculations	
	$V = \sqrt{u^2 + w^2}$
	$\alpha_f = \arctan\left(\frac{w}{u}\right)$
Wing	$u_w = V\cos\left(\alpha_f\right) - q d_{x,w}$
	$w_w = V\sin\left(\alpha_f\right) - q d_{z,w}$
	$V_w = \sqrt{u_w^2 + w_w^2}$
	$\gamma_w = \arctan\frac{w_w}{u_w}$
	$\alpha_w = \gamma_w + i_w$
	$C_{L,w} = C_{l_{\alpha,w}}\left(\alpha_w - \alpha_{0L,w}\right)$
	$C_{D,w} = C_{D0,w} + \frac{C_{L,w}^2}{\pi AR_w e_w}$
	$L_W = \frac{1}{2}\rho V_w^2 S_W C_{L_w}$
	$D_w = \frac{1}{2}\rho V_w^2 S_w C_{D_w}$
	$X_w = L_w\sin\left(\gamma_w\right) - D_w\cos\left(\gamma_w\right)$
	$Z_w = -L_w\cos\left(\gamma_w\right) - D_w\sin\left(\gamma_w\right)$
	$M_w = \frac{1}{2}\rho V_w^2 S_W C_{m_{ac},w}$
Horizontal stabilizer	$u_{hs} = V\cos\left(\alpha_f\right) - q d_{x,hs}$
	$w_{hs} = V\sin\left(\alpha_f\right) + q d_{z,hs}$
	$V_{hs} = \sqrt{u_{hs}^2 + w_{hs}^2}$
	$\gamma_{hs} = \arctan\frac{w_{hs}}{u_{hs}}$
	$\alpha_{hs} = \gamma_{hs} + i_{hs}$
	$C_{L,hs} = C_{l_{\alpha,hs}}\left(\alpha_{hs} - \alpha_{0L,hs}\right) + \frac{dCl_{hs}}{dElev}\frac{dElev}{d\theta_{1s}}\theta_{1s}$
	$C_{D,hs} = C_{D0,hs} + \frac{C_{L,hs}^2}{\pi AR_{hs}e_{hs}}$
	$L_{hs} = \frac{1}{2}\rho V_{hs}^2 S_{hs} C_{L_{hs}}$
	$D_{hs} = \frac{1}{2}\rho V_{hs}^2 S_{hs} C_{D_{hs}}$
	$X_{hs} = L_{hs}\sin\left(\gamma_{hs}\right) - D_{hs}\cos\left(\gamma_{hs}\right)$
	$Z_{hs} = -L_{hs}\cos\left(\gamma_{hs}\right) - D_{hs}\sin\left(\gamma_{hs}\right)$
	$M_{hs} = \frac{1}{2}\rho V_{hs}^2 S_{hs} C_{m_{ac},hs}$
Control plane	$\alpha_{DP} = \theta_{1s} - \alpha_f - \eta$
	$\mu_{CP} = \frac{V}{\Omega R}\cos\left(\alpha_{CP}\right)$
	$\lambda_{CP} = \frac{V}{\Omega R}\sin\left(\alpha_{CP}\right)$
	$d_{x,dp} = l_n\sin\left(\theta_c\right) + d_{z,n}\sin\left(\theta_c - \eta\right) + d_{x,n}\cos\left(\theta_c - \eta\right)$
	$d_{z,cp} = l_n\cos\left(\theta_c\right) - d_{x,n}\sin\left(\theta_c - \eta\right) + d_{z,n}\cos\left(\theta_c - \eta\right)$
	$\gamma = \frac{\rho C_{l_\alpha,b} c_b R^4}{I_b}$

Table A.1 continues on the next page

Control plane cont*	$\hat{q} = \frac{q}{\Omega}$ $\sigma = \frac{N_b c_b}{\pi R}$ $d_{x,hub} = l_n \sin(\eta) + d_{x,n}$ $d_{z,hub} = -l_n \cos(\eta) - d_{z,n}$ $\lambda_{qt} = \frac{q d_{z,cp}}{\Omega R}$ $\lambda_{qp} = \frac{q d_{x,cp}}{\Omega R}$
Inflow	$\lambda_i = \arg\min\ (C_{T\,BEM} - C_{T\,GLAU})$ $a_1 = f\left(\mu_{CP}, \lambda_{qt}, \lambda_{qp}, I_b, \theta_0, \lambda_{CP}, \lambda_i, \gamma, \Omega, q, K_\beta\right)$ (See equation A.2 $C_{TBEM} = \frac{N I_b \gamma}{4R^5 \rho \pi}\left(\left(\lambda_{qt}^2 - 2\mu_{CP}\lambda_{qt} + \mu_{CP}^2 + \frac{2}{3}\right)\theta_0 - \frac{a_1 \lambda_{qt}}{2} + \frac{a_1 \mu_{CP}}{2} + \lambda_{qt} - \lambda_{CP} - \lambda_i\right)$ $C_{TGLAU} = 2\lambda_i \sqrt{\left(\frac{V}{\Omega R}\cos(\alpha_{CP} - \alpha_1)\right)^2 + \left(\frac{V}{\Omega R}\sin(\alpha_{CP} - \alpha_1) + \lambda_i\right)^2}$
Actuator limits	$\theta_{0_{max}}(\eta) = \frac{\partial \theta_0}{\partial X_{COL}}(\eta) X_{COL_{max}} + \theta_{0LL,0tw}(\eta) + \theta_{0G_{max}}$ $\theta_{0_{min}}(\eta) = \frac{\partial \theta_0}{\partial X_{COL}}(\eta) X_{COL_{min}} + \theta_{0LL,0tw}(\eta) + \theta_{0G_{min}}$ $\theta_{1s} = (\partial \theta_{1s} / \partial X_{LN}) X_{LN}$
State equations	$a_0 = f\left(\mu_{CP}, \lambda_{qt}, \lambda_{qp}, I_b, \theta_0, \lambda_{CP}, \lambda_i, \gamma, \Omega, K_\beta\right)$ (See equation A.1) $b_1 = f\left(\mu_{CP}, \lambda_{qt}, \lambda_{qp}, I_b, \theta_0, \lambda_{CP}, \lambda_i, \gamma, \Omega, q, K_\beta\right)$ (See equation A.3) $T = N_R C_{TBEM} \rho \Omega^2 \pi R^4$ $H = f\left(I_b, N_b, \gamma, \mu_{CP}, \theta_0, a_0, a_1, b_1, \lambda_i, \hat{q}, \lambda_{qp} \lambda_{qt}, q, \Omega, \lambda_{CP}, R, c_R, \rho, C_{l_\alpha}, C_{d_{0,b}}, C_{d_{1,b}}, C_{d_{2,b}}\right)$ $M_{K\beta} = \frac{N_R N_b K_\beta a_1}{2}$ $D_f = \frac{1}{2}\rho V^2 A_{eq}$ $\theta_{DP} = \theta_c - a_1 - \eta$ $\dot{u} = -g\sin(\theta_f) - \frac{D_f}{m}\cos(\alpha_f) + \frac{T}{m}\sin(\theta_{DP}) - \frac{H}{m}\cos(\theta_{DP}) - qw + \frac{X_w}{m} + \frac{X_{hs}}{m}$ $\dot{w} = g\cos(\theta_f) - \frac{D_f}{m}\sin(\alpha_f) - \frac{T}{m}\cos(\theta_{DP}) - \frac{H}{m}\sin(\theta_{DP}) + qu + \frac{Z_w}{m} + \frac{Z_{hs}}{m}$ $\dot{q} = \frac{T}{I_y}\left(\sin(\theta_{DP})\, d_{z,hub} - \cos(\theta_{DP})\, d_{x,hub}\right) - \frac{H}{I_y}\left(\cos(\theta_{DP})\, d_{z,hub} + \sin(\theta_{DP})\, d_{x,hub}\right) + \frac{M_{K\beta}}{I_y} + \frac{M_w}{I_y} + \frac{M_{hs}}{I_y} + \frac{Z_w d_{x,w} - X_w d_{z,w}}{I_y} + \frac{Z_h d_{x,hs} - X_{hs} d_{z,hs}}{I_y}$ $\dot{\theta}_f = q$

Rotor dynamics

$$a_0 = \frac{\left(3\mu_{cp}^2\theta_0 - 6\mu_{cp}\theta_0\lambda_{qt} + 3\theta_0\lambda_{qt}^2 + 3\theta_0 - 4\lambda_{cp} - 4\lambda_i + 4\lambda_{qp}\right) I_b\gamma\Omega^2}{24\left(I_b\Omega^2 + K_\beta\right)} \tag{A.1}$$

$$\begin{aligned} a_1 = & \frac{32\Omega\gamma I_b}{\left(I_b\Omega^2 + K_\beta\right)\left(I_b^2\gamma^2\Omega^4\left(\mu_{cp}^2 - 2\mu_{cp}\lambda_{qt} + \lambda_{qt}^2 + 2\right)\left(\mu_{cp}^2 - 2\mu_{cp}\lambda_{qt} + \lambda_{qt}^2 - 2\right) - 256K_\beta^2\right)}\Bigg(qI_b^2\Omega^4\left(\mu_{cp}^2 - 2\mu_{cp}\lambda_{qt} + \lambda_{qt}^2 + 2\right) + \\ & + \frac{\left(\mu_{cp}^2 - 2\mu_{cp}\lambda_{qt} + \lambda_{qt}^2 + 2\right)\left(\lambda_{qp} + \frac{4\theta_0}{3} - \lambda_{cp} - \lambda_i\right)\left(-\mu_{cp} + \lambda_{qt}\right)\gamma I_b^2\Omega^5}{8} + qI_bK_\beta\left(\mu_{cp}^2 - 2\mu_{cp}\lambda_{qt} + \lambda_{qt}^2 + 3\right)\Omega^2 + K_\beta^2 q + \\ & + \frac{\left(\left(\lambda_{qp} + \frac{8\theta_0}{3} - \lambda_{cp} - \lambda_i\right)\lambda_{qt}^2 - 2\mu_{cp}\left(\lambda_{qp} + \frac{8\theta_0}{3} - \lambda_{cp} - \lambda_i\right)\lambda_{qt} + \left(\lambda_{qp} + \frac{8\theta_0}{3} - \lambda_{cp} - \lambda_i\right)\mu_{cp}^2 + \frac{34\left(\lambda_{qp} - \lambda_{cp} - \lambda_i\right)}{9} + 4\theta_0\right)K_\beta\left(-\mu_{cp} + \lambda_{qt}\right)\gamma I_b\Omega^3}{8}\Bigg) \end{aligned} \tag{A.2}$$

$$\begin{aligned} b_1 = & \frac{-2\Omega I_b}{\left(I_b\Omega^2 + K_\beta\right)\left(I_b^2\gamma^2\left(\mu_{cp}^2 - 2\mu_{cp}\lambda_{qt} + \lambda_{qt}^2 + 2\right)\left(\mu_{cp}^2 - 2\mu_{cp}\lambda_{qt} + \lambda_{qt}^2 - 2\right)\Omega^4 - 256K_\beta^2\right)}\Bigg(\left(256 + \left(\mu_{cp}^2 - 2\mu_{cp}\lambda_{qt} + \lambda_{qt}^2 - 2\right)\gamma^2\right)qK_\beta I_b\Omega^2 + \\ & + \frac{2\left(\frac{3\lambda_q^2\theta_0}{4} - \frac{3\lambda_{qt}\mu_{cp}\theta_0}{2} + \frac{3\mu_{cp}^2\theta_0}{4} + \lambda_{qp} + \frac{3\theta_0}{4} - \lambda_{cp} - \lambda_i\right)\left(\mu_{cp}^2 - 2\mu_{cp}\lambda_{qt} + \lambda_{qt}^2 - 2\right)\left(-\mu_{cp} + \lambda_{qt}\right)\gamma^3 I_b^2\Omega^5}{9} + qI_b^2\gamma^2\left(\mu_{cp}^2 - 2\mu_{cp}\lambda_{qt} + \lambda_{qt}^2 - 2\right)\Omega^4 + \\ & + 32\left(\lambda_{qp} + \frac{4\theta_0}{3} - \lambda_{cp} - \lambda_i\right)K_\beta\left(-\mu_{cp} + \lambda_{qt}\right)\gamma I_b\Omega^3 + 32\left(\lambda_{qp} + \frac{4\theta_0}{3} - \lambda_{cp} - \lambda_i\right)\Bigg)K_\beta^2\left(-\mu_{cp} + \lambda_{qt}\right)\gamma\Omega + 256K_\beta^2 q\Bigg) \end{aligned} \tag{A.3}$$

$$
\begin{aligned}
H = &-\frac{\Omega N_b}{96R}\left(-b_1\left(c_{d_2,b}\theta_0-\frac{c_{d_1,b}}{2}\right)^2 a_0\lambda_{qt}^3+3\left(\mu_{cp}a_0b_1-\frac{a_0^2}{3}-\frac{a_1^2}{6}-\frac{b_1^2}{6}\right)\left(c_{d_2,b}\theta_0-\frac{c_{d_1,b}}{2}\right)^2\lambda_{qt}^2+\right.\\
&+\left(-3b_1\left(c_{d_2,b}\theta_0-c_{d_1,b}\frac{1}{2}\right)^2 a_0\mu_{cp}^2+2\left(c_{d_2,b}\theta_0-c_{d_1,b}\frac{1}{2}\right)^2\left(a_0^2+\frac{1}{2}a_1^2+\frac{1}{2}b_1^2\right)\mu_{cp}-\right.\\
&-2\left(\frac{1}{4}a_0b_1+a_1\left(\lambda_{cp}+\lambda_i-\lambda_{qp}\right)\right)c_{d_2,b}^2\theta_0^2+2c_{d_1,b}\left(\frac{1}{4}a_0b_1+a_1\left(\lambda_{cp}+\lambda_i-\lambda_{qp}\right)\right)c_{d_2,b}\theta_0-12c_{d_2,b}\Omega a_0b_1+\\
&+\left(-\frac{1}{8}a_0b_1-\frac{1}{2}a_1\left(\lambda_{cp}+\lambda_i-\lambda_{qp}\right)\right)c_{d_1,b}^2+12\Omega c_{l_\alpha,bl}a_0b_1\Big)\lambda_{qt}+b_1\left(c_{d_2,b}\theta_0-c_{d_1,b}\frac{1}{2}\right)^2 a_0\mu_{cp}^3-\left(c_{d_2,b}\theta_0-c_{d_1,b}\frac{1}{2}\right)^2\left(a_0^2+\frac{1}{2}a_1^2+\frac{1}{2}b_1^2\right)\mu_{cp}^2+\\
&+\left(2\left(\frac{1}{4}a_0b_1+a_1\left(\lambda_{cp}+\lambda_i-\lambda_{qp}\right)\right)c_{d_2,b}^2\theta_0^2-2c_{d_1,b}\left(\frac{1}{4}a_0b_1+a_1\left(\lambda_{cp}+\lambda_i-\lambda_{qp}\right)\right)c_{d_2,b}\theta_0+12c_{d_2,b}\Omega a_0b_1+\right.\\
&+\left(\frac{1}{8}a_0b_1+\frac{1}{2}a_1\left(\lambda_{cp}+\lambda_i-\lambda_{qp}\right)\right)c_{d_1,b}^2-12\Omega c_{l_\alpha,bb}a_0b_1\Big)\mu_{cp}-4c_{d_2,b}\left(\left(\lambda_{cp}+\lambda_i-\lambda_{qp}\right)^2 c_{d_2,b}+\Omega\frac{1}{2}\right)\theta_0^2+4c_{d_1,b}\left(\left(\lambda_{cp}+\lambda_i-\lambda_{qp}\right)^2 c_{d_2,b}+\Omega\frac{1}{2}\right)\theta_0-\\
&-6c_{d_2,b}b_1\Omega\hat{q}-\left(\lambda_{cp}+\lambda_i-\lambda_{qp}\right)^2 c_{d_1,b}^2+6\left(\hat{q}c_{l_\alpha,bl}b_1-c_{d_0,b}\frac{1}{3}\right)\Omega\Big)\rho c\left(\mu_{cp}-\lambda_{qt}\right)R^4\\
&+12\gamma I_b\left(\Omega a_0b_1\lambda_{qt}^2+\left(-2b_1\Omega\mu_{cp}a_0+2\Omega\left(\lambda_{cp}+\lambda_i-\lambda_{qp}\right)\theta_0+\frac{1}{4}\Omega b_1^2+\frac{1}{4}qb_1+\Omega\left(a_0^2+\frac{3}{4}a_1^2\right)\right)\lambda_{qt}+\Omega a_0b_1\mu_{cp}^2+\right.\\
&+\left.\left(-2\Omega\left(\lambda_{cp}+\lambda_i-\lambda_{qp}\right)\theta_0-\frac{1}{4}\Omega b_1^2-\frac{1}{4}qb_1-\Omega\left(a_0^2+\frac{3}{4}a_1^2\right)\right)\mu_{cp}-2\frac{1}{3}\Omega a_1\theta_0+2\frac{1}{3}qa_0+\Omega a_1\left(\lambda_{cp}+\lambda_i-\lambda_{qp}\right)\right)
\end{aligned}
\tag{A.4}
$$

B

Aircraft parameters

In this appendix the numerical values of the parameters will be presented.

Table B.1: Parameter values[8]

Environmental			
ρ	Air density	1.225	kg/m^3
g	Gravitational acceleration	9.81	m/s^2
Aircraft			
m	Aircraft mass	5896.7	kg
I_y	Moment of inertia w.r.t C.G.	28960.272	kgm^2
A_{eq}	Equivalent flat plate drag area	0.84	m^2
N_R	Number of rotors	2	[-]
Rotor			
m_b	Blade mass	113.9	kg
Ω	Rotorspeed	517	RPM
R	Rotor radius	3.81	m
c_b	Average chord length	0.3557	m
I_b	Blade Moment of inertia w.r.t blade C.G.	139	kgm^2
K_β	Flapping spring constant	17478	$\frac{kgm^2}{s^2 rad}$
θ_{tw}	Thrust weighted average twist	8.59	deg
N_b	Number of blades	3	$[-]$
$C_{l_\alpha,b}$	Blade lift curve slope	6.56	rad/s
$C_{D0,w}$	0th order blade airfoil drag coefficient	5	$[-]$
$C_{d_1,b}$	1th order blade airfoil drag coefficient	0.068	rad^{-1}
$C_{d_2,b}$	2th order blade airfoil drag coefficient	0.81	rad^{-1}
Wing			
$C_{l_{\alpha,w}}$	Wing lift curve slope	5.31	rad^{-1}
$C_{D0,w}$	Wing zero-lift angle of attack	-4.02	$[-]$
$c_{m_{ac}}$	Wing profile drag coefficient	0.017	$[-]$
S_w	Wing surface area	-0.02	m^2
AR_w	Wing aspect ratio	5.7	$[-]$
e_w	Wing Oswald factor	1	$[-]$
i_w	Wing incidence angle	0	deg
$d_{x,w}$	Wing a.c. x-distance w.r.t. C.G.	-0.1348	m
$d_{z,w}$	Wing a.c. y-distance w.r.r. C.G.	0.361	m
Horizontal stabilizer (HS)			
$C_{l_\alpha,hs}$	HS lift curve slope	4.03	rad^{-1}
$\alpha_{0L,hs}$	HS zero-lift angle of attack	0	rad
$C_{D0,hs}$	HS profile drag coefficient	0.0088	$[-]$
$c_{m_{ac},hs}$	HS pitching moment coefficient w.r.t. a.c.	0	$[-]$
$S_{hs}S$	HS area	4.66	m^2
AR_{hs}	HS aspect ratio	3.27	$[-]$
e_{hs}	HS Oswald factor	1	$[-]$
i_{hs}	Incidence angle	0	rad
$\frac{dCl_{hs}}{dElev}$	HS effectiveness w.r.t. Elevator	2.29	rad^{-1}
$d_{x,hs}$	x-distance w.r.t. C.G. in b-frame	6.696	m
$d_{z,hs}$	y-distance w.r.t. C.G. in b-frame	0.542	m

Table B.1 continues on the next page

Nacelle			
l_n	Mast length	1.422	m
$d_{x,n}$	Nacelle pivot x-distance in b-frame	0.09	m
$d_{z,n}$	Nacelle pivot z-distance in b-frame	0.466	m
Controls			
$\delta_{e,min}$	Min elevator limit	-20	deg
$\delta_{e,max}$	Max elevator limit	20	deg
$\delta_{e,r\ max}$	Max deflection rate	± 100	deg/s
$\delta_{e,\tau}$	Elevator deflection rate time-constant	0.05	s
η_{min}	Min mast angle limit	-90	deg
η_{max}	Max mast angle limit	5	deg
$\eta_{r\ max}$	Mast angle rate	$\pm 2.5/\pm 7.5$	deg/s
$\frac{\partial \theta_0}{\partial X_{COL}}$	See table B.2		
$\theta_{0,r\ max}$	Max collective rate	60	deg/s
$\theta_{0,\tau}$	Collective rate time-constant	$1/13$	s
$\frac{\partial \theta_{1s}}{\partial X_{LON}}$	See table B.3		
$\theta_{1s,r\ max}$	Max longitudinal cyclic rate		deg/s
$\theta_{1s,\tau}$	Longitudinal cyclic rate time-constant	$1/13$	s
$X_{COL,max}$	Maximum collective stick deflection	10	inch
$X_{COL,min}$	Minimum collective stick deflection	0	inch
$X_{LON,max}$	Maximum longitudinal stick deflection	4.8	inch
$X_{LON,min}$	Minimum longitudinal stick deflection	-4.8	inch

Table B.2: Collective control gearing and lower pitch bounds.[9]

Nacelle angle, η, [deg]	$\frac{\partial \theta_0}{\partial X_{COL}}$**, [deg/in]**	θ_{0LL}**, [deg]**
0 (helicopter mode)	1.6	-2.3
-10	1.5	-1
-20	1.35	1
-30	1.13	4
-40	0.92	7
-50	0.71	10.2
-60	0.52	13.5
-70	0.34	16.7
-80	0.15	19.5
-90 (airplane mode)	0	21.3

Table B.3: Longitudinal cyclic gearing[9]

Nacelle angle, η, [deg]	$\frac{\partial \theta_{1S}}{\partial X_{LN}}$**, [deg/in]**
0 (helicopter mode)	2.1
-10	2.09
-20	1.98
-30	1.81
-40	1.60
-50	1.35
-60	1.04
-70	0.71
-80	0.362
-90 (airplane mode)	0

C

Active set solving algorithm

This appendix presents the active set algorithm that is used to solve weighted least squares (WLS) problem for the control allocation problems will be presented. This method has been introduced for control purposes in the work of Härkegård in [54] and was adapted for incremental control by Smeur in [41]. A fully implemented matlab example is accesible online via [72]

The objective function as defined for the control allocation problem is:

$$u_W = \arg\min_{\underline{u} \le u \le \bar{u}} \gamma \left\| W_v (Gu - v) \right\|^2 + \left\| W_u \left(u - u_p \right) \right\|^2 \tag{C.1}$$

The active set solving algorithm solves this problem as a least squares problem formulated as:

$$u = \arg\min \|Au - b\|^2 \tag{C.2}$$

with the constraints:

$$Bu = v \tag{C.3}$$

$$Cu \ge U \tag{C.4}$$

C is defined as $\begin{pmatrix} 1 \\ -1 \end{pmatrix}$ and U as $\begin{pmatrix} \underline{u} \\ -\bar{u} \end{pmatrix}$ This objective function will be rewritten as:

$$\left\| \underbrace{\begin{pmatrix} \gamma W_v G \\ W_u \end{pmatrix}}_{A} u - \underbrace{\begin{pmatrix} \gamma W_v v \\ W_u u_p \end{pmatrix}}_{b} \right\|^2 \tag{C.5}$$

Equation C.1 is reformulated in this form and becomes:

$$u_W = \arg\min_{\underline{u} \le u \le \bar{u}} \|Au - b\|^2 \tag{C.6}$$

This problem is then solved via the following algorithm:

Let u_0 be a feasible starting point. Let the working set W contain (a subset of) the active inequality constraints at u_0.

for k = 0,k,2,....N-1:

To determine the free columns in A. Given u^k, find the optimal perturbation p, considering the constraints in the working set as equality constraints and disregarding the remaining inequality constraints. Solve:

$$u_W = \arg\min_p \left\| A(u^k + p) - b \right\|^2 \tag{C.7}$$

$$Bp = 0 \tag{C.8}$$

$$p_i = 0, i \in W \tag{C.9}$$

if $u^k + p$ is feasible:

Set $u^{k+1} = u^k + p$ and compute the Lagrange multipliers, $\begin{pmatrix} \mu \\ \lambda \end{pmatrix}$, where μ is associated with equation C.3 and λ with the constraints from equation C.4. The Lagrange multipliers can be computed with:

$$A^T(Au - b) = \begin{pmatrix} B^T & C_0^T \end{pmatrix} \begin{pmatrix} \mu \\ \lambda \end{pmatrix} \tag{C.10}$$

where C_0 contains the rows of C that correspond to constraints in the working set.

if all $\lambda \geq 0$:

u^{k+1} is the optimal solution to equation C.7.

else:

Remove the constraints associated with the most negative λ

else:

Determine the maximum step length α such that $u^{k+1} = u^k + \alpha p$ is feasible. Add the primary bounding constraint to the working set.